Electrophysiological Characterization of the Acid Sensing Ion Channel shark ASIC1b and Identification of Amino Acids Controlling the Gating of ASIC1

Von der Fakultät für Mathematik, Informatik und Naturwissenschaften der RWTH Aachen University zur Erlangung des akademischen Grades eines Doktors der Naturwissenschaften genehmigte Dissertation

vorgelegt von

Diplom-Biologe

Andreas Springauf

aus Würzburg

Berichter: Universitätsprofessor Dr. rer. nat. Stefan Gründer
Universitätsprofessor Dr. rer. nat. Hermann Wagner

Tag der mündlichen Prüfung: 04. Februar 2011

Table of contents

Summary

Acid sensing ion channels (ASICs) are sodium-selective and proton-sensitive members of the DEG/ENaC gene family and are expressed in the chordate lineage while being absent in evolutionary older animals. Although members of the DEG/ENaC family share similarities with respect to topology, selectivity for sodium and sensitivity to the blocking agent amiloride, the family comprises ion channels of various functions and diverse gating mechanisms.

So far, four ASIC genes have been identified in mammals (*asic*1-*asic*4) that code for at least six different ASIC subunits.

Amino acid sequences of the members of the ASIC subfamily are at least 45% identical and they are composed, like all members of the DEG/ENaC family, of two transmembrane domains, a large extracellular loop domain and rather short intracellular termini.

So far, ASICs have been cloned from urochordates, jawless vertebrates, cartilaginous shark and bony fish, from chicken and different mammals. Proton-sensitivity, however, was postulated to have evolved with the rise of bony fish and ASICs from lower chordate species were characterized as proton-insensitive.

Since the crystal structure of chicken ASIC1 was resolved in 2007 it is known that functional ASIC channels are trimeric structures that assemble in a homo- or heteromeric fashion *in vivo* and *in vitro*. Depending on the subunit composition they exhibit different functional features regarding proton sensitivity or gating kinetics.

Some ASICs, like the abundant ASIC1a, are broadly expressed in the peripheral as well as in the central nervous system whereas the expression pattern of other ASICs, for example ASIC1b and ASIC3, is restricted to the peripheral nervous system. Predominantly located at the postsynaptic membrane, ASICs are supposedly implicated in modulation of synaptic transmission and pain perception, but they also contribute to pathophysiological processes like ischemia, epilepsy as well as to axonal degeneration during neuroinflammation. Moreover, knockout of the *asic1* gene leads to deficits in spatial memory and learned fear, suggesting a contribution to higher brain functions. Because of such important implications and the limited pharmacological toolkit for ASIC modulation, it is desirable to find new specific drugs for ASIC modulation and understanding of the gating process of ASICs would be of great benefit for designing new highly specific drugs.

The first part of this work shows that proton-sensitivity evolved latest in cartilaginous fish and that ASIC1b from shark (*Squalus acanthias*) indeed responds to extracellular acidification. Furthermore, a detailed characterization of homomeric shark ASIC1b channels revealed that the current of these channels exhibit unique features and that it can be divided into two components. The fast transient current component shows a time constant of desensitization (τ) of less than 50 ms and is followed by a highly proton sensitive sustained current component that does not completely desensitize as long as protons are present in the extracellular solution.

In addition, the second part of this thesis elucidates the amino acids that are crucial for the unique sustained current component of shark ASIC1b. An amino acid triplet ($M^{109}DS$) in the proximal region of the extracellular domain that is located in the linker region between two β-sheets partially controls the time constant of desensitization and is necessary for the generation of the sustained current of shark ASIC1b. Additionally, it is shown that the same triplet is also sufficient to introduce a sustained current in rat ASIC1a, a channel that usually completely desensitizes during prolonged acidification.

Moreover, when the most critical residue of this triplet at position 110 is mutated to cysteine, different MTS-modification rates at this position in the closed and the desensitized state, respectively, provide evidence that this residue is moving during the gating transition.

Finally, engineering of a cysteine at position 110 (position 82 in rat) and at an adjacent position in the β11-β12-linker leads to spontaneous formation of a disulfide bond that traps shark ASIC1a and rat ASIC1a in the desensitized conformation.

Collectively the results presented in this work suggest that the β1-β2 and β11-β12 linkers are dynamic during gating and tightly oppose each other during desensitization gating. Obstruction of this tight opposition leads to reopening of the channel. It results that the β1-β2 and β11-β12 linkers modulate gating movements of ASIC1 and may thus be drug targets for modulation of ASIC activity.

Zusammenfassung

Acid sensing ion channels (ASICs) sind Natrium-selektive und protonen-aktivierbare Ionenkanäle der DEG/ENaC-Genfamilie. Sie werden in Wirbeltieren exprimiert, sind jedoch nicht in entwicklungsgeschichtlich älteren Lebewesen zu finden. Obwohl die Mitglieder der DEG/ENaC Familie Gemeinsamkeiten hinsichtlich ihrer Topologie, ihrer Selektivität für Natrium und der Sensitivität für den Kanalblocker Amilorid zeigen, erfüllen die verschiedenen Mitglieder jedoch sehr unterschiedliche physiologische Funktionen und benötigen diverse Aktivierungs-Stimuli.

Bisher konnten in Säugern vier ASIC-Gene (*asic1* – *asic4*) identifiziert werden, die für mindestens sechs ASIC-Untereinheiten kodieren. Die Sequenzen innerhalb der Mitglieder der ASIC-Unterfamilie sind zu mindestens 45% homolog. ASICs haben, wie auch die anderen Mitglieder der DEG/ENaC Familie, zwei Transmembran-Domänen, eine große extrazelluläre Domäne und kurze Enden, die ins Zellinnere gerichtet sind.

ASIC-Untereinheiten konnten bisher aus entwicklungsgeschichtlich verschiedenen Spezies wie Urochordaten, kieferlosen Vertebraten, Knorpel- und Knochenfischen, sowie aus dem Huhn und verschiedenen Säugern kloniert werden. Jedoch wurde geraume Zeit angenommen, dass Protonen-sensitive ASICs erst mit der Entstehung von Knochenfischen entstanden sind, da ASICs aus dem Manteltier, dem Neunauge und dem Haifisch als insensitiv gegenüber Protonen charakterisiert wurden.

Seit im Jahre 2007 die Kristallstruktur von ASIC1 aus dem Huhn bekannt ist, weiß man, dass funktionelle Kanäle durch drei ASIC-Untereinheiten gebildet werden, die sich *in vivo* und *in vitro* zu Homomeren oder Heteromeren zusammenlagern können. Abhängig von der Zusammensetzung der Untereinheiten haben die Kanäle unterschiedliche Eigenschaften bezüglich ihrer Protonen-Sensitivität oder ihrer Kinetik.

Während manche ASIC-Untereinheiten sowohl im peripheren als auch im zentralen Nervensystem exprimiert werden, ist die Expression anderer Untereinheiten, wie etwa von ASIC1b und ASIC3, auf das periphere Nervensystem beschränkt. ASICs sind vorzugsweise an der postsynaptischen Membran zu finden, wobei sie an der Modulation der synaptischen Übertragung und der Schmerzwahrnehmung beteiligt sind, aber auch mit pathophysiologischen Prozessen wie Ischämie, Epilepsie oder axonaler Degeneration während neuronaler Entzündungen in Verbindung gebracht

werden. Darüber hinaus ist aus Studien mit Knockout-Mäusen bekannt, dass der Verlust des *asic1*-Gens zu Defiziten im räumlichen Gedächtnis und bei Furcht-Konditionierung führt, was zudem eine Beteiligung an höheren Gehirnfunktionen vermuten lässt. Da ASICs mit solch wichtigen Symptomen in Verbindung gebracht werden können und da pharmakologische Werkzeuge für ASICs sehr begrenzt sind, ist es außerordentlich wünschenswert, neue und für ASICs spezifische Pharmaka zu entwickeln. Ein besseres Verständnis des Gating-Prozesses dieser Kanäle wäre in diesem Zusammenhang von großem Nutzen.

Der erste Teil dieser Arbeit zeigt, dass Protonen-Sensitivität von ASICs bereits in Knorpelfischen entwickelt war und dass shark ASIC1b aus dem Dornhai (*Squalus acanthias*) darüber hinaus einen einzigartigen Protonen-aktivierten Ionenstrom zeigt. Die detaillierte Charakterisierung ließ erkennen, dass die Ströme von shark ASIC1b in zwei Komponenten unterteilt werden können. Die sehr schnell desensitivierende transiente Komponente weist eine Zeitkonstante von weniger als 50 ms auf und wird von einer zweiten Stromkomponenten gefolgt, die auch durch sehr geringe Protonenkonzentrationen aktiviert werden kann und die nicht desensitiviert solange Protonen extrazellulär vorhanden sind.
Zusätzlich werden im zweiten Teil der Arbeit die Aminosäuren identifiziert, die für das außergewöhnliche Gating-Verhalten von shark ASIC1b verantwortlich sind. Ein Aminosäuretriplet ($M^{109}DS$) in der proximalen Region der extrazellulären Domäne, das kurz hinter der ersten Transmembrandomäne und zwischen zwei β-Faltblatt-Strukturen liegt, kontrolliert zum Teil die Geschwindigkeit der Desensitivierung und ist maßgeblich für die Generierung des nicht-desensitivierenden Stromes verantwortlich. Weiterhin konnte gezeigt werden, dass dieses Triplet nicht nur für den nicht-desensitivierenden Strom in shark ASIC1b verantwortlich ist, sondern auch einen nicht-desensitivierenden Strom in ASIC1a der Ratte induzieren kann, einem Kanal der typischer Weise selbst in Anwesenheit von Protonen komplett desensitiviert.
Weiterhin wurde durch MTS-Modifikations-Versuche an Position 110 gezeigt, dass diese Aminosäure während der Gating-Bewegung dynamisch ist und daher direkt Einfluss auf den Gating-Vorgang ausüben kann. Schließlich wurden Doppel-Cystein-Mutanten an Positionen 110 und 428 konstruiert. Beide Positionen liegen in der Krystallstruktur zwischen zwei β–Faltblättern und befinden sich im desensitivierten Zustand in unmittelbarer Nähe zueinander. Durch die spontane Formation einer

Disulfidbrücke zwischen diesen beiden Positionen, die den Kanal im desensitivierten Zustand festhalten, konnte die direkte Wechselwirkung dieser Positionen in der desensitivierten Konformation von ASIC1 gezeigt werden.

Mit den in dieser Arbeit präsentierten Ergebnissen kann ein Modell für ASIC1 vorgeschlagen werden, bei dem sich während der Desensitivierung des Kanals zwei Linker-Regionen, die jeweils zwischen zwei β-Faltblatt-Strukturen liegen, aufeinander zu bewegen und im desensitivierten Zustand in direkter Wechselwirkung zueinander stehen. Aus diesem Grund sind beide Positionen vielversprechende Bereiche für die Entwicklung spezifischer Pharmaka zur Modulierung von ASICs.

1. General Introduction

Cells of every Phylum are surrounded and delimited from the environment or other cells by a membrane consisting of a lipophilic lipid bilayer. To interact with other cells, transfer information and maintain a certain physiological state of homeostasis cells need to exchange substances and ions. Because most hydrophilic substances and ions cannot cross the membrane, certain structures and proteins are required to allow such an exchange.

Ion channels are a class of proteins that span the cell membrane and form water filled pores through those lipid bilayers, thus providing a selective or unselective gate for ions to cross cell membranes. They can be found in every phylum and are expressed in almost every cell of all organisms. Most functional ion channels are built up by several similar or identical subunits giving rise to a high number of possible quaternary structures and different functional characteristics. Despite their high variety regarding topologies and three-dimensional structures, most subunits of ion channels contain at least two hydrophobic regions of around 20 amino acids which form the transmembrane domains and which are connected to each other via a loop region, that can be located intra- or extracellularly. The pore regions of all ion channels are formed by the transmembrane domains or by special pore loops located between the transmembrane domains.

Most ion channels display selectivity for certain ions thus acting as molecular sieves. This capacity is achieved by the architecture of the pore, its size or its pore lining amino acids, which can interact with certain ions and retract others. Thus the pore can differentiate ions with regard to their size and their charge.

Taking a look at the open probability of ion channels, two main characters can be distinguished at first sight: constitutively open channels and channels that need special ligands or other stimuli such as changes in the membrane potential or membrane tension to be transferred from the closed to the open state.

Ligands that open ion channels are even more diverse than the class of ion channels itself, comprising protons as the simplest ligands possible as well as complex oligopeptides with intricate three-dimensional structures.

Ion Channels can be classified into ion channel families according to their structure, their ion - selectivity, their ligands and even to their physiological function. Until

today, most molecular correlates for physiological currents through cell membranes are identified, cloned and characterized.

1.1 The Superfamily of DEG/ENaC Ion Channels

1.1.1 Discovery and classification

Discovered at the beginning of the 1990s, the DEG/ENaC gene family comprises ion channels with diverse properties according to their gating mechanisms, their expression patterns and their physiological functions (Mano and Discroll, 1999). The first part of the designation of the DEG/ENaC superfamily refers to one of the first genes that have been identified, deg-1 (the second is called mec-4) (Chalfie and Au, 1989; Chalfie and Wolinsky, 1990). Deg-1 encodes a mechanosensitive protein that is required for touch sensation in *C. elegans*. Mutation of this gene causes neuronal degeneration. At the same time a channel was cloned and identified that was already known to play a crucial role in sodium absorption in distal tubule of the kidney. This channel was the α-subunit of the amiloride-sensitive epithial sodium channel, αENaC. Sequence comparison revealed a substantial homology between αENaC and Degenerins thus suggesting a common family of ion channels, the DEG/ENaC ion channel family (Canessa *et al*., 1993, Lingueglia, *et al*., 1993). New subfamilies emerged within this ion channel family, formed by subsequently found members, which have been identified by sequence homology.

All members of this channel family identified so far are exclusively expressed in animals of the metazoan kingdom, which are characterized by a body plan including organs for reproduction, digestion and coordination. The expression restricted to the metazoan kingdom distinguishes them from very ancient channels in evolution like potassium, chloride or water channels.

Another striking feature of the members of this ion channel family is their functional heterogeneity associated with and caused by the wide tissue distribution of the different family members. Gating features are as diverse as mechanosensitivity of the degenerins and ligand gating of other members. The ligands themselves are very different just as protons (ASICs) or small peptides (FaNaC and HyNaCs). Furthermore, ENaCs that are expressed in the kidney, are constitutively open. One

can conclude that the divergent evolution of the DEG/ENaC gene family was directed by the task to achieve very different functions in the cell.

1.1.2 Common sequence features and characteristics

The sizes of the proteins that are encoded by DEG/ENaC genes range from approximately 500 to 800 amino acids. All channels share a common topology with two transmembrane domains (TM1 and TM2), a large extracellular loop and rather small intracellular N- and C-termini. The extracellular loop makes up two thirds of the whole protein and represents a unique structural feature that is not found in other ion channel families (Kellenberger and Schild, 2002). The channels contain domains or at least several amino acids that are highly or even completely conserved among all family members (Fig. 1.1). The conserved residues are thought to represent elements that are crucial for proper channel folding and function (Kellenberger and Schild, 2002).

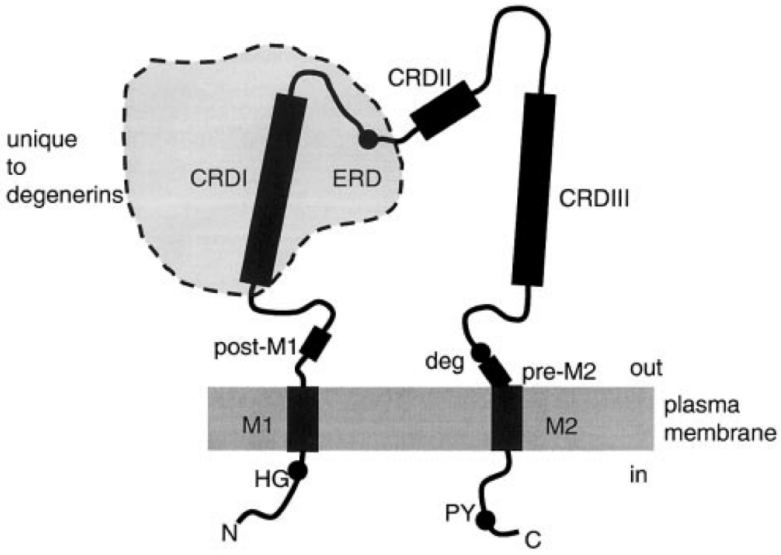

Figure 1.1. Members of the DEG/ENaC family of ion channels show highly conserved residues. Schematic transmembrane topology organization of the DEG/ENaC superfamily of ion channels that shows localization of conserved domains. Scheme shows a single subunit. (CRD, cysteine rich domain; ERD, extracellular regulatory domain unique to *C. elegans* degenerins; M1/M2, transmemebrane domain 1 and 2; deg, mutation at this site causes degeneration of cells expressing this mutant channel. (Adapted from Kellenberger and Schild, 2002).

The highest degree of conservation is displayed by the Histidine-Glycine pair located intracellularly upstream of the first transmembrane domain (Fig. 1.1), the FPxxTxC sequence that follows TM1 and several residues upstream from and within the second transmembrane domain (Kellenberger and Schild, 2002). Additionally, the extracellular loop contains two cysteine rich domains (Fig. 1.1). Through conformation of disulfide bridges these domains ensure the precise formation and maintenance of the tertiary structure. Moreover, two cysteine-pairs of ENaCs were identified to play a crucial role for trafficking of the channel to the plasma membrane (Firsov *et al*., 1999). Other residues, even if not conserved within the entire DEG/ENaC family, are at least shared by members of the same subfamilies. For example, the members of the ASIC subfamily, which are activated by extracellular protons, display several extracellular sequence features that distinguish them from other subfamilies (see also 1.2.3).
Other common characteristics of the DEG/ENaC family are a selectivitiy for Na^+ over K^+ and Ca^{2+} and sensitivity regarding to the diuretic amiloride.
Nevertheless, it has to be considered that a lot of channels of this family have not been characterized electrophysiologically *in-vivo* or *in-vitro* and it remains unclear if the mentioned features are indeed shared by all members of this family.

1.1.3 Subfamilies of the DEG/ENaC Superfamily

According to sequence homology, the identified members of the DEG/ENaC family can be divided into eight subfamilies (Fig 1.2). These are the SCNN (sodium channel gene family) genes encoding the α–, β–, γ- and δ–subunits of ENaC subfamily and the UNC, MEC, DEG and DEL genes from *C. elegans* forming the degenerin subfamily.
Another major subfamily comprises the acid sensing ion channels (ASICs) that are gated by protons. Other subfamilies like the pickpocket (PPK/dmdNaC1) and ripped pocket (RPK/dGNaC1) genes and the peptide gated sodium channels FaNaC were found in *Drosophila* and the snail *Helix aspersa,* respectively. The FLR-1 genes from *C. elegans,* which are clearly distinct from the degenerins provide another subfamily. Moreover, the DEG/ENaC family also comprises the mammalian BLINaC gene (brain-liver-intestine amiloride Na^+-channel), which was cloned from rat and from mouse, and its human ortholog INaC (intestine Na^+ channel). The most recently described subfamily comprises the HyNaC genes, which were cloned from the cnidarian *Hydra magnipapillata*, the most ancient known organism that encodes DEG/ENaC genes.

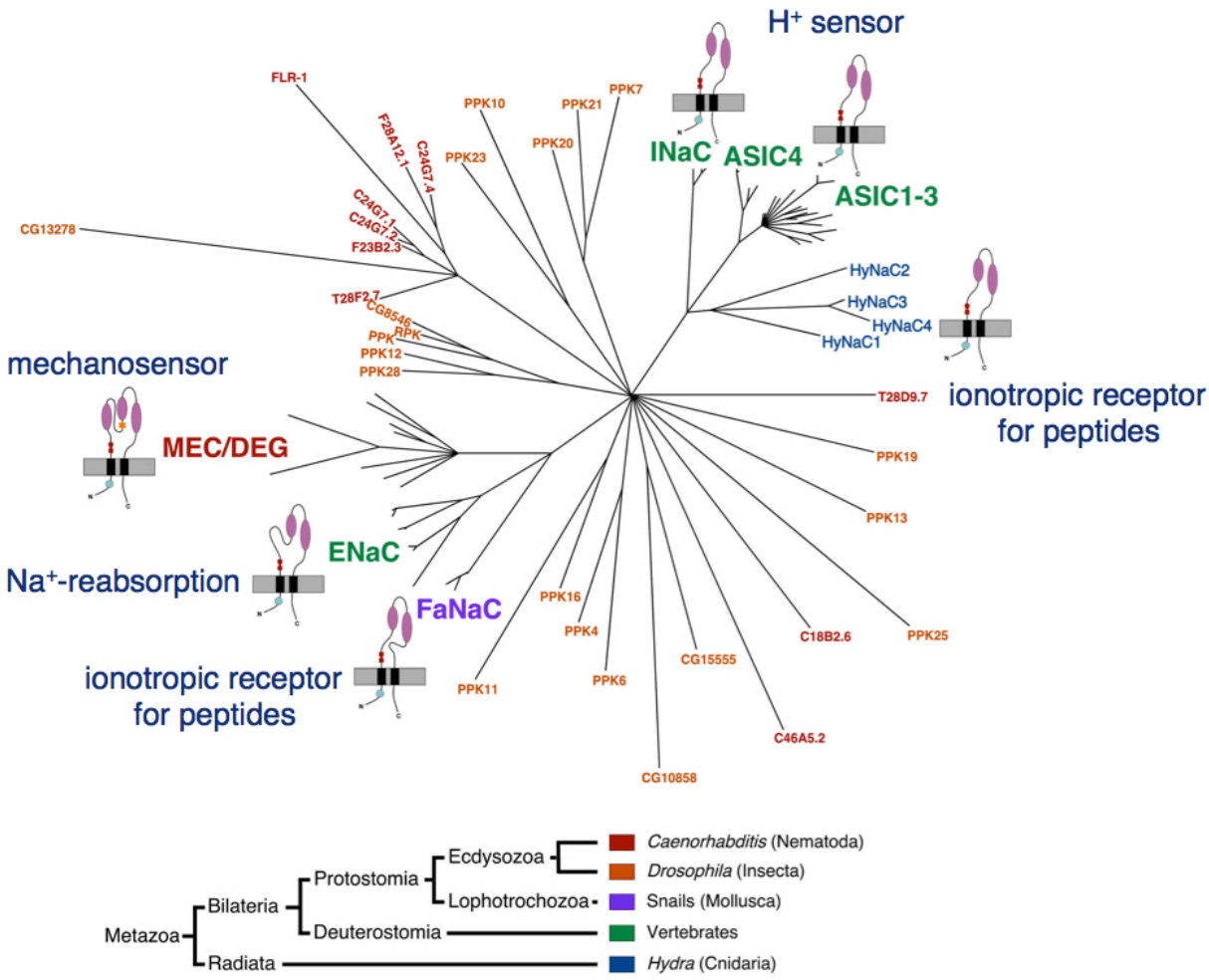

Figure 1.2. Phylogenetic tree created with the software Treepuzzle-50.
The length of the branches are proportional to the evolutionary distances. Different colors represent animal groups that are also indicated in the cladogram at the bottom. (Adapted from Golubovic *et al*., 2007)

1.1.3.1 ENaC (epithelial sodium channel)

In mammals the subfamily of the epithelial sodium channels comprises the four subunits α–, β–, γ– and δ-ENaC, which share an amino acid homology of 30 – 35%. Expressed in *Xenopus* oocytes the three subunits α, β and γ form functional heteromeric and constitutively open channels that produce higher currents than the homomeric α–subunit alone (Canessa *et al*., 1994; McDonald, 1995). Currents from the heterotrimeric channels are very similar to those observed *in vivo* (Palmer and

Frindt, 1986). The β– and γ– subunit cannot form functional channels alone or in combination.

The δ-subunit, identified in 1995 (Waldmann *et al*., 1995), shows a different expression pattern than the other three subunits, (Waldmann *et al*., 1995; Yamamura *et al*., 2004), and it can substitute the α-subunit and is suspected to have a regulatory function.

Like all other members of the DEG/ENaC family, functional ENaC channels are voltage independent with a linear current-voltage relationship and display a high selectivity for Na^+ over K^+ (Lingueglia *et al*., 1993; Canessa *et al*., 1994, Garty and Palmer, 1997). Located at the apical membrane of the epithelia of kidney, lung, colon, sweat and salivary glands, ENaC is the central component of the pathway that controls sodium reabsorption from the exterior medium back into the cell thus maintaining salt homeostasis (Garty and Palmer, 1997). Because of this important function, ENaC is tightly controlled by hormones such as aldosterone, vasopressin and insulin (Rossier *et al*., 2002). Furthermore, mutations in ENaC can cause several severe diseases in humans like hypertension, Liddle's syndrome, hypokalemia and salt-wasting syndrome (Gründer, 2000) further confirming the important function of this channel.

1.1.3.2 BLINaC/hINaC

Three orthologs of the BLINaC subfamily from rat, mouse and human have been cloned by homology to other DEG/ENaC channels. RT-PCR analysis for rat BLINaC revealed a predominant tissue distribution in brain, liver and small intestine hence the name BLINaC. For mouse, additional expression of BLINaC has been shown in kidney and lung (Sakai *et al*., 1999). In contrast, the human ortholog, hINaC, is predominantly expressed in the intestine (human intestine Na^+ channel) (Schaefer *et al*., 2000). Only very little is known about the physiological role of these channels but the tissue distribution with the emphasis on expression in non-neural tissues like kidney suggests a participation in epithelial transport similar to ENaC.

Recently, a functional study shed light on rat and mouse BLINaC and showed very different behaviours of both channels when expressed in *Xenopus* oocytes despite the high amino acid sequence homology of 97% (Wiemuth and Gründer, 2010). Rat BLINaC exhibits small and unselective currents that are only weakly sensitive to

amiloride. Removal of extracellular Ca^{2+} leads to robust currents with much higher Na^{+}-selectivity. On the other hand, the mouse ortholog shows a 250-fold lower sensitivity for Ca^{2+}, thus leading to constitutively open channels under physiological conditions. Additionally, mBLINaC displays a much higher Na^{+}-selectivity and amiloride-sensitivity (Wiemuth and Gründer, 2010). The different affinities for Ca^{2+} and amiloride are determined by the difference at one single amino acid (A387S) between rat and mouse (Wiemuth and Gründer, 2010).

1.1.3.3 FaNaCs (FMRF-amide gated sodium channels)

Another subfamily of the DEG/ENaC family of ion channels are the FaNaCs, which are exclusively expressed in snails. The first FaNaC was cloned from the snail *Helix aspersa* in 1995 (Lingueglia *et al*., 1995) and during the last years three orthologs have been identified from *Helisoma trivolvis* (Jeziorski *et al*., 2000), *Lymnaea stagnalis* (Perry *et al*., 2001) and *Aplysia kurodai* (Furukawa *et al*., 2006). In general, FaNaC was the first ionotropic receptor that could be directly activated by the neuropeptide FMRFamide, a common peptide in the nervous system of snails (Cottrell *et al*., 1990; Lingueglia, 1995). The expression of FaNaCs is restricted to neurons (Davey, 2001). Although their function and physiological role remains unknown there are speculations about a participation in fast synaptic transmission (Lingueglia, 2006).

1.1.3.4 HyNaCs (Hydra Sodium Channels)

So far, four genes have been cloned and characterized from the HyNaC subfamily. An additional gene, *hynac1*, is probably a pseudogene (Golubovic *et al*., 2007; Dürrnagel *et al*., 2010). As mentioned above, *Hydra magnipapillata* belongs to the phylum *Cnidaria* and displays a radial symmetry and a primitive nervous system that extensively uses neuropeptides for neuronal transmission (Grimmelikhujizen *et al*., 1982). This suggests that peptide-gating is an ancient feature of DEG/ENaC channels which was preserved during evolution in members of the Protostomia, such as snails, but was probably lost in Deuterostomia, such as mammals (Golubovic *et al*., 2007; Dürrnagel *et al*., 2010). Whole-mount *in situ* hybridization revealed a location of the

three functional subunits around the base of the tentacles (Golubovic *et al*., 2007) and thus shows a co-localization with the *Hydra* neuropeptides Hydra-RFamides I and II (Hansen *et al*., 2000), which had previously been isolated and identified from the *Hydra* nervous system (Moosler *et al*., 1996). Functional HyNaCs that can be activated by Hydra-FRamides are composed of the HyNaC-subunits 2 and 3 or 2, 3 and 5. Both functional assemblies exhibit markedly different characteristics regarding surface expression and sensitivity for the activating peptides and to the blocking agent amiloride (Golubovic *et al*., 2007; Dürrnagel *et al*., 2010). In this regard, the trimeric assembly of the HyNaC subunits 2, 3 and 5 displays a higher surface expression, higher selectivity for Na^+ and a higher sensitivity for amiloride (Dürrnagel *et al*., 2010).

By investigating the feeding reaction of Hydra in the absence and presence of amiloride it has been observed that the channels are not required for the general movement of the tentacles but that they might be involved in the coordinated tentacle movement associated with the feeding reflex (Golubovic *et al*., 2007; Dürrnagel *et al*., 2010).

Besides the characterization of the gating behaviour and regulation of the HyNaCs themselves, these channels provide interesting insights into the development of the DEG/NaC channel family and shed light on the question how distinct features of this channel family have been changed or are conserved during evolution.

1.1.3.5 DEGs (Degenerins)

The mechanosensory degenerins are exclusively expressed in *C. elegans* and are used to convert mechanical forces into cellular responses (Driscoll and Chalfie, 1991; Huang and Chalfie, 1994; Liu *et al*., 1996; Tavernarakis *et al*., 1997). They have been shown to play crucial roles in different physiological functions, such as touch sensation and proprioception, while also being involved in the development, survival, proper function and regulation of touch receptor neurons (Chalfie and Au, 1989). A genetic analysis identified 16 so-called *mec* genes that disrupt body touch sensation when mutated. Not all of them belong to the family of DEG/ENaC ion channels but mutations of genes that cause cell degeneration, such as MEC-4 and MEC-10, are members of this family. Cells that express other mutant proteins like UNC-8, UNC-105 or DEG-1 show similar phenotypes, meaning swelling and subsequent death of

these cells hence resulting in the name degenerins (DEGs) for this subfamily (Chalfie and Wolinsky, 1997; Tavernarakis and Driscoll, 1997). Although the mechanosensitivity remains to be shown in heterologous expression systems constitutively active channels were obtained after co-expression of MEC-4 and MEC-10 together with MEC-2. With regard to these findings it is postulated that MEC-4 and MEC-10 are core elements of a touch-transducing complex and the co-expression of multiple subunits plus associated cytosolic or extracellular proteins are required for proper function and expression (Gu *et al*., 1996; Tavernarakis and Driscoll, 1997; Goodman *et al*., 2002). MEC-4 and MEC-10 expression is restricted to mechanosensitive neurons (Huang and Chalfie, 1994), whereas two other genes of the degenerin subfamily, UNC-8 and DEG-1 are expressed in motoneurons (Tavernarakis *et al*., 1997). It is believed that in this class of neurons, UNC-8 and DEG-1 form a similar core of a stretch-sensitive complex as MEC-4 and MEC-10 in mechanosensitive neurons, thus mediating *C. elegans* locomotion (Tavernarakis and Driscoll, 2000).

1.1.3.6 Pickpocket/Ripped Pocket (PPK/RPK) genes of *Drosophila melanogaster*

The PPK/RPK subfamily of DEG/ENaC channels comprises a rather diverse group of ion channels. Since the first two members (RPK and PPK) were identified in the genome of *Drosophila melanogaster* (Adams *et al*., 1998; Darboux *et al*., 1998) about 25 candidates have been identified so far (Littleton and Ganetzky, 2000).

Until today, 16 members have been cloned (Darboux *et al*., 1998; Liu *et al*., 2003) and RPK is the only member that generates currents when heterologously expressed in *Xenopus* oocytes. These currents exhibit a high Na^+-selectivity and a low affinity to amiloride (Adams *et al*., 1998). Although little is known about the gating characteristics and pore features of these channels, transgenic *Drosophila* models, *in-situ*-hybridization- and RNAi-approaches, as well as behavioural assays shed light into the expression patterns and associated functions of these channels. RPK, for example, was shown to be maternally derived and to play a role in early development (Adams *et al*., 1998; Darboux *et al*., 1998). The PPK gene product, on the other hand, appears at later developmental stages of *Drosophila*. It is expressed in sensory dendrites of peripheral neurons in late-stage embryos and early larvae. This finding led to speculations about an involvement of PPK in the function rather than in the

differentiation of these neurons (Darboux *et al*., 1998). Additionally, nine PPK genes show distinct temporal and spatial expression patterns in the tracheal system of *Drosophila* as development progresses and especially PPK4 and PPK11 point to an involvement in liquid clearance when the airways develop, a function similar to ENaCs in mammals (Liu *et al*., 2003a). Furthermore, it has also been shown that PPK11 together with PPK19 is expressed in neurons of the taste bristles of labelum, legs and wing margins, where they play a key role in detecting Na^+ and K^+ salts (Liu *et al*., 2003b).

Finally, a recent study identified PPK28 as the molecular correlate for water taste in *Drosophila* and raised the possibility that DEG/ENaC ion channels may also participate in osmosensation of flies as well as in other animals, including humans (Cameron *et al*., 2010).

1.1.3.7 Fluoride Resistant Mutation proteins (FLRs)

Eight members of this subfamily have been defined so far. All genes were identified by a conserved extracellular region (Take-Uchi *et al*., 1998). FLR-1, which is expressed in intestine of *C. elegans* and is thought to control defecation rhythm (Take-Uchi *et al*., 1998), is the only gene that was cloned but has yet not been expressed heterologously (Take-Uchi *et al*., 1994). The subfamily got their name from *C. elegans*-FLR-1 mutants that display resistance to fluoride ions (Katsura *et al*., 1998).

1.1.3.8. Acid Sensing Ion Channels

Since this work particularly deals with ASICs, this subfamily of the DEG/ENaC superfamily is discussed in detail in the next chapter.

1.2 Acid Sensing Ion Channels (ASICs)

The acid sensing ion channels (ASICs) are a small subfamily of the DEG/ENaC family. The first member of this subfamily, ASIC1a from rat brain, was cloned in 1997 by sequence homology of around 25% to ENaC (Waldmann *et al*., 1997). ASICs are restricted to chordates and the evolutionary oldest ASIC gene is found in the genome

of the urochordate *Ciona intestinalis* (Coric *et al*., 2008). To date, ASIC genes were cloned from very diverse species like the jawless vertebrate lamprey (Coric *et al*., 2008), from the cartilaginous fish spiny dogfish (Coric *et al*., 2008), from the bony fish toadfish and zebrafish (Coric *et al*., 2003; Paukert *et al*., 2004), from chicken (Coric *et al*., 2005) and from different mammals. Six different members of the ASIC subfamily have been identified in mammals (ASIC1a, ASIC1b, ASIC2a, ASIC2b, ASIC3 and ASIC4). ASIC1a and ASIC1b as well as ASIC2a and ASIC2b are splice forms of the same gene (Chen *et al*., 1998; Bässler *et al*., 2001). The definition of ASICs is based on their sequence homology and the ASIC subunits ASIC2b and ASIC4 are not sensitive to protons (Lingueglia *et al*., 1997; Akopian *et al*., 2000).
Although belonging to the same subfamily and sharing a lot of similarities, channels that are composed of different subunits display differences with regard to expression patterns, proton-affinity and gating behaviour.

1.2.1 The apparent affinity for H^+

Especially the proton-affinity is a crucial feature of ASICs from a physiological point of view. Figure 1.3 shows a basic scheme of different possible states of ASICs. Protons can bind to closed ASIC channels (C), upon binding ASICs undergo conformational changes causing channel opening (O) and currents that are mainly based on an influx of Na^+-ions. Open channels are of high potential energy and unstable thus reaching a desensitized state (D) after a characteristic and rather short time even in the presence of protons. As shown in the scheme, the channel can also enter the desensitized state without reaching an apparent open conformation. This mechanism is called steady-state desensitization. For both, activation and steady-state desensitization, the apparent proton affinities are different for each ASIC and can be determined and fitted using the Hill-equation.

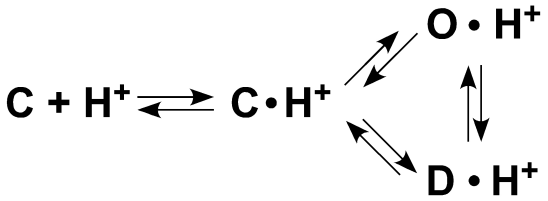

Figure 1.3. Scheme of the different possible states of an ASIC channel
Upon binding of protons, ASICs can open. After a certain time they reach the desensitized state while protons are still bound to the channel. The desensitized state can also be directly reached from the closed state without opening of the channel (steady-state-desensitization).

For example, ASIC1a displays apparent proton affinities for half-maximal activation and steady-state desensitization of pH 6.5 and 7.25, respectively, leading to the assumption that activation and steady-state desensitization are processes completely separate from each other (Gründer and Chen, 2010). Additionally, the values for half-maximal activation and steady-state desensitization suggest that acidification in small steps leads to complete desensitization of all channels without any apparent current.
A contrary hypothesis, however, is that activation and steady-state desensitization are tightly linked. Slight acidification can cause channel opening with low probability within a certain time. And such an un-concerted opening of only a few channels at one time will not lead to visible currents at whole cell level thus remaining unnoticed (Gründer and Chen, 2010). Moreover, mutagenesis studies of ASIC1a report changes in the apparent H^+-affinity for activation that also affect affinities of steady-state desensitization (Babini *et al*., 2002). Another publication reports a mutation in ASIC3, which causes a shift in the curve for steady-state desensitization without affecting the activation curve (Cushman *et al*., 2007) and thus suggesting that the reported mutation uncouples the mechanisms of activation and steady-state desensitization.
Irrespective of the two suggested possibilities, it was shown in several publications that ASICs are sensitive sensors for protons and are also implicated in several physiological and pathophysiological states.

1.2.2 Biophysical characteristics and physiological functions

1.2.2.1 ASIC1a/ASIC1b

Alternative splicing of the ASIC1 gene leads to ASIC1a- and ASIC1b-subunits, which differ in the first transmembrane domain and the proximal part of the large ectodomain (Chen *et al*., 1998; Bässler *et al*., 2001). The last two thirds of both channels are identical. Both subunits display several differences when forming homomeric channels.
ASIC1a, as the best investigated ASIC, is expressed in sensory neurons and throughout the brain, with the highest expression levels in cerebellum, hippocampus and other distinct areas (Waldmann *et al*., 1997), whereas ASIC1b is specifically found in sensory neurons (Chen *et al*., 1998). Both channels exhibit fast transient currents that completely desensitize in the continued presence of extracellular

protons. When strongly activated with an acidic solution of pH 5.0, ASIC1b shows a desensitization time constant of around 500 ms whereas ASIC1a desensitizes slower with a time constant of around 1.5 s (Chen *et al*., 2006). Homomeric ASIC1a and ASIC1b channels are selective for Na^+ over K^+ and ASIC1a is the only ASIC channel that also displays a slight permeability for Ca^{2+}-ions (Waldmann *et al*., 1997; Bässler *et al*., 2001).

A unique feature of ASIC1a and ASIC1b is the sensitivity to Psalmotoxin1 (PcTx1), a polypeptide toxin of the South American tarantula *Psalmopoeus cambridgei*. Interestingly, both ASIC1 channels show different behaviours upon modification by PcTx1. ASIC1a is inhibited by PcTx1 with an EC_{50} of around 1 nM (Escoubas *et al*., 2000). The toxin increases its apparent H^+ affinity, pushing the channel into a desensitized state at a resting pH of 7.4 (Chen *et al*., 2005). Contrary, steady-state desensitization of ASIC1b is just weakly affected by PcTx1 while activation is strongly promoted (Chen *et al*., 2006a). These observations lead to the conclusion that the affinity of PcTx-binding strongly depends on the state of both channels (Chen *et al*., 2006). In the desensitized state ASIC1a shows a much higher affinity for PcTx than in the open state. On the other hand, ASIC1b affinity for PcTx1 is maximal in the open state thus explaining the promotion and stabilization of the open state and the slowing of the time course for desensitization of ASIC1b (Chen *et al*., 2006a).

Another possibility to shift the proton affinity of ASICs is the alteration of the extracellular Ca^{2+} concentration. In general, rising extracellular concentrations of Ca^{2+} stabilize the closed state (Waldmann *et al*., 1997; de Weille and Bassilana, 2001; Zhang and Canessa, 2002) and shift the curves for H^+-dependent activation and steady-state desensitization of ASICs while at the same time exhibiting an open channel block (Babini *et al*., 2002; Immke and McCleskey, 2003). This sensitivity to Ca^{2+} is shared with other ion channels like P2X receptors (Cook *et al*., 1998), nicotinic actylcholine receptors (Mulle *et al*., 1992) and the metabotropic glutamate receptors (Kubo *et al*., 1998). A possible mechanism is illustrated by a model where H^+ and Ca^{2+} compete at a common binding site and a relief of Ca^{2+}, which keeps the channel in the closed conformation, is achieved when H^+ is applied extracellularly to the channel (Immke and McCleskey, 2003; Paukert *et al*., 2004a). Although most observations confirm this model, there are also results, which point to a more complicated mechanism with at least two Ca^{2+}-binding sites and an additional modulating-site within the extracellular loop domain of ASICs (Paukert *et al*., 2004a).

Knock-out studies and behavioural assays increased our knowledge of the physiological function of ASIC1a.

First of all, ASIC1a was shown to be particularly expressed at postsynaptic membranes of synapses in the hippocampus (Zha *et al*., 2006). In a scenario where synaptic vesicles, which also contain protons as co-transmitters, release their content into the synaptic cleft leads to a possible activation of ASIC1a at the postsynapse and thus ASIC1a can contribute to the excitatory postsynaptic current. The knock-out of ASIC1a would lead to a reduced postsynaptic reaction that can cause several pathophysiological states. Indeed, knock-out mice revealed an involvement of ASIC1 in long-term-potentiation (Wemmie *et al*., 2002), in fear conditioning (Wemmie *et al*., 2003; Coryell *et al*., 2007), spatial learning and memory (Wemmie *et al*., 2002) and also a participation in seizure termination (Zieman *et al*., 2008) and pain-sensitivity (Mogil *et al*., 2005).

1.2.2.2 ASIC2a/ASIC2b

The ASIC2 gene also gives rise to two splice forms, ASIC2a and ASIC2b, where only ASIC2a forms a functional homomeric channel when heterologously expressed. ASIC2b, on the other hand, cannot form functional homomeric channels but was shown to tune ASIC currents when forming heteromeric channels together with other ASIC subunits (Lingueglia *et al*., 1997; Askwith *et al*., 2004; Hesselager *et al*., 2004). It was already shown, for example, that hippocampal and cortical neurons exhibit acid evoked currents that arise from ASIC1a/ASIC2-heteromers (Baron *et al*., 2002; Askwith *et al*., 2004; Gao *et al*., 2004). Compared to ASIC1a, homomeric ASIC2a displays a much lower sensitivity to protons (Lingueglia *et al*., 1997; Benson *et al*., 2002) and the desensitization kinetics of ASIC2a for upon half-maximal activation is significantly slower (Baron *et al*., 2008). The expression patterns of ASIC2a and ASIC2b in the brain are similar to ASIC1a (Kellenberger and Schild, 2002) but ASIC2a is additionally found in taste buds of the circumvallate papillae where it may contribute to sour taste perception (Ugawa *et al*., 1998). Furthermore, ASIC2a plays a role in facilitating ASIC1a localization to dendritic spines, where they form heteromeric channels (Zha *et al*., 2009). This suggests ASIC2a as a partner for ASIC1a that brings ASIC1a to or retains it from excitatory synapses (Zha *et al*., 2009). Hence it can be proposed that ASIC2a indirectly modulates the proper function of

ASIC1a. Finally, two independent ASIC2-knock-out mice lines suggested involvements of ASIC2 in mechanosensation (Prize *et al*., 2000; Roza *et al*., 2004).

1.2.2.3 ASIC3

In contrast to other ASIC subunits, ASIC3 is exclusively expressed in sensory neurons of the peripheral nervous system (Waldmann *et al*., 1997), where it is localized at nerve terminals and possibly transduces various sensory stimuli (Price *et al*., 2001). Specifically, ASIC3 has been proposed to play a role as H^+ sensor in cardiac afferents (Sutherland *et al*., 2001) and has been implicated in the development of mechanical hyperalgesia (Sluka *et al*., 2003) and high intensity pain sensations (Chen *et al*., 2003). Detailed analysis revealed co-localization and heteromeric assemblies of ASIC3 with other subunits *in vivo* and *in vitro* (Chen *et al*., 2006; Hattori *et al*., 2009). Homomeric ASIC3, together with homomeric ASIC1a, exhibits the highest H^+-sensitivity of mammalian ASICs (Waldmann *et al*., 1997; Sutherland *et al*., 2001). The time constant of desensitization of ASIC3 is in the range of 300 to 400 ms (Sutherland *et al*., 2001). ASIC3 has the unique capacity to encode sustained currents when activated with solutions of pH 5 and lower. Additionally, a striking feature of ASIC3 is the capacity to encode slight acidification in a narrow physiological range between pH 7.3 and 6.7 by the generation of a sustained current (Fig. 1.4 *A*) (Yagi *et al*., 2006). The overlap of dose-response curves for steady-state desensitization and activation accounts for the ability of ASIC3 to encode such small changes in H^+ concentration (Fig. 1.4 *B*) (Yagi *et al*., 2006). Thus, the sustained current between pH 7.3 and 6.7 is a so-called window current, which can be described by a condition where a small fraction of channels is always in the open state (Fig. 1.4 *C*). This feature underlines the role of ASIC3 as a sensor for nociceptive stimuli that are caused by mild acidification like muscle ischemia, and that last longer than a few seconds (Prize *et al*., 2001; Yagi *et al*., 2006). The window current was the first explanation for a possible mechanism of generating a sustained current in the physiological range and underlined the importance of ASIC3 for encoding long lasting changes in extracellular pH.

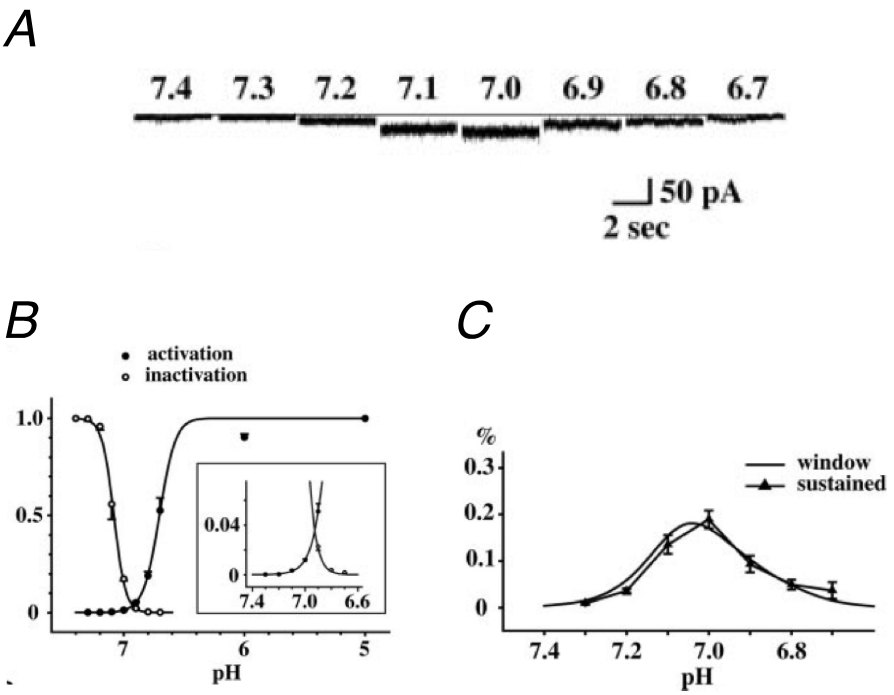

Figure 1.4. Sustained currents of ASIC3.
(A) Representative acid-evoked sustained currents of CHO cells transfected with ASIC3. (B) Hill plots of the activation and inactivation of peak, transient ASIC3 currents, normalized to pH 7.4 (inactivation) and pH 5.0 (activation). The blow-up shows the tight overlap of inactivation and activation curves. (C) The current vs. pH relationship of measured sustained currents (triangles) from (A) and predicted window currents (smooth curve) calculated by multiplying values at each pH of activation and inactivation fits in (B). (Adapted from Yagi *et al*., 2006)

1.2.2.4 ASIC4

Besides ASIC2b, ASIC4 is the second ASIC-subunit that is not activated by protons when expressed as a homomer. In addition, no functional heteromeric assembly with other subunits was examined so far and the function of this subunit remains unkown (Akopian *et al*., 2000; Gründer *et al*., 2000). However, ASIC4 is broadly expressed in the mammalian nervous system, especially in pituitary gland (Gründer *et al*., 2000). Some observations suggest that ASIC4 assembles with ASIC1a and downregulates the expression of ASIC1a (Donier *et al*., 2008). A yeast two-hybrid assay revealed a unique interaction of ASIC4 with polyubiquitin and other proteins of various functions that might be a first step to uncover the possible role of ASIC4 (Donier *et al*., 2008).

1.2.3 Crystal-structure of chicken ASIC1

In 2007 ASIC1 from chicken was crystallized at a resolution of 1.9 Å (Jasti *et al*., 2007). The first crystal, however, was resolved from a non-functional deletion mutant that lacked most of its C- and N-termini. A functional chicken ASIC1 was crystallized two years later at a resolution of 3.0 Å (Gonzales *et al*., 2009). Most of the C-terminus of this functional chicken ASIC1 was also deleted, but not the N-terminus that is essential for the gating of the channel (Gonzales *et al*., 2009). The most striking difference between both channels was the symmetric order of the transmembrane domains of the functional channel (Gonzales *et al*., 2009).

Because both structures were resolved at acidic pH values, the crystal represents the desensitized conformation of the channel. Surprisingly, the chicken ASIC1 crystallized in units of two trimers (Jasti *et al*., 2007). Since rat ASIC1 and human ASIC1 show an amino acid identity of about 70% to chicken ASIC1 it is likely that the structures and even structural details are highly conserved between chicken ASIC1 and ASIC1 of mammals.

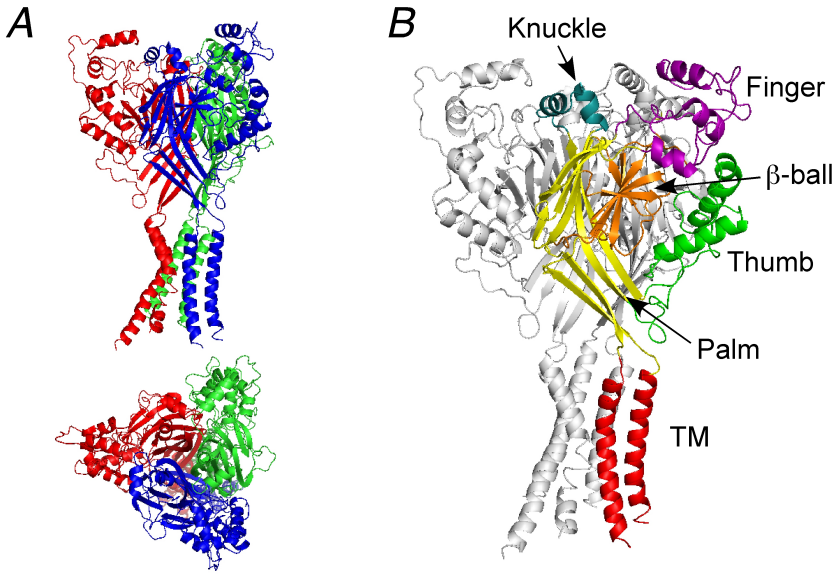

Figure 1.5. Crystal structure of chicken ASIC1.
(A) Functional channels are built by three channel subunits. Each subunit consists of two transmembrane domains (TM) with rather short cytosolic C- and N-termini and a large extracellular loop that is connected to TM via a flexible wrist. (B) The extracellular domain of a single subunit has the shape of a clenched hand and is divided into five subdomains named knuckle, finger, thumb, palm, β-ball and two transmembrane domains.

The shape of the large extracellular domain of each subunit resembles a clenched hand (Fig. 1.5) that can be divided into five subdomains that are named palm, finger, knuckle, thumb and β-ball (Jasti *et al*., 2007). The central subdomain of the extracellular loop is the palm domain, because it spans almost the entire height of the extracellular loop and it connects the extracellular domain with both, transmembrane domain 1 and 2 via the so-called β1- and β12-strand, respectively (Jasti *et al*., 2007). Identified subunit contacts, built mainly by hydrogen bonds and disulfide bridges, are between different domains of the palm of the same subunit and the palm domain of one subunit to the thumb domain of another. Five disulfide bridges within one thumb domain are thought to provide structural integrity and a faithful transduction of conformational changes to the ion pore forming transmembrane domain (Jasti *et al*., 2007).

The so-called acidic pocket containing several acidic residues, which form three pairs of carboxylic acid-carboxylate groups, was another noticeable feature of the chicken ASIC1 structure. This acidic pocket is formed by several intra- and inter-subunit contacts and has a rather far distance of 45 Å from the ion pore (Jasti *et al*., 2007). The acidic pocket provides an attractive site for H^+-sensing in ASICs. While the negatively charged side chains coordinates a Ca^{2+} ion in the closed state, upon protonation of one of the two carboxylates from each pair both side chains would come close to each other in the desensitized state by forming an acidic residue pair (Paukert *et al*., 2008).

The transmembrane domains form α-helices that cross the membrane in a symmetric fashion while, in line with previous studies (Waldmann *et al*., 1995; Kellenberger *et al*., 1999; Schild *et al*., 1997), the second transmembrane domain of each subunit lines the ion pore.

Because the crystal of the chicken ASIC1 is a snapshot of the desensitized state of the channel, it would be interesting to resolve the channel also in the closed and the open state, to get a clear picture of conformational changes during the gating motions.

1.2.4 Evolution of proton-sensitivity and important amino acids

The first ASIC genes were identified and cloned from mammals like mouse, rat and human and were named ASIC1 – ASIC4 (Waldmann *et al*., 1998; Akopian *et al*.,

2000; Gründer *et al*., 2000). So far, many ASIC homologs were cloned from very diverse members of the chordate lineage that belong to different evolutionary stages (Fig. 1.6). The most ancient one is the ASIC1 gene from the ascidian *Ciona intestinalis* that gives rise to two spliced forms and exhibits no H^+-sensitive currents when expressed in *Xenopus* oocytes (Coric *et al*., 2008). Other ASIC homologs were cloned from cyclostome lamprey (Coric *et al*., 2005), from the chondrichthyes spiny dogfish shark (*Squalus acanthias*) (Coric *et al*., 2005) and elephant shark (Li *et al*., 2010c), from the teleosts toadfish (Coric *et al*., 2003, 2005) and zebrafish (Paukert *et al*., 2004b), from the frog *Xenopus laevis* (Li *et al*., 2010b), and from chicken (Coric *et al*., 2005). Moreover, genetic analysis and the rising number of sequenced genomes revealed that ASICs are only expressed in the chordate lineage and that ASIC genes are absent from evolutionary older organisms. Comparison of sequences and related currents that are conducted by ASIC channels of the diverse species and a broad mutagenesis screen for rat ASIC1a shed light to the questions: When did H^+-sensitivity arise? What are the crucial domains that are sufficient for H^+-sensitivity? And what are the gating-properties of ancient ASIC channels?

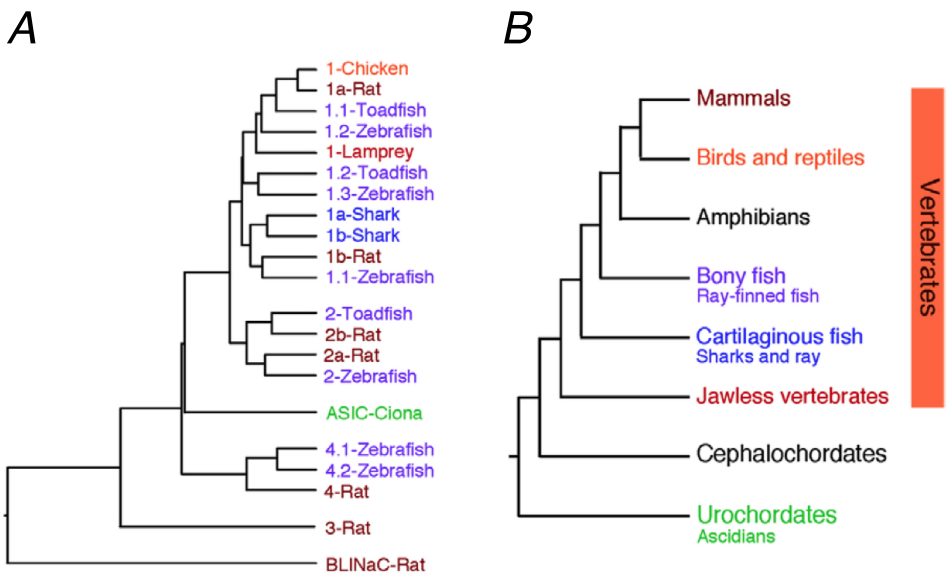

Figure 1.6. Relationship of ASICs from different species.
(A) Phylogenetic tree representing selected ASICs from evolutionary different species and their relationship to each other. (B) Phylogenetic tree of the main chordate clades. The colors of the ASICs in (A) corresponds to the colors of the different clades in (B). (Adapted from Gründer and Chen, 2010)

So far, no H^+ sensitivity could be determined for ASICs from Ciona, lamprey and shark suggesting that proton-sensitivity arose with bony fish approximately 450 million years ago (Coric *et al*., 2005, 2008) and led to different suggestions that evolutionary early ASICs might be activated by ligands different from protons.

1.3 Aims of this study

A recent broad mutagenesis screen uncovered four amino acids (Glu63, His72/His73 and Asp 78) that are involved in proton gating of rat ASIC1a (Paukert *et al*., 2008). All four amino acids are highly conserved among diverse proton sensitive ASIC homologs and orthologs and so far only two exceptions are known: zASIC2 from zebrafish and sASIC1b from shark contain all four crucial amino acids but were described as proton insensitive.

These controversial data were the main reason for the first part of this work:

(1) to re-evaluate the H^+-sensitivity of shark ASIC1b, which is closely related to rat ASIC1a and zebrafish ASIC1.1 and to electrophysiologically characterize the currents of shark ASIC1b that are elicited by extracellular acidification.

The electrophysiological characterization of shark ASIC1b revealed currents that are unique among the members of the ASIC subfamily. Shark ASIC1b exhibits a very fast desensitizing transient current that is followed by a highly proton sensitive sustained current, which does not desensitize as long as extracellular protons are present.

Thus, the second part of this work addressed the question:

(2) What are the crucial amino acids that control the sustained current of shark ASIC1b and are there possible interacting regions that are involved in controlling of the gating kinetics of this channel?

2. Material and Methods

2.1 Material

2.1.1 Chemicals

All used standard chemicals were purchased from Sigma-Aldrich (Diesenhofen), Merck (Darmstadt), Abbott (Wiesbaden) and Roth (Karlsruhe) in analytic quality.

2.1.2 Biological Materials

2.1.2.1 TOP10 E. coli Competent Cells; Invitrogen

Top10 Competent Cells were used for all transformations of double stranded plasmid-DNA performed in this work. They were deduced from the DH10B™strain, have a high transformation efficiency of 10^9 cfu/μg and are characterized by the genotype:

F$^-$ *mcr*A (*mrr-hsd*RMS-*mcr*BC) 80*lac*Z M15 *lac*X74 *rec*A1 *ara* 139 (*ara-leu*)7697 *gal*U *gal*K *rps*L (Str^R) *end*A1 *nup*G.

2.1.2.2 *Xenopus laevis* oocytes

Xenopus laevis oocytes are precursors of mature egg cells (Fig. 3.1). Oocytes of development stages V and VI were used as expression system for all wildtyp -, mutant - and chimeric channels for electrophysiological purposes. The oocytes are around 1 mm in diameter and show a characteristic bipolar look. These two poles are the dark brown animal pole and the yellow vegetal pole. One to four days after injection of RNA whole cell currents of the oocytes were measured with the two-electrode-voltage-clamp-technique.

Figure 2.1. Healthy oocytes of *Xenopus laevis* (left) are composed of a dark brown animal pole and a yellow vegetal pole (right).

2.1.2 Materials for molecular biological purposes

2.1.3.1 Ready-to-use materials

DNA-ladder, 1 kb	Gene Ruler, Fermentas, St. Leon-Rot
DNA-ladder, 100 bp	NEB, Frankfurt
DNA-ladder	Ribo Ruler, Fermentas, St. Leon-Rot
DNA-loading buffer	Ambion, Austin, USA
DEPC-H_2O	Roth, Karlsruhe
Ethidiumbromide	Roth, Karlsruhe
Red-Save	Hiss, Freiburg

2.1.3.2 Oligonucleotides (Primers)

All primers used in this project were ordered from MWG Eurofins, Martinsried, as HPLC purified, unmodified DNA oligos. Working concentrations were 10ng/µl.

2.1.3.3 Oocyte expression vector

All used constructs were cloned in the oocyte expression vector pRSSP-6009. Containing the 5'-untranslated region from Xenopus β-globin and a poly-A-tail at the

3' region of the constructs this vector was optimized for expression in *Xenopus* oocytes.

2.1.3.4 Commercially available Kit systems

The following Kit systems were used according to manufacturer's instructions

High Pure PCR Product Purification Kit	Roche, Mannheim
High Pure Plasmid Isolation Kit	Roche, Mannheim
mMessage Machine Kit, SP6	Ambion, Austin, USA

2.1.3.5 Enzymes

Taq-DNA-polymerase	New England Biolabs, Frankfurt
Kappa Hifi-DNA-polymerase	Clontech, Erlangen
Alkaline phosphatase	New England Biolabs, Frankfurt
T4-Ligase	New England Biolabs, Frankfurt
Ligate-IT™ Rapid Ligation Kit	Wooburn Green, UK

2.1.3.6 Antibodies

anti-HA Klon 3F19 (rat, monoclonal)	Roche, Mannheim
anti-rat-IgG-HRP	Jackson ImmunoResearch
(goat, F(ab')2 fragment (H+L)	Laboratories

2.1.3.7 Solutions and Buffers for molecular biology

Agarplates	15 g Agar-Agar ad 1 l ddH_2O
Agarose-Gels	x g Agarose ad 30 ml bzw. 100 ml 1xTAE
Antibiotics	Ampicilin: 50 mg/ml

dNTPs für PCR	concentration: 10 mM ⇒1:10-dilution of the 100 mM-stock solution dATP, dCTP,dGTP, dTTP
LB-medium	LB Broth Base 20 g/1000 ml pH 7-7.4
MOPS (5x)	0.1 M MOPS (pH 7,0) 40 mM NaAc 5 mM EDTA (pH 8) ad 1 l DEPC-H_2O
TFB I	300 mM NaAc 50 mM $MnCl_2$ 100 mM NaCl 10mM CaCl 15% Glycerin (99%)
TFB II	10 mM MOPS 110 mM NaCl 75 mM $CaCl_2$ 15% Glycerin
TAE (50x)	242 g Tris Base 57.1 ml pure acetic acid 100% 100 ml 0,5 M EDTA (pH 8) ad 1 l ddH_2O

2.1.4 Electrophysiological materials and setups

2.1.4.1 Capillaries and electrodes

Glas capillaries for RNA-Injektion: 1.14 mm OD, 0.5 mm ID, World Precision Instruments

Borosilicate capillaries for TEVC-measurements: 0.7 mm-1.0 mm, Science Products GmbH

Silverwire for current and voltage electrodes: AG-15T, Science Products, Hofheim.

2.1.4.2 Setup for measuring oocytes with the two-electrode-voltage-clamp-technique (TEVC)

Cellworks software 5.1.1 was used for electrophysiological characterization and measurement of the mutant and chimeric channels. Cellworks was connected to the oocyte testing carousel, OTC-20 (npi, electronic instruments) via an interface. The automated, pump-driven solution exchange together with the small chamber for the oocyte allows exchange of 80 % of the solution within 300 ms (Chen et al. 2006b). The oocyte chamber is located in the center of the grounded acryl glass frame (Fig. 2.2; 6). The intracellular current and voltage electrodes were connected to the acryl glass frame (Fig. 2.2; 2, 7). The solutions were applied to the
oocytes while the testing carousel is turning the solution underneath the induction pipe. Opening of the valve as well as rotation of the dishes are also controlled by the Cellworks 5.1.1 software.

Further components of the setup are the TurboTec03X amplifier (npi electronic imstruments), an oscilloscope HM507 (Hameg instruments) (Fig. 2.3) and a computer (Macintosh G4). Data acquisation was also managed by Cellworks 5.1.1 software (npi electronic imstruments).

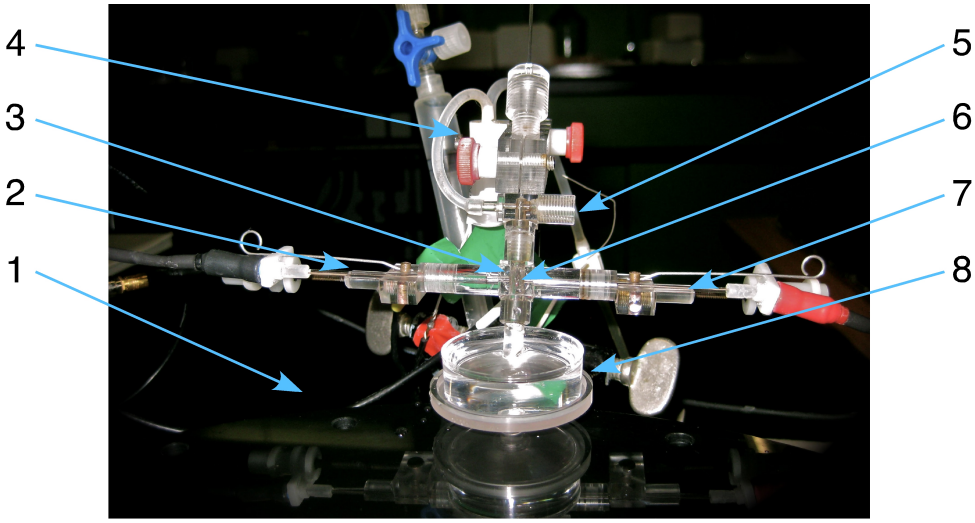

Figure 2.2. Experimental chamber of the carousel solution exchange system. 1: Solution containing dish carousel for the transport of solutions; 2: Voltage electrode; 3: Reference electrode; 4: Automated valve for the solution exchange; 5: Ground electrode 6: "Maltese cross" bath chamber containing the oocyte; 7: Current electrode; 8: Petri dish containing the soltions that is applied to the oocyte

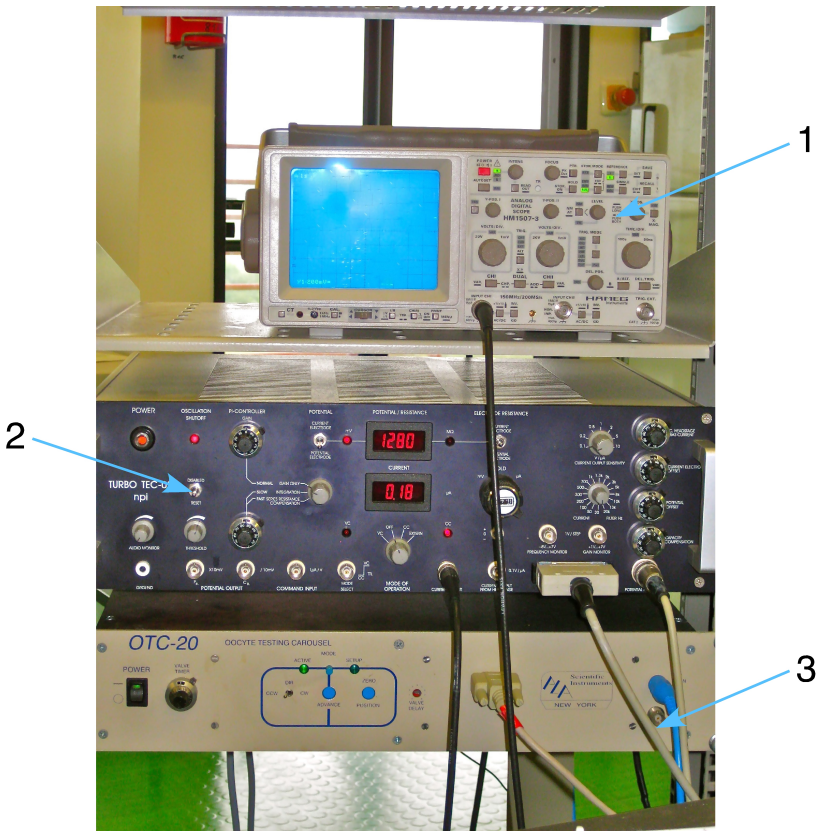

Figure 2.3. Components of the TECV-setup:1. oscilloscope (HM 507, Hameg); 2.TEVC-amplifier (Turbo Tec-03X, npi); 3. Interface to control (OTC-20, Oocyte Testing Carousel, npi)

2.1.4.3 Solutions for electrophysiology and bioluminescence assay

OR-2; pH = 7.3

NaCl	82.5 mM
KCl	2.5 mM
Na_2HPO_4	1 mM
HEPES	5 mM
PVP	0.5 g/l
$MgCl_2$	1 mM
$CaCl_2$	1 mM
H_20	ad 1 l

ND-96-Solution; pH = 7,4

NaCl	96 mM
KCl	2 mM
$CaCl_2$	1.8 mM
$MgCl_2$	2 mM
HEPES	5 mM

Standard bath – solution; pH 7.8 – pH 6.8

NaCl	140 mM
HEPES	10 mM
$CaCl_2$ (1M)	1.8 mM
$MgCl_2$ (1M)	1.0 mM

Standard bath – solution; pH 6,7 – pH 4,0

NaCl	140 mM
MES	10 mM
$CaCl_2$ (1M)	1.8 mM
$MgCl_2$ (1M)	1.0 mM

2.1.4.4 Disulfide-bridge building chemicals and channel blockers

Amiloride	Sigma, Diesenhofen
Psalmotoxin	Alamone Labs Ltd, Jerusalem
Aminoethyl Methanethiosulfonate Hydrobromide (MTSEA-Bromide)	Toronto Research Chemicals, Kanada

2.2 Methods

2.2.1 Molecular biological Methods

The methods described below were used to create chimeric ion channels, to insert HA-tags into ORFs of certain ion channels, to create point mutants of ion channels and to synthesize cRNA of all constructs for expression in *Xenopus laevis* oocytes.

2.2.1.1 Agarose gel electrophoresis

Agarose gel electrophoresis is a standard method to analyze DNA and RNA according to its length and its concentration/amount or to isolate different DNA-fragments in the same sample from each other. In this project, agarose gel electrophoresis was carried out in horizontal BioRad chambers (Munich). Agarose concentrations from 0.8 to 1.5 % (w/v) were used in 1xTAE buffer. After boiling the agarose solution, 0.1 ‰ (w/v) red safe was added and the solution was poured into the gel cast chamber. Wells were formed by a plastic comb. After cooling down, the gel was placed in a running chamber. 1xTAE was used as running buffer. Before loading the wells, DNA loading buffer was added to the samples and a voltage of 100 V was applied for approximately 30 to 40 min to separate the DNA fragments. A DNA ladder running parallel to the samples was used to determine the size of the DNA fragments. To visualize the DNA, safe and print the data, a UV-Transilluminator (BioRad, Munich) was used in combination with a PC and the software Quantity One (BioRad, Munich).

Agarose gel electrophoresis was also used to isolate DNA-fragments of interest. After cutting out of a gel a distinct DNA band, the DNA was purified from the gel using the High Pure PCR Product Purification Kit (Roche, Mannheim). This kit uses a silica gel

matrix that binds DNA in a pH and salt dependent manner. After one or two washing steps the DNA was finally eluted with a special elution buffer and the concentration was determined by measuring the absorption at 260 nm.

2.2.1.2 Polymerase Chain Reaction (PCR)

The polymerase chain reaction technique (PCR), invented in the mid 1980s (Saiki et al. 1985) is an effective method to amplify specific DNA fragments. The method is based on the elongation of two oligonucleotides (primers), which flank a particular DNA sequence, by a thermostable DNA-polymerase enzyme. The sequence between the two primers serves as a template for DNA polymerase.

The PCR can be divided into different phases. The initial step is the denaturation of the template DNA at a temperature of 95°C. Afterwards the annealing of the primers to the DNA template is achieved at temperatures between 45°C and 60°C, depending on the length and the GC-base content of the primers. The third step is performed at 72°C when the thermo-stable DNA polymerase elongates the primers with the result that the specific template DNA sequence was copied. Several repeats of the three steps lead to a high amplification rate of the template DNA sequence. Several parameters contribute to the success of a PCR.

The most important ones are the number and duration of the amplification steps, the salt concentrations, especially of $MgCl_2$, and the annealing temperature.

All standard PCR procedures were performed with the Biometra T3000 Thermocycler with the following volumes:

template-DNA (cDNA, 100 ng)	x µl
Primer 1, sense (10 pmol/µl)	2 µl
Primer 2, antisense (10 pmol/µl)	2 µl
DNA-polymerase reaction buffer (10x)	5 µl
dNTPs (10 mM each)	1 µl
taq-polymerase (2.5 U/ml)	0.5 µl
H_2O, bidest.	x µl
total volume	20 µl

2.2.1.2.1 Colony-PCR

The colony PCR was used to proof the success of plasmid transformations. False-positive colonies could be easily distinguished from the right ones. Several bacterial colonies served as the template. They were harvested with a pipette tip from an antibiotica plate and were pipetted in a reaction tube that contains all ingredients for a PCR-reaction. Before transferring the colony in the reaction tube, it was stamped on a second antibiotica plate to easily assign each reaction tube to a harvested clone.
The hypotonic reaction mix cracked the bacteria membrane and set free the DNA and all containing plasmids. Appropriate primer pairs were used to control if the plasmids in the harvested clones carried the inserts of interest.

2.2.1.2.2 Recombinant PCR

The method of the recombinant PCR was used to insert mutations of more than 6 bases, to clone chimeric channels and to insert the HA-epitope into the open reading frame of the sharkASIC1b and the related M27-sharkASIC1b construct.
Two distinct reactions were performed in the first step. Each reaction is executed with a gene-specific primer and a second recombinant primer (Fig. 2.4, A). This second recombinant primer carries a gene-specific sequence at the 3' end and the sequence of the HA-tag, the desired mutation or the sequence of a second gene that is inserted in the gene of interest at the 5'-end. The gene-specific 3' end anneals with the template DNA while the 5' end overlaps in the first reaction. This overlapping sequence should be at least 12 bases in length.
The 5' ends of the two primers overlapped so that each of the two reactions contain complementary sequences and they can hybridize in a third PCR reaction (Fig. 2.4, C).
In this third reaction the amplification starts when the two products of the first two reactions overlap and hybridize. The resulting products contain the desired mutations, the HA-epitope or the chimeric border (Fig. 2.4, D). In the next amplification steps, the reaction starts again with the elongation of the outer primers.
The annealing temperature was determined according to the content of GC-bases and the length of overlapping sequences.

A gel electrophoresis was performed to proof the success of each individual reaction and to isolate the DNA products of interest from buffers and enzymes used in the PCR reactions in order to prepare them for further downstream reactions.

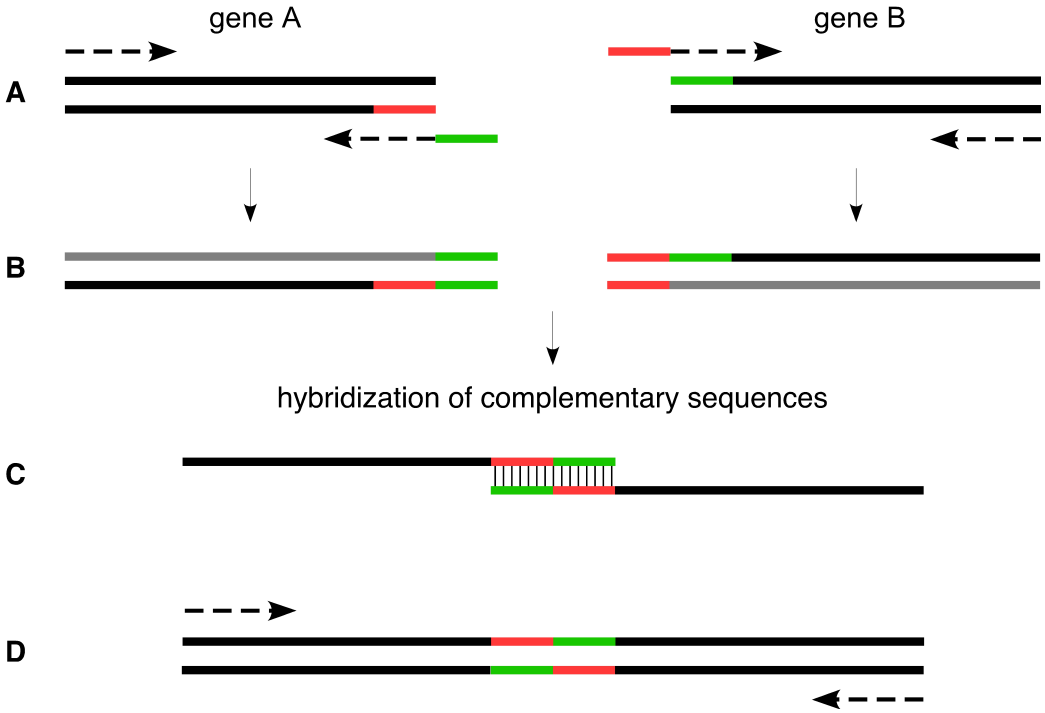

Figure. 2.5: The recombinant PCR is an effective method for creating recombinant DNA fragments. The method requires recombinant primers that contain sequence fragments of two dfferent genes and that are also complementary to each other (indicated red and green).

2.2.1.2.3 Targeted point mutagenesis with the Quick-Change-Method

The Quick-Change-Method is a time saving method to insert point mutations into plasmid-DNA. Complementary primers with a length of 24 bases are used that carry the desired mutation in the middle of its sequences (Fig. 2.6). After primer annealing, the polymerase amplifies the whole plasmid in each amplification step. Because of the long sequence that is amplified during each step it is important to use a polymerase with a 3'-5'-exonuclease-activity („proof-reading") to avoid unwanted mutations that are caused by the error rate of the polymerase. In contrast to the

mutated plasmid DNA products the template plasmid DNA is methylated. A restriction digest with the enzyme DpnI follows the PCR reaction because DpnI cuts only methylated DNA-sequences (Fig. 2.6). This restriction digest leaves only the unmethylated mutated plasmid DNA products that are subsequently transformed into competent cells.

The standard PCR approach for the Quick-Change mutagenesis was as follows:

5x Kappa Hifi polymerase reactions buffer	10 µl
template plasmid-DNA (20 ng)	x µl
mutagenesis Primer 1 (10 pmol/µl)	1,5 µl
mutagenesis Primer 2 (10 pmol/µl)	1,5 µl
dNTPs (10 mM each)	1,0 µl
kappa Hifi DNA-polymerase (1 U/µl)	0,5 µl
H_2O, bidest.	y µl
total volume	50 µl

Standard conditions for the Quick-Change mutagenesis:

Denaturation	95°C	30 sec
Annealing	55°C	60 sec
Elongation	72°C	180 sec (30 sec/1kb plasmid length)

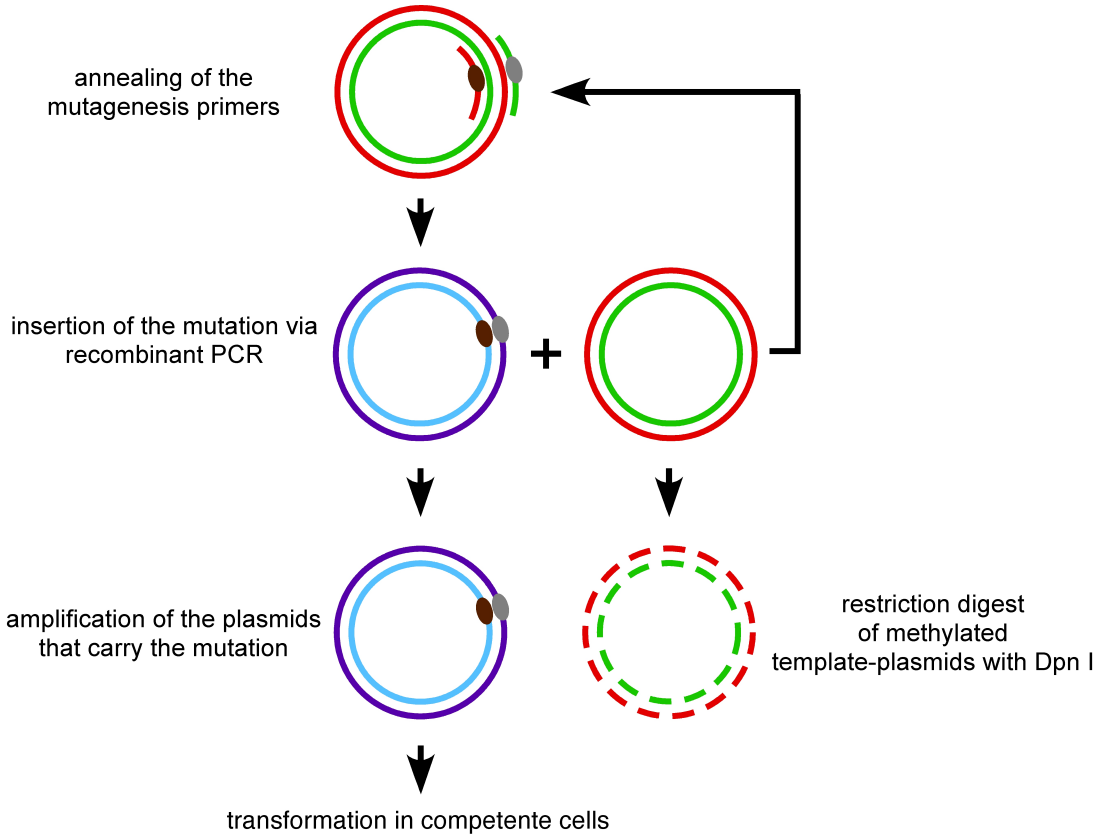

Figure 2.6. Mutagenesis with the Quick-Change-method is a time saving method for mutating few bases of a gene which is inserted in a plasmid vector.

2.2.1.3 Restriction digest of PCR-products und plasmid vectors

PCR products were cloned into appropriate vector backgrounds with restriction enzymes.

The digestion of PCR products and vectors with adequate restriction enzymes produced 5' or 3' prime overhangs that were complementary to each other. This allows the insertion of a PCR fragment into a plasmid vector. In most cases a site-directed insertion was necessary. For this purpose a double digest with two different restriction enzymes was used.

All restriction enzymes used in this project were purchased from NEB (Frankfurt).

2.2.1.4 Ligation of PCR fragments into plasmid vectors

In the ligation reaction the enzyme ligase catalyses the generation of a phosphodiester bond between the 3'-hydroxyl group and the 5' phosphate of double stranded DNA under the consumption of one molecule ATP.

Before the reaction was started, the concentration ratio between PCR fragment and vector had to be determined with an analytical gel electrophoresis.

The ratio was calculated with the following formula:

$$\text{volume (insert)} = \frac{\text{x µl volume (vector)}}{\text{concentration factor (insert) (gel)}} \times \frac{\text{3 x size (insert)}}{\text{size (vector)}}$$

Subsequently the reaction was carried out with the „Ligate IT™ Rapid Ligation Kit" for ten minutes at room temperature.

2.2.1.5 Preparation of heat-competent cells (E.coli, Top10)

A single colony of the bacterial strain E.coli, Top10 was picked from a tetracycline containing agar plate, inoculated as a starter culture in 3 ml LB medium, and incubated over night at 37°C with vigorous shaking at 220 rpm.

The next day the culture was transferred into 50 ml of fresh LB medium without antibiotics and incubated until an OD_{600} of 0.5 to 0.6 was reached. The cells were centrifuged at 5000 rpm (rotor JA20, centrifuge J2-MC, Beckmann, Osterode) and the pellet was resuspended in 12.5 ml ice cold TFBI. After 10 min on ice the suspension was centrifuged again for 5 min at 4°C and 5000 rpm. The pellet was resuspended again in 4 ml TFBII buffer and aliquots of 200 µl were shock frozen in liquid nitrogen and then stored at -80°C.

2.2.1.6 Transformation of heat-competent cells (E.coli, TOP10)

Plasmid vectors were transformed into heat-competent cells in order to amplify them with a high efficiency. To amplify plasmid vectors they were transformed into competent cells, which take up the plasmid DNA through the cell wall and amplify

the plasmid DNA while the cells are growing and dividing.
In this project heat competent E. coli cells of the strain TOP10 were used. The cells were thawed on ice and 20 µl of a ligation reaction was added to the suspension. After 30 min incubation on ice, a 45 sec heat shock at 42°C was followed by another 1 min incubation on ice. 200 µl LB medium was then added and the cells were incubated at 37°C for 1 h with vigorous shaking at 220 rpm.
In the last step the whole volume or just part of it was plated on an ampiciline containing agar plate.

2.2.1.7 Isolation of plasmid DNA – „Miniprep“

A commercially available kit from Roche was used to purify plasmid DNA from competent cells. The plasmid preparation was performed according to the manufacturer's instruction.
The method is based on the principle that the competent cells are lysated and the plasmid DNA is bound to silica membrane. After one or two washing steps the plasmid DNA is eluted from the silica membrane and diluted in an appropriate buffer.
In this thesis 4 ml LB medium containing ampiciline was inoculated with a colony transformed with a specific plasmid. After incubation at 37°C over night at 220 rpm the medium was ready for plasmid isolation.

2.2.1.8 DNA-sequencing

To verify the identity of cloned plasmid-DNA, DNA-sequencing was carried out at MWG-Eurofins, Martinsried.
For each reaction, an aliquot of 1 µl plasmid DNA diluted in 15 µl was sent to MWG. The result of each sequencing was downloaded from the Company's website.

2.1.2.9 cRNA-production via *in-vitro*-Transcription

For electrophysiological measurements of ion channels expressed in *Xenopus* oocytes cRNA synthesized from the plasmid DNA templates by *in-vitro*-transcription. In the first step, the plasmid DNA was cut and opened (linearized) 3' from the clone of interest in order to avoid the transcription of the whole plasmid. The DNA was extracted from the reaction mix using phenol/chloroform and was then precipitated over night at -20°C with ethanol (100%) and 3 M NaAc.

After centrifugation and resuspension of the linearized DNA, the *in-vitro*-transcription was performed using the mMessage Machine kit (Ambion, Austin, USA) according to manufacturer's instructions.

The reaction mix was precipitated over night at -20°C for a second time using LiCl.

After centrifugation, the cRNA was dried and resuspended in DEPC-H_2O and the concentration was determined via an analytical gel electrophoresis and the synthesized cRNA was visually adjusted to a standard cRNA with a concentration of 200 ng/µl.

2.2.2 Electrophysiological Methods

The methods illustrated in the following chapters were performed to electrophysiologically analyze the cloned ion channels and to determine the surface expression of certain channels.

Channels were electrophysiologically characterized using the two-electrode-voltage-clamp technique (TEVC) on oocytes of the South American frog *Xenopus laevis.* This expression system was introduced by Gurdon (Gurdon 1971) and refined by Miledi who could show that injection of cRNA leads to the expression of proteins and especially membrane spanning proteins (Barnard 1982). The oocyte expression system is ideal for measuring channels and receptors located at the membrane because they contain only few endogenous channels. Another advantage is the relatively big size and robustness that provides an uncomplicated handling.

However, channels expressed in oocytes may function differently than in their native invironment because the posttranslational modification may be different.

Nevertheless, *Xenopus* oocytes have become a common expression system to investigate and characterize various ion channels and receptors.

The electrophysiological measurements were complemented by a bioluminescence approach to determine the expression of certain ion channels on the cell surface of oocytes

Only oocytes in developmental stages V to VI were used for all performed experiments as previously described (2.1.2.2).

2.2.2.1 Preparation und handling of *Xenopus laevis* oocytes

Before operation and removal of the oocytes, the frog was anaesthetized with 2.5 g/l Tricaine for around 30 min. The anaesthetized frog was placed on its back and was opened by a small cut along its body axis. A sufficient number of oocytes was removed from the ovary and put in a dish containing OR-2 medium. The cuts in the subcutaneous musculature and in the abdominal skin were stitched separately. The frog was kept in a bucket of a small volume for one to two hours before it was set back in the aquarium. The same frog can be operated 4-6 times and the interval between the operations should be at least 3 months (Goldin 1992).

The follicle cell layer surrounding the oocyte was removed by a two-hour incubation in OR-2 medium containing 1 mg/ml collagenase Type IIA (Sigma-Aldrich, Diesenhofen). Three to four washing steps were applied to remove the collagenase from the oocytes and to prepare the oocytes for cRNA injection.

2.2.2.2 cRNA-microinjection in *Xenopus laevis* oocytes

For injection of cRNA into oocytes, pulled glass capillaries (1.14 mm OD and 0.5 mm ID, World Precision Instruments, Inc.) were used. Capillaries were pulled with an automatic Puller (Flaming/Brown Micropipette Puller Model P-97; Sutter Instrument Co.) and the tips were broken manually to a diameter of about 10-20 µm, which allowed more easy penetration of the oocyte membrane. In order to reduce the air volume and water evaporation from the RNA solution, capillaries were filled with paraffin oil before they were attached to the injector. A hand-driven coarse manipulator (Nanoliter 2000, World Precision Instruments, Inc.) was used to pilot the injection. A total volume of about 40 nl of diluted cRNA was injected for each oocyte.

2.2.2.3 Bioluminescence analysis to determine surface expression of ion channels

The HA-epitope (amino acid sequence: YPYDVPDYA) was inserted in the extracellular loop of sASIC1b between residues R161 and N162 by recombinant PCR in order to determine the surface expression of the ion channels. If the tagged ion channels are expressed at the cell surface the monoclonal anti-HA-antibody is able to bind to the HA-epitope. A second antibody against the anti-HA-antibody was coupled to the enzyme horseradish peroxidase (HRP), which emits a luminescence signal when stimulated. This luminescence could be detected and quantified. The amount of luminescence is proportional to the expression of ion channels at the surface of the oocytes.

After injection of cRNA, the oocytes were incubated for two days at 19°C. After a mild incubation with collagenase (0.3 mg/ml), the follicle membrane of each individual oocyte was removed manually. Oocytes were blocked in ND-96/1% BSA at 4°C for 30 min. Afterwards incubation with the first antibody (anti-HA, clone 3F19, (rat, monoclonal; 0,5 μg/ml) in ND-96/1 % BSA was performed at 4°C for 60 min. Five washing steps were performed in 24-well-plates with ND-96/1 %BSA before the oocytes were incubated with the second antibody (anti-rat-IgG-HRP (goat, $F(ab')_2$ fragment (H+L)) in ND-96/1% BSA-solution for 40 min. After incubation with the second antibody, the oocytes were washed thoroughly in ten washing steps. The first four washing steps were performed in ND-96/1 % BSA-solution, the last six washing steps were performed in ND-96 solution without BSA to avoid background signals. For detection of the luminescence signal the oocytes were placed in 96-well plates and the signal was recorded in an Orion II Microplate Luminometer. Two seconds after 50 µl of the substrate (SuperSignal ELISA Femto Maximum Sensitivity Substrate, Pierce) was added to each individual oocyte, the signal was recorded for five seconds. The luminescence was expressed as relative light units (RLUs). The oocytes expressing sharkASIC1b-wt channels without HA-epitope were used as a negative control.

2.2.2.4 Two-electrode-voltage-clamp technique (TEVC)

The method of the two-electrode-voltage-clamp technique (TEVC) was invented by von Marmont und Cole in 1949. Generally, an electric capacitor is defined as two conductive materials that are separated by an isolator. Cellular membranes

are excellent capacitors. Basic characteristic of a capacitor is its ability to store positive and negative charges simultaneously on its surface. Capacitance of membranes (C_m) is the ability to store charge (Q) when there is a voltage change (ΔV) across the two sides of the membrane:

$$Q = C_m * \Delta V_m$$

The capacitance of all biological membranes (C_m) is about 1 $\mu F/cm^2$. Since C is constant, the current flow through the capacitor is proportional to the voltage change with time:

$$I_c = \Delta Q_m / \Delta t = C_m * \Delta V_m / \Delta t$$

The total current I_m flowing through the membrane is the sum of the resistance or ionic current I_i, and the capacitative current I_c:

$$I_m = I_i + I_c$$

If V_m does not change, Q_m is constant and there is no capacitative current I_c flowing through the membrane. In this case, measured I_m is nearly equal to I_i, flowing exclusively through ion channels in the membrane. Applying above-mentioned principles, Marmont and Cole (1949) invented the voltage- clamp technique to overcome the problem of disturbing capacitative currents. With this method they uncoupled the opening and closing of voltage dependent ion channels from the membrane potential. In voltage clamp measurements, it is possible to control the membrane voltage (clamping the voltage) and measure the transmembrane current that is required to maintain the clamped voltage. As mentioned above, elimination of capacitative currents is a big advantage of this system and that is why the current flow through the membrane is only proportional to the number of open channels and, thus, can be correctly measured.

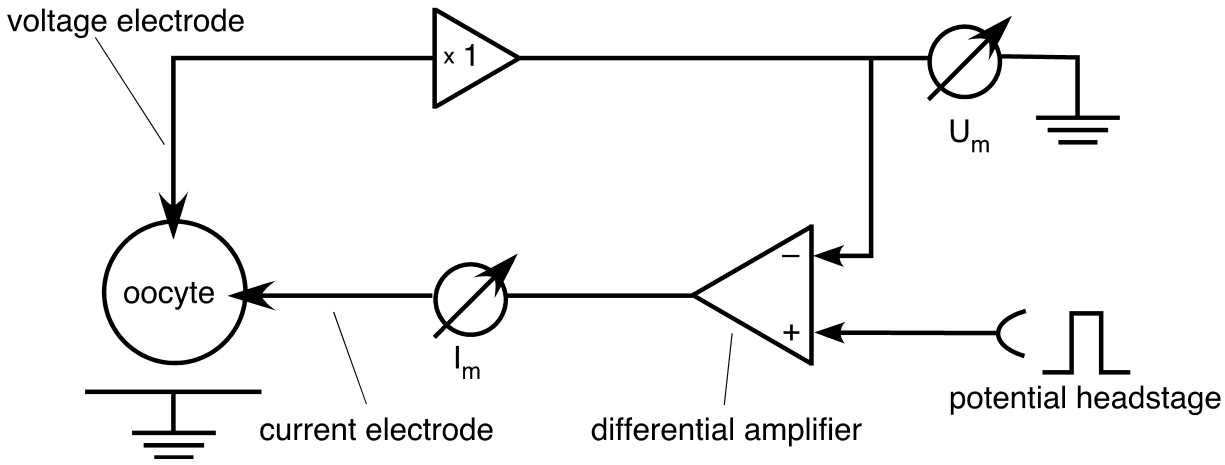

Figure 2.7. Circuit diagram of the TEVC setup.

The voltage clamp is a negative feedback mechanism where the membrane potential is kept stable and the current necessary for keeping that potential is measured. In the two electrode voltage clamp technique, two intracellular electrodes are used, one to pass the feedback current and the other to measure the membrane potential (see Fig. 2.7). Latter (V_m) is recorded by a unity-gain amplifier (A1) connected to the voltage-recording potential electrode (v). A second high-gain differential amplifier (A2) compares V_m to the command potential (V_{hold}) and adjusts the difference between V_m and V_{hold}. The voltage at the output of A2 forces the current to flow through the current-passing microelectrode (i) into the cell.

Thus, there is a negative feed back loop: the membrane potential is clamped at a determined value by the command voltage. So, current is produced via the clamping amplifier output if the membrane potential is different from this command voltage and this current flows through the microelectrode i to compensate the difference. This compensating current is the measured parameter.

An additional potential recording electrode (reference electrode) was placed in the bath solution in our voltage clamp studies to avoid polarization errors that arise from the current passing through the ground electrode. In this configuration, the difference between the intracellular potential electrode and the reference electrode was equated with the transmembrane potential.

Several considerations have to be made when measuring big cells, like *Xenopus* oocytes, with the two-electrode voltage clamp technique. The most important is that oocytes possess a large surface of around 10^6 μm^2 that has to be charged in order to clamp the cell. Additionally, invaginations of the surface are doubling or tripling the amount of surface compared to an ideal spherical oocyte. Another point is that injection of mRNA, depending on the protein, can lead to high expression levels. Currents up to 50 µA or even larger can cause enormous resistance errors. Since the response time (τ) of a voltage clamp to a step voltage change is,

$$\tau = R_i * C_m / A ,$$

where R_i is the resistance of the current electrode, C_m is the membrane capacitance, and A is the gain of the command amplifier, the lowest R_i and the largest A possible are usually used to achieve fast clamping of the oocyte.

2.2.2.5 Recording and analysis of the data

As mentioned in chapter 3.1.4.2, the electrophysiological data was recorded with the Cellworks 5.1.1 software (npi, electronic instruments) with a sampling rate of 1 kHz. Statistical analysis and determination of significances were calculated in Micrsosoft Excel 2008 using Student's *t* test. The software IgorPro 4.02 (Wave Metrics, Lake Oswego, OR) was used for fitting of dose-response-curves and for fitting ASIC currents with an exponential function for analysis of the time constants of desensitization.

Concentration-response-curves were determined by fitting the data to the Hill-function:

$$I = a + (I_{max} - a) / (1 + (EC_{50} / [H]^n) ,$$

where

I_{max} = maximal current amplitude

a = residual current

H = proton concentration

EC_{50} = pH/concentration at which half-maximal activation/block of the transient current component was achieved

n = Hill-coefficient

Current decay kinetics of the fast transient currents were fitted with a mono-exponential function:

$$I = A_0 + Ae^{-1/\tau} ,$$

where

A_0 = relative amplitude of the non-desensitizing current

A = relative amplitude of the desensitizing current

τ = time constant of desensitization

Current decay kinetics of the slow sustained currents were best fit with the sum of two exponential functions:

$$I = A_0 + A_1e^{-1/\tau 1} + A_2e^{-1/\tau 2} ,$$

where

A_0, A_1, A_2 = relative amplitudes of the corresponding various components

$\tau 1$, $\tau 2$ = time constants of the slow and the fast time constants, respectively

To determine the reversal potentials of the slow and the fast current components activated with different pH solutions, the currents were described by a linear function:

$$I = ax + y ,$$

where

a = slope of the linear function

y = relative current amplitude at 0 mV clamped voltage

Graphs and figures were generated using the Canvas 10 software (Deneba Systems) and Photoshop CS3 (Adobe Systems Incorporated, San Jose, USA).

If not otherwise indicated, all measurents were performed at a holding potential of -70 mV and at room temperature (20 – 25°C). For each experiment oocytes from two different frogs were used.

All results are reported as means s.e.m. They represent the mean of n individual experiments of different oocytes.

3. An acid-sensing ion channel from shark (Squalus acanthias) mediates transient and sustained responses to protons

3.1 Abstract

Acid-sensing ion channels (ASICs) are proton-gated Na^+ channels. They are implicated in synaptic transmission, detection of painful acidosis, and possibly sour taste. The typical ASIC current is a transient, completely desensitizing current that can be blocked by the diuretic amiloride. ASICs are present in chordates but are absent in other animals. They have been cloned from urochordates, jawless vertebrates, cartilaginous shark and bony fish, from chicken and different mammals. Strikingly, all ASICs that have so far been characterized from urochordates, jawless vertebrates, and shark are not gated by protons, suggesting that proton-gating evolved relatively late in bony fish and that primitive ASICs had a different and unknown gating mechanism. Recently, amino acids that are crucial for proton-gating of rat ASIC1a have been identified. These residues are completely conserved in shark ASIC1b (sASIC1b), prompting us to re-evaluate proton-sensitivity of sASIC1b. Here we show that, contrary to previous findings, sASIC1b is indeed gated by protons with half-maximal activation at pH 6.0. sASIC1b desensitizes quickly but incompletely, efficiently encoding transient as well as sustained proton signals. Our results show that the conservation of the amino acids crucial for proton-gating can predict proton sensitivity of an ASIC and increase our understanding of the evolution of ASICs.

3.2 Introduction

Acid-sensing ion channels (ASICs) are ligand-gated channels that are gated open by the binding of protons – the simplest ligand possible. In the continued presence of protons, ASICs desensitize. They are involved in synaptic transmission (Wemmie *et al*., 2002) and transduction of painful acidosis (Jones *et al*., 2004; Yagi *et al*., 2006; Deval *et al*., 2008) and have been implicated in cell death accompanying stroke (Xiong *et al*., 2004), in autoimmune inflammation of the central nervous system (Friese *et al*., 2007), and in seizure termination during epilepsy (Ziemann *et al*., 2008). Mammals contain four genes coding for ASICs: ASIC1 – 4 (Waldmann & Lazdunski,

1998; Gründer *et al*., 2000); the use of alternative first exons gives rise to the variants ASIC1b (Chen *et al*., 1998; Bässler *et al*., 2001) and ASIC2b (Lingueglia *et al*., 1997). One characterizing feature of ASIC subtypes is their time course of desensitization: time constants vary over a 100-fold range from 10 ms (Paukert *et al*., 2004b) to several seconds (Lingueglia *et al*., 1997). Usually, desensitization is complete; among homomeric ASICs, only rat ASIC3 desensitizes incompletely (Waldmann *et al*., 1997; Hesselager *et al*., 2004; Salinas *et al*., 2009), but at rather low pH values (pH ≤5,0).

The primary sequence of ASICs shows two hydrophobic domains that could span the membrane, a large loop (>350 amino acids) between these domains and rather short N- and C-termini. A topology with two transmembrane domains, a large ectodomain and intracellular N- and C-termini has been experimentally confirmed (Saugstad *et al*., 2004). All ASICs contain 14 conserved cysteine residues within the ectodomain (Paukert *et al*., 2004b) that may stabilize its structure (Firsov *et al*., 1999). In addition, each ASIC contains at least one consensus sequence for N-glycosylation and glycosylation may assist the proper folding of the ectodomain (Kadurin *et al*., 2008). These features have recently been confirmed by the crystal structure of a chicken ASIC1 deletion mutant (Jasti *et al*., 2007). Moreover, the crystal structure revealed the three-dimensional folding of the ectodomain: it is composed of five subdomains which are connected to the membrane-spanning domains by an apparently flexible wrist (Jasti *et al*., 2007). The crystal represents the desensitized conformation of the channel (Gonzales *et al*., 2009); thus, it does not provide direct evidence for the proton sensor of ASICs. A recent comprehensive mutagenesis screen of conserved titratable amino acids identified four amino acids of ASIC1a that are important for proton-gating: Glu63, His72/His73, and Asp78 (Paukert *et al*., 2008). The presence of these amino acids correlated well, though not perfectly, with proton sensitivity of ASICs (Paukert *et al*., 2008).

To gain further insight into the structural determinants of proton-sensitivity of ASICs and to understand whether proton-sensitivity is an ancient feature of ASICs, ASICs have been cloned from different chordate species; they are absent in other animals like Drosophila or *C. elegans*. ASICs have been cloned from the urochordate Ciona (Coric *et al*., 2008), the simple, jawless vertebrate lamprey (Coric *et al*., 2005), the cartilaginous shark spiny dogfish (Coric *et al*., 2005), and the teleosts toadfish (Coric*et al*., 2003; Coric *et al*., 2005) and zebrafish (Paukert *et al*., 2004b); moreover from chicken (Coric *et al*., 2005) and different mammals. It has been reported that

ASICs from Ciona, lamprey and shark are not gated by protons (Coric *et al*., 2005; Coric *et al*., 2008), suggesting that proton-gating first evolved in bony fish and that ASICs of primitive chordates have a different and unknown gating stimulus. Since related channels from the Cnidaria Hydra are gated by neuropeptides (Golubovic *et al*., 2007), it is, for example, conceivable that early ASICs were gated by neuropeptides.

From shark, so far two ASICs have been cloned, sASIC1a and sASIC1b; both have been cloned from brain. sASIC1a and 1b have highest sequence homology to rat ASIC1b and zebrafish ASIC1.1 (zASIC1.1; (Coric *et al*., 2005). The amino acids that are critical for H^+-sensitivity of rat ASIC1a are completely conserved in sASIC1b, prompting us to re-evaluate proton-sensitivity of sASIC1b. Here we show that sASIC1b is indeed gated by protons and produces typical rapidly desensitizing Na^+ currents that are sensitive to amiloride. In addition and in contrast to other ASICs, a small sustained current persists during even slight acidification (pH <7.0). Our results show that proton-sensitivity of ASICs arose earlier in evolution than previously thought, at latest in cartilaginous fish. Moreover, they consolidate the definition of a "proton-sensitivity signature" in ASICs.

3.3 Methods

3.3.1 Electrophysiology

The cDNA of shark ASIC1b was cloned from the brain of the spiny dogfish Squalus acanthias (Coric *et al*., 2005); it was a kind gift of C.M. Canessa (Yale University). Our sequence analysis of this cDNA differs from the sASIC1b sequence, which is in the DDBJ/EMBL/GenBank databases (accession no. AY956392), at two residues in the cytoplasmic C-terminus: an R instead of a K at position 496 and an A instead of a V at 498. The same amino acids (R and A) are found at the corresponding positions in the closely related toadfish ASIC1.1 and zASIC1.1.

We subcloned this cDNA into expression vector pRSSP, which is optimized for functional expression in Xenopus oocytes, containing the 5´- untranslated region from *Xenopus* β-globin and a poly(A) tail (Bässler *et al*., 2001). Chimeric and mutant channels were generated by recombinant PCR using standard protocols with KAPA HiFi DNA polymerase (Peqlab). All PCR-derived fragments were entirely sequenced.

Oocytes were surgically removed under anaesthesia from adult *Xenopus* laevis females and kept in OR-2 medium (82.5 mM NaCl, 2.5 mM KCl, 1.0 mM Na_2HPO_4, 5.0 mM HEPES, 1.0 mM $MgCl_2$, 1.0 $CaCl_2$, and 0.5 g/liter polyvinylpyrrolidone). Anaesthetized frogs were killed after the final oocyte collection by decapitation. Animal care and experiments followed approved institutional guidelines at RWTH University Aachen.

Synthesis of cRNA was done as previously described (Paukert *et al*., 2004b). We injected 0.8 - 8 ng of sASIC1b cRNA per oocyte. Whole cell currents were recorded after 1 - 4 days with a TurboTec 03X amplifier (npi electronic, Tamm, Germany) using an automated, pump-driven solution exchange system together with the oocyte testing carousel controlled by the interface OTC-20 (npi electronic) (Madeja *et al*., 1995). With this system, 80% of the bath solution (10 – 90%) is exchanged within 300 ms (Chen *et al*., 2006b). Data acquisition and solution exchange were managed using CellWorks version 5.1.1 (npi electronic). Data were filtered at 20 Hz and acquired at 1kHz. Holding potential was -70 mV if not otherwise indicated. All experiments were performed at room temperature (20-25°C). Psalmotoxin was purchased from Alomone Labs (Jerusalem, Israel).

Bath solution for the two-electrode voltage clamp contained 140 mM NaCl, 1.8 mM $CaCl_2$, 1.0 $MgCl_2$, 10 mM HEPES. For the acidic test solutions, HEPES was replaced by MES buffer. Solutions containing PcTx1 were supplemented with 0.05% BSA (Sigma-Aldrich) in order to avoid absorption by the tubing. Glass electrodes filled with 3M KCl and a resistance of 0.3-1.5 MΩ were used.

3.3.2 Determination of surface expression

The hemagglutinin (HA) epitope (YPYDVPDYA) of influenza virus was inserted in the extracellular loop of sASIC1b between residues R161 and N162. HA-tagged sASIC1b formed a proton-activated channel with an estimated apparent H^+ affinity indistinguishable from untagged channels (results not shown). The oocytes were injected with 8 ng of cRNA and surface expression was determined as previously described (Zerangue *et al*., 1999; Chen & Gründer, 2007; Chen *et al*., 2007). Briefly, oocytes expressing shark ASIC1b were placed for 30 min in ND96 with 1% BSA to block unspecific binding, incubated for 60 min with 0,5 µg/ml of rat monoclonal anti-HA antibody (3F10, Roche), washed extensively with ND96/1% BSA, and incubated

for 90 min with 2 µg/ml of horseradish peroxidase-coupled secondary antibody (goat anti-rat Fab fragments, Jackson ImmunoResearch). Oocytes were washed six times with ND96/1% BSA and three times with ND96 without BSA. All steps were performed on ice. Oocytes were then placed individually in wells of microplates and luminescence was quantified in a Berthold Orion II luminometer (Berthold detection systems; Pforzheim, Germany). The chemiluminescent substrates (50 µl Power Signal Elisa; Pierce) were automatically added and luminescence measured after 2 sec for 5 sec. Relative light units (RLUs)/s were calculated as a measure of surface expressed channels. RLUs of HA-tagged channels were at least 400-fold higher than RLUs of untagged channels. The results are from two independent frogs; at least eight oocytes were analyzed for each experiment and each condition.

3.3.3 Data analysis

Data were analyzed with the software IgorPro (Wave metrics, Lake Oswego, OR). Concentration response curves were fit to the Hill-Function

$$I = a + (I_{max} - a)/(1 + (EC_{50}/[H]^{n}))$$

where I_{max} is the maximal current, a is the residual current, EC_{50} is the pH/concentration at which half-maximal activation/block of the transient current component was achieved, and n is the Hill-coefficient. For pH-activation and steady-state-desensitization curves, I_{max} was set to 1 and a to 0.

Current decay kinetics of the fast transient currents were fit with a mono-exponential function:

$$I = A_0 + Ae^{-1/\tau}$$

where A_0 is the relative amplitude of the non-desensitizing component, A is the relative amplitude of the desensitizing component and τ is the time constant of desensitization.

Current decay kinetics of the slow "sustained" currents were best fit with the sum of two exponential components

$$I = A_0 + A_1 e^{-1/\tau 1} + A_2^{-1/\tau 2},$$

where A_0, A_1, and A_2 are the relative amplitudes of the of various components, and τ_1 and τ_2 are the slow and fast time constants, respectively.

Results are reported as means ± S.E.M. They represent the mean of n individual measurements on different oocytes. Statistical analysis was done with Student´s unpaired t test.

3.4 Results

3.4.1 Functional characterization of shark ASIC1b.

Oocytes expressing sASIC1b generated robust currents when stimulated by pH 6.4. These currents were typical rapidly activating and desensitizing ASIC currents (Fig. 3.1); we did not observe such currents in oocytes that did not express sASIC1b (Fig. 3.1). The sASIC1b current desensitized with a time constant < 50 ms; the rapid gating of this channel precluded a more precise determination of the time course of desensitization. Most of the current rapidly declined due to desensitization, a small fraction (~5%), however, persisted even after prolonged (90 s) acid application without any sign of desensitization (Fig. 1).

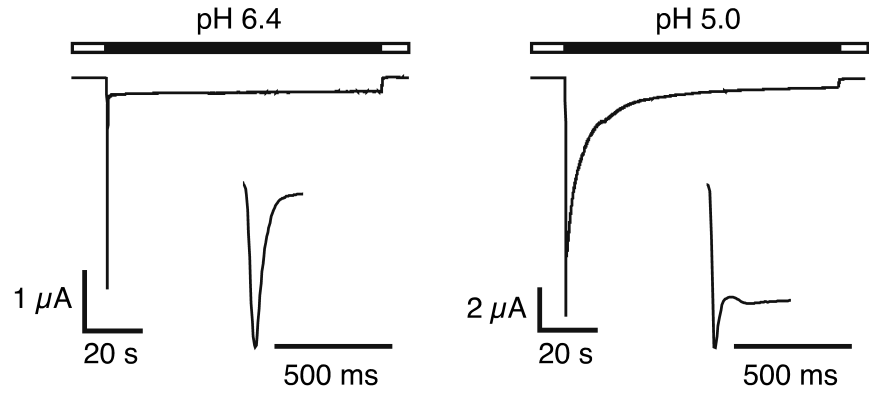

Figure 3.1. Shark ASIC1b is H^+-sensitive.
Top, representative traces of sASIC1b currents at pH 6.4 and pH 5.0. Note the sustained current at pH 6.4 and the two current components at pH 5. The current rise phase and the initial desensitization phase are also shown on an expanded time scale. **Bottom,** representative current trace of an uninjected oocyte. No currents are elicited by pH 5.0.

Such a sustained current is known from ASIC3 (Waldmann *et al*., 1997); ASIC3, however, generates a sustained current only at very acidic pH ≤5 (Waldmann *et al*., 1997; Salinas *et al*., 2009). Application of pH 5.0 to oocytes expressing sASIC1b generated transient currents of larger amplitude than pH 6.4. Moreover, at pH 5, after a short delay a second current component developed with a variable amplitude around 50% of the amplitude of the transient current. This second current component desensitized much slower than the initial transient current. The time course of desensitization of the slow current component was best fit by a double-exponential function with time constants τ_1 = 16 ± 4 s and τ_2 = 3.1 ± 0.2 s (n = 7; Table 1). Similar to the current at pH 6.4, the current at pH 5.0 did not completely desensitize but relaxed to a sustained steady-state level; the double-exponential fit revealed a level of 2.6 ± 0.5% of the initial amplitude of the slow component at steady-state (Table 1), which is on the same order as the sustained level at higher pH (normalized to the transient current at pH 5; see below). At pH 5, the sASIC1b current is, thus, qualitatively very similar to the ASIC3 current (Salinas *et al*., 2009). In the remainder of this study, we will refer to the typical transient ASIC current as the “transient current” and to the second slow current component at pH 5.0 as the “slow current”.

Parameter	Value	SEM	*n*
a_0	2,6%	0,5%	7
a_1	24,1%	2,2%	7
a_2	73,3%	2,4%	7
t_1	16 s	4 s	7
t_2	3,1 s	0,2 s	7

Table 1: Parameters describing desensitization of the slow current component of shark ASIC1b at pH 5.0.

Repetitive application of pH 6.4 to oocytes expressing sASIC1b with an interval of 30 s elicited transient currents of similar amplitude (Fig. 3.2A), showing that recovery from desensitization was complete in 30 s. As expected for a non-desensitizing current, also the amplitude of the sustained current did not change with repetitive applications of pH 6.4. Repetitive application of pH 5 also elicited transient currents of similar amplitude (Fig. 3.2A); in contrast, the initial amplitude of the slow current diminished progressively towards a steady-state level (Fig. 3.2A). Even after intervals

of 3 min, the slow current did not recover (not shown). This result shows that the slow current recovers slowly from desensitization, if at all, similar to ASIC3 (Salinas *et al*., 2009).

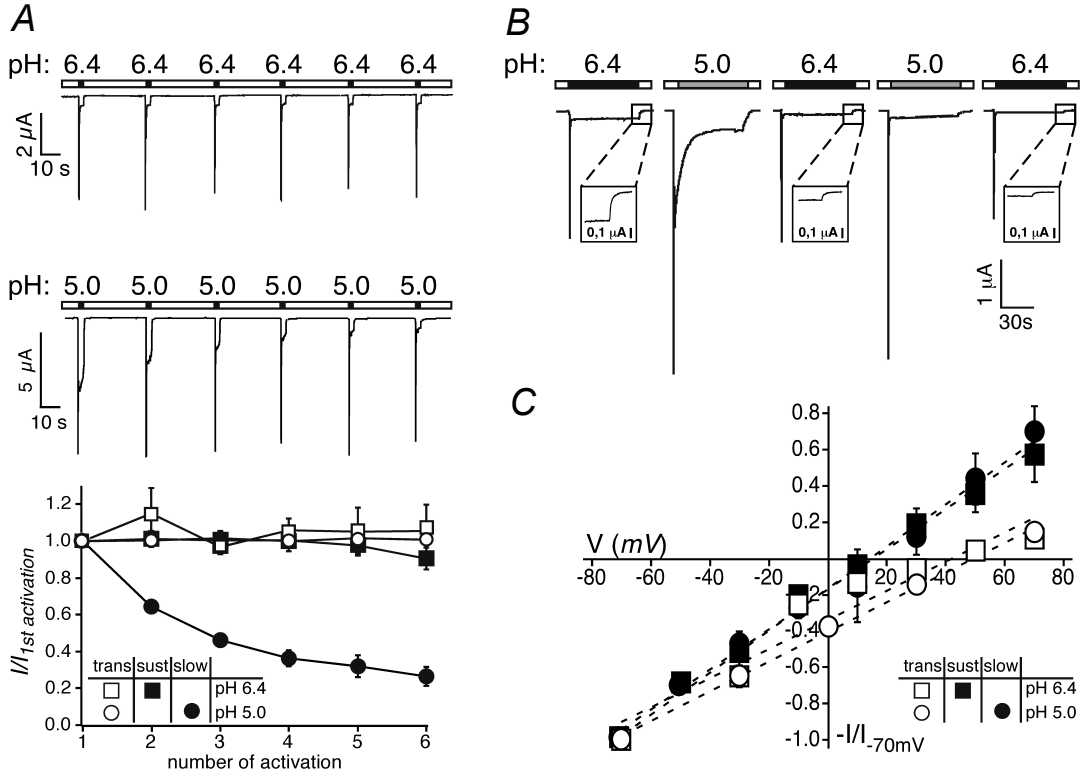

Figure 3.2. Characterization of the sustained sASIC1b current.
(A) Top, representative current traces of sASIC1b that was repeatedly activated by application of either pH 6.4 or 5 for 3 s. Channels were allowed to recover in conditioning pH 7.4 for 30 s. Bottom, current amplitudes were normalized to the first amplitude. The initial amplitude of the slow current component at pH 5 decreased progressively. Absolute values of the initial amplitudes were 4.1 ± 0.5 mA (transient current at pH 6.4; *n* = 7), 0.3 ± 0.05 mA (sustained current at pH 6.4; *n* = 7), 5.8 ± 1.8 mA (transient current at pH 5; *n* = 6), and 1.7 ± 0.4 mA (slow current at pH 5; *n* = 6), respectively. (B) Desensitization of the sustained current at pH 6.4 by application of pH 5.0. Channels were alternatively activated by pH 6.4 and pH 5.0. The amplitude of the sustained current (magnified in the insets) successively decreased after application of pH 5.0. (C) Current-voltage relationship for the transient and the sustained current at pH 5.0 and 6.4, respectively. For the transient currents, channels had been repeatedly activated at different holding potentials; for the sustained and slow currents, channels had been activated with pH 6.4 or 5.0, respectively, and voltage steps from -70 to +70 mV of 1 s duration were applied. Voltage steps at pH 5.0 were applied 60 s after activation when the slow current had relaxed to a constant amplitude. Absolute values of the current amplitudes at -70 mV were 19.4 ± 4.5 mA (transient current at pH 5.0; *n* = 6), 0.78 ± 0.12 mA (transient current at pH 6.4; *n* = 12), 0.33 ± 0.07 mA (sustained current at pH 5.0; *n* = 9 - 11 for voltage jumps between -70 mV and +30 mV; *n* = 3 - 5 for voltage jumps at +50 mV and +70 mV) and 0.44 ± 0.09 mA (sustained current at pH 6.4; n = 7), respectively.

Since the slow current developed after the transient current and did not completely desensitize, we wondered whether this current has the same basis as the sustained current at pH 6.4. In order to address this question, we asked whether the slow

current at pH 5.0 cross-desensitizes the sustained current at pH 6.4. This was indeed the case: after a 1 min-application of pH 5.0 the amplitude of the sustained current at pH 6.4 was significantly smaller (49 ± 10% of the initial amplitude, $p < 0.01$) than before the pH 5.0 application (Fig. 3.2B). A second pH 5.0-application further decreased the sustained current at pH 6.4 (42 ± 10% of the initial amplitude, $p < 0.05$; Fig. 3.2B). This is in contrast to several applications of pH 6.4, which did not desensitize the sustained current (Fig. 3.2A). Cross-desensitization of the sustained current at pH 6.4 by pH 5.0 suggests that the sustained current has a similar basis as the slow current. This interpretation implies that the slow current starts to desensitize only at pH values <6.4 (see also below).

The reversal potential of the transient current was around 50 mV (Fig. 3.2C), indicating a Na^+-selective current, which is typical for ASICs. For the sustained current at pH 6.4, the reversal potential was shifted by approximately 30 mV to the left (Fig. 3.2C), indicating a lower Na^+ selectivity. The reversal potential of the slow current at pH 5.0 was similar to the reversal potential of the sustained current (Fig. 3.2C), supporting the

idea that both currents have the same basis. Similar nonselective sustained currents are also carried by the ASIC3/2b heteromer (Lingueglia *et al*., 1997).

The amplitude of the transient sASIC1b current increased with increasing H^+ concentrations and saturated at pH 5.0 (Fig. 3.3A); half-maximal activation was reached at pH 6.0 ± 0.04 (n = 15; Fig. 3.3C). Due to the long-lasting desensitization, the apparent H^+ affinity of the slow current could not be determined precisely. Pre-conditioning by slight acidification for 60 s revealed that the number of channels available for activation diminished at pH values below 7.4 so that at a pre-conditioning pH of 6.55 no transient currents could be recorded any more (Fig. 3.3B). Steady-state desensitization of the transient current was half-maximal at pH 6.9 ± 0.01 (n = 11; Fig. 3.3C). In contrast, even at a conditioning pH of 6.4, small sustained currents were still elicited (Fig. 3.3B).

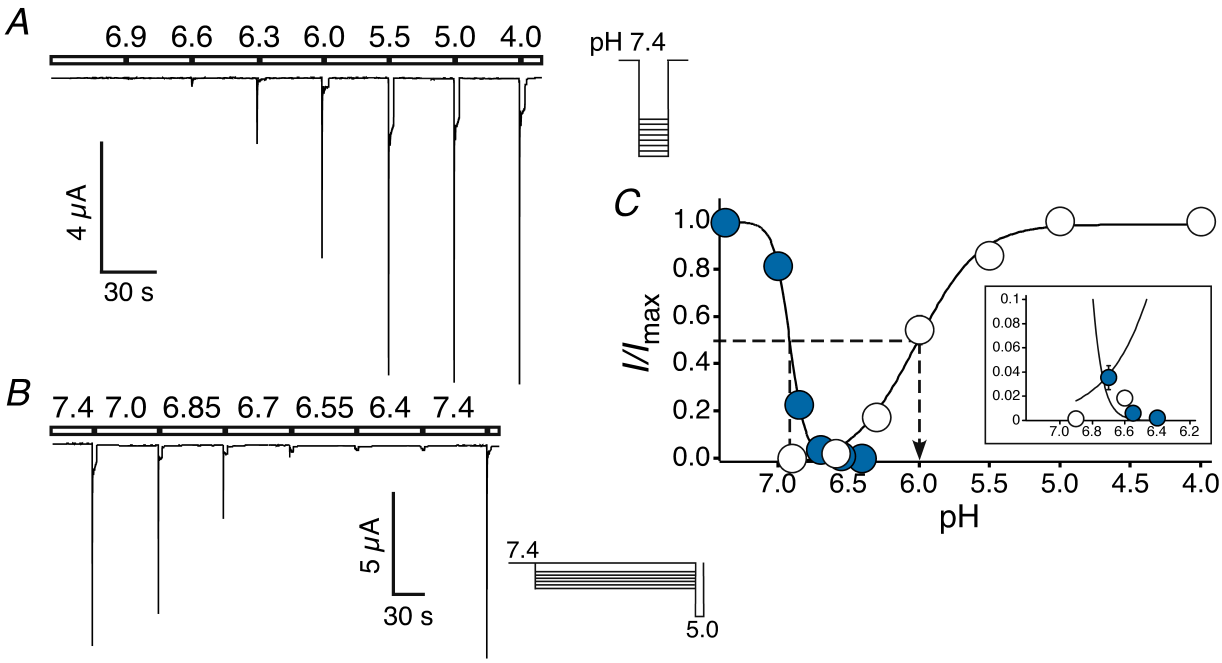

Figure 3.3. Apparent H^+ affinity of shark ASIC1b.
(A) Representative current trace of oocytes expressing sASIC1b. Channels were activated for 3 s by varying low pH, as indicated. Conditioning pH 7.4 was applied for 30 s. (B) Channels were activated by pH 5.0 with varying pre-conditioning pH, as indicated. Conditioning pH was applied for 60 s. (C) pH-response curves for activation (open circles) and steady-state desensitization (grey circles); lines represent fits to the Hill function. Dotted lines indicate EC_{50} values. Only the transient current was analyzed. The overlapping region of the activation and inactivation curves is magnified (inset). Absolute values of the current amplitudes were 4.9 ± 1.2 mA (activation curve, pH 5.0; *n* = 15) and 8.4 ± 1.9 mA (steady-state desensitization curve, conditioning pH 7.4; *n* = 11), respectively.

3.4.2 Pharmacology of shark ASIC1b

The sASIC1b current was sensitive to amiloride: the transient current was half-maximally blocked by 78 ± 12 µM amiloride (n = 21; Fig. 3.4A), similar to other ASICs (Paukert *et al.*, 2004b). Amiloride at concentrations up to 4 mM did not completely block this current (not shown); however, the fast desensitization of the transient current may mask a higher amiloride affinity of the channel. In agreement with this hypothesis, 1 mM amiloride blocked the slow current to a larger extent than the transient current (Fig. 3.4B). The kinetics, Na^+ selectivity, pH activation and steady-state desensitization curves, and block by amiloride all identify the transient sASIC1b current as a typical ASIC current.

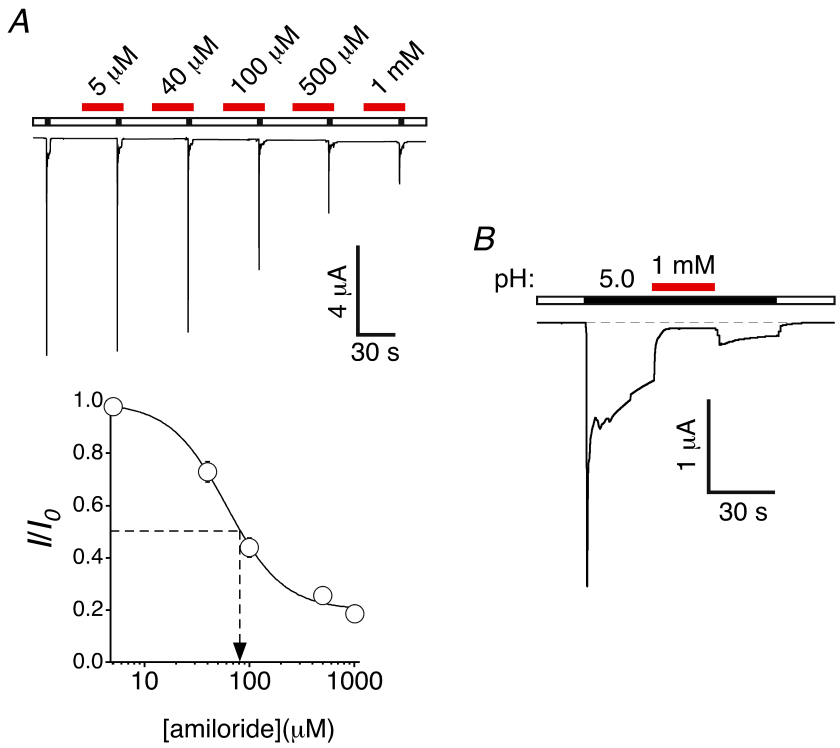

Figure 3.4 Apparent H^+ affinity of shark ASIC1b.
(A) Representative current trace of oocytes expressing sASIC1b. Channels were activated for 3 s by varying low pH, as indicated. Conditioning pH 7.4 was applied for 30 s. (B) Channels were activated by pH 5.0 with varying pre-conditioning pH, as indicated. Conditioning pH was applied for 60 s. (C) pH-response curves for activation (open circles) and steady-state desensitization (grey circles); lines represent fits to the Hill function. Dotted lines indicate EC_{50} values. Only the transient current was analyzed. The overlapping region of the activation and inactivation curves is magnified (inset). Absolute values of the current amplitudes were 4.9 ± 1.2 mA (activation curve, pH 5.0; *n* = 15) and 8.4 ± 1.9 mA (steady-state desensitization curve, conditioning pH 7.4; *n* = 11), respectively.

The spider toxin psalmotoxin 1 (PcTx1) is a specific inhibitor of homomeric ASIC1a (Escoubas *et al*., 2000); it inhibits ASIC1a by increasing its apparent H^+ affinity (Chen *et al*., 2005), transferring all channels into the desensitized conformation at pH 7.4. By contrast, homomeric ASIC1b is not inhibited by PcTx1 but opened at slight acidification (Chen *et al*., 2006a). Thus, binding of PcTx1 is state-dependent: for ASIC1a, it binds with highest affinity to the desensitized state and for ASIC1b, to the open state (Chen *et al*., 2006a). So far, modulation has been shown for rat, mouse, and chicken ASIC1 (Escoubas *et al*., 2000; Chen *et al*., 2005, 2006a; Samways *et al*., 2009). To investigate whether ASIC1b from shark is also modulated by PcTx1, we investigated the effect of PcTx1 on the steady-state desensitization and pH activation curves of sASIC1b. This tests the stabilization of the desensitized and the open conformation, respectively. 100 nM PcTx1 did not significantly shift the steady-state desensitization or the activation curve of sASIC1b (Fig. 3.5A).

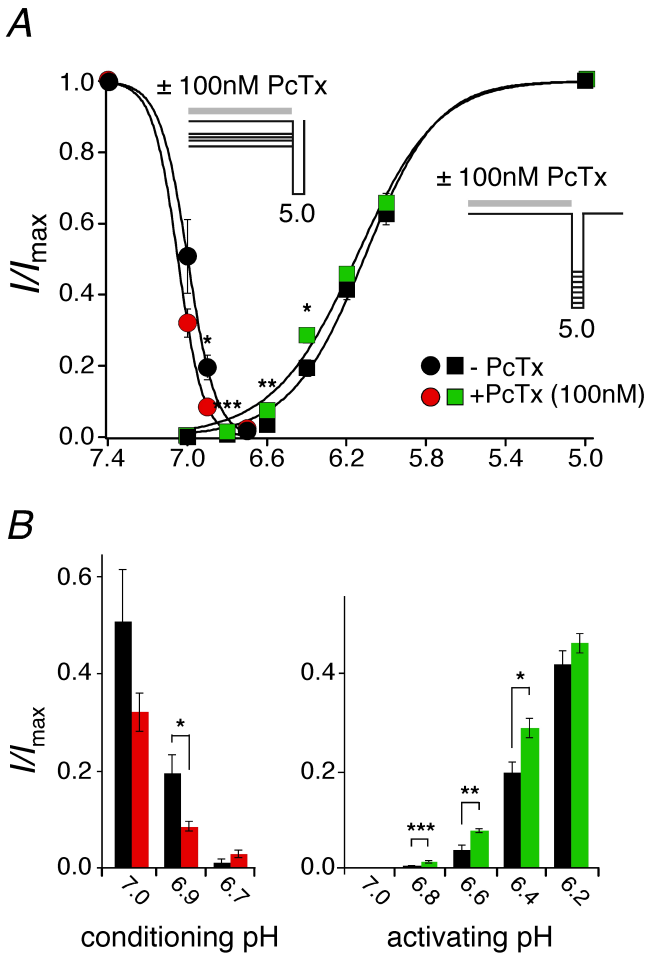

Figure 3.5. Shark ASIC1b is slightly modulated by psalmotoxin 1.
A) pH-response curves for activation (squares) and steady-state desensitization (circles) with (black symbols) and without (open symbols) pre-application of 100 nM psalmotoxin (PcTx); PcTx was present only in the conditioning period (60 s). For activation curves, channels had been activated for 3 s by varying low pH, as indicated. For steady-state desensitization curves, channels had been activated for 3 s by pH 5.0 with varying pre-conditioning pH, as indicated. Lines represent fits to the Hill function. Absolute values of the current amplitudes were 8.4 ± 2.6 mA (activation curve, pH 5.0, without PcTx; *n* = 6), 8.3 ± 1.8 mA (activation curve, pH 5.0, with PcTx; *n* = 6), 8.9 ± 2.7 mA (steady-state desensitization curve, conditoning pH 7.4, without PcTx; *n* = 6) and 4.5 ± 1.4 mA (steady-state desensitization curve, conditoning pH 7.4, with PcTx; *n* = 6), respectively. (B) Bar graphs comparing normalized current amplitudes at slight acidification for the data from (A). White bars, without PcTx1; black bars, with PcTx1. For conditioning pH 6.9, significantly more channels were desensitized when PcTx was present; similarly, for activation by pH 6.8 - 6.4 current amplitudes were significantly larger when PcTx was present. *, $p < 0.05$; **, $p < 0.01$; ***, $p < 0.001$.

For comparison, 30 nM PcTx1 shifts the steady-state desensitization curve of rat ASIC1a by ~0.3 pH units (Chen *et al*., 2005) and 100 nM PcTx1 shifts the activation curve of rat ASIC1b by ~0.4 pH units (Chen *et al*., 2006a). In contrast to rat ASIC1b (Chen *et al*., 2006a), there were also no effects of PcTx1 on the desensitization of sASIC1b. Furthermore, the amplitude of the sustained current relative to the transient current at pH 6.6 was not significantly different when PcTx1 was present or absent

(results not shown). Thus, PcTx1 does not strongly stabilize the desensitized or the open state of sASIC1b.

There were subtle effects of PcTx1, however, that led to significant changes of the current amplitudes at certain pH values. At steady-state and a conditioning pH of 6.9, significantly more channels were desensitized when PcTx1 was present than when it was absent (Fig. 3.5B). Similarly, slight acidification (pH 6.8 - 6.4) opened significantly more channels in the presence than in the absence of PcTx1 (Fig. 3.5B). This result shows that PcTx1 slightly promotes desensitization and opening of sASIC1b at low agonist-concentrations, suggesting that PcTx1 indeed binds to and stabilizes the desensitized and the open conformation of sASIC1b, qualitatively similar to rat ASIC1 (Chen *et al*., 2006a). The comparatively subtle effects of PcTx1 can be due to either a low PcTx1 affinity of sASIC1b or a subtle effect of PcTx1 binding on gating of sASIC1b. In summary, subtle effects of PcTx1 on sASIC1b suggest that the PcTx1 binding site (Pietra, 2009; Qadri *et al*., 2009) is partially conserved in sASIC1b, suggesting that it is an evolutionary old pocket in the three-dimensional structure of ASIC1.

3.4.3 Mutational analysis of shark ASIC1b

A pair of histidines that is indispensable for H^+ sensitivity of rat ASIC1a is conserved in sASIC1b (Paukert *et al*., 2008). When both histidines were exchanged by asparagines (H101/H102N), sASIC1b was no longer sensitive to H^+ (pH ≥ 4; Fig. 3.6A): both the transient and the slow current were no longer elicited by H^+. This result shows that also fundamental structural requirements for H^+ sensing are conserved in sASIC1b. Collectively, these results suggest that the gating mechanism of ASICs is conserved from shark to mammals. Amplitudes of transient sASIC1b currents usually ranged between 1 and 10 µA (Fig. 3.6B, first bar). Amplitudes of rat ASIC1b, which are of similar magnitude, can be increased by deletion of an N-terminal domain (Bässler *et al*., 2001), which is conserved in sASIC1b. Deletion of this N-terminal domain increases surface expression of zASIC4.1 (Chen *et al*., 2007).

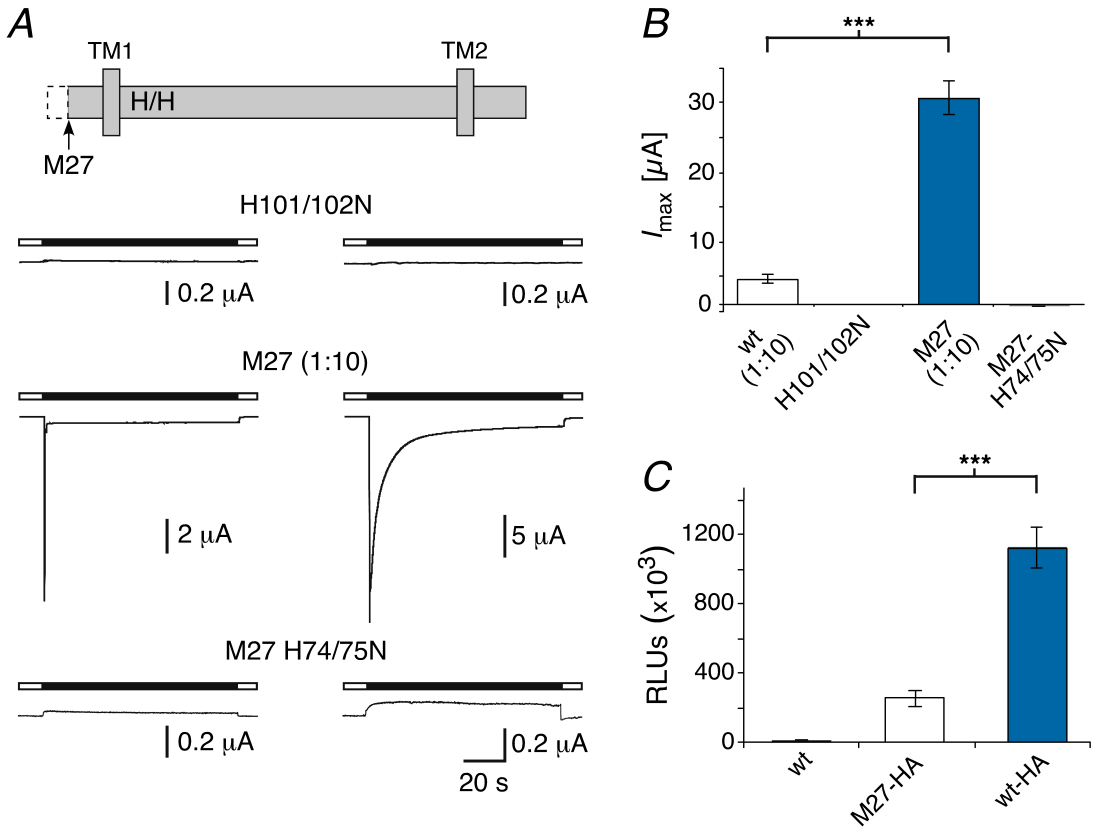

Figure 3.6. A pair of histidines is indispensable for H^+-sensitivity of shark ASIC1b. (A) Top, schematic illustration of the topology of sASIC1b. TM1, TM2: transmembrane domains. The arrow indicates the position of the N-terminal truncation in construct M27; the two conserved histidines localize to the proximal ectodomain. Bottom, representative current traces for sASIC1b-H101/102N, -M27, and -M27-H74/75N. Note that for M27-H74/75N, application of H^+ slightly reduced the background current. (B) Bars representing the peak current amplitude (mean ± SEM) of oocytes expressing wild-type sASIC1b (wt), the histidine mutant (H101/102N), and the two M27-mutants ($n \geq 6$); channels had been activated by pH 5.0. The amounts of cRNA that had been injected into each oocyte were 0.8 ng (wt and M27) or 8 ng (H101/102N and M27-H74/75N), respectively. ***, $p << 0.01$. (C) Bars representing surface expression of sASIC1b and -M27; untagged sASIC1b served as a control (left bar). Results are expressed as relative light units (RLUs)/oocyte/s ($n = 36$). ***, $p << 0.01$.

Deletion of this domain in sASIC1b (sASIC1b-M27) increased current amplitudes by about ten-fold (Fig. 3.6B, third bar), indicating that the N-terminal domain controls surface expression of sASIC1b. Substitution of the conserved histidine pair (H74/H75, corresponding to H101/102 in the wild-type) rendered also the highly expressing variant sASIC1b-M27 H^+-insensitive (Fig. 3.6A and 3.6B, fourth bar), confirming the importance of these histidines. Sustained and slow current were identical between wild-type sASIC1b and sASIC1b-M27 (Fig. 3.6A), as well as the apparent affinity for H^+ of the transient current (not shown), suggesting that the N-terminal domain has a specific role in the trafficking of sASIC1b.

To more specifically address surface expression of sASIC1b-M27, we introduced an HA-epitope in the ectodomain of sASIC1b and sASIC1b-M27 and assessed the presence of epitope-tagged channels on the surface of intact oocytes using a monoclonal anti-HA antibody and a luminescence assay (see Methods). Deletion of the N-terminal domain in sASIC1b-M27 increased surface-expression 4.5-fold compared to wild-type (Fig. 3.6C), showing that the N-terminal domain indeed leads to inefficient surface expression of shark ASIC1b. Inefficient surface expression together with the fast kinetics may be the reason why a previous study reported that sASIC1b is H^+-insensitive (Coric *et al*., 2005).

3.4.4 The sustained current of shark ASIC1b

A striking feature of sASIC1b was the sustained current at mild acidification (Fig. 3.1). It endows this ASIC with the capacity to encode also sustained H^+ signals of small amplitude, as illustrated in Fig. 3.7. Similar to a previous study that mimicked the effect of mild acidification on ASIC3 (Yagi *et al*., 2006), pH was decreased from 7.4 to 6.2 in steps of 0.2 units, with each step held for 10 seconds (Fig. 3.7A). Under these conditions, sASIC1b generated non-desensitizing currents already at pH 7.0. Slightly stronger acidification to pH 6.8 and 6.6 generated transient currents in addition to sustained currents, which were of slightly larger amplitude than at pH 7.0. Below pH 6.6, due to steady-state desensitization of the transient current (Fig. 3.3C), only the sustained currents remained, the amplitude of which further increased. Only at pH 6.2, some desensitization of the sustained current became apparent. This result demonstrates that sASIC1b generates sustained H^+ signals over a pH range from 7.0 to 6.4 without any apparent desensitization.

As was previously shown for ASIC3, overlap of steady-state activation and desensitization curves can generate a sustained “window current” (Yagi *et al*., 2006). In order to determine the window current of sASIC1b, we multiplied values of the two curves that were fit to the data in Fig. 3.3C (Fig. 3.7B, smooth curve). We then compared the predicted window current with the current amplitude of the sustained current (expressed as a fraction of the transient current amplitude at pH 5) that we actually measured. As can be seen in Fig. 3.7B, both curves matched well from pH 7.4 to 7.0, suggesting that the sustained current at pH 7.0 is a pure window current.

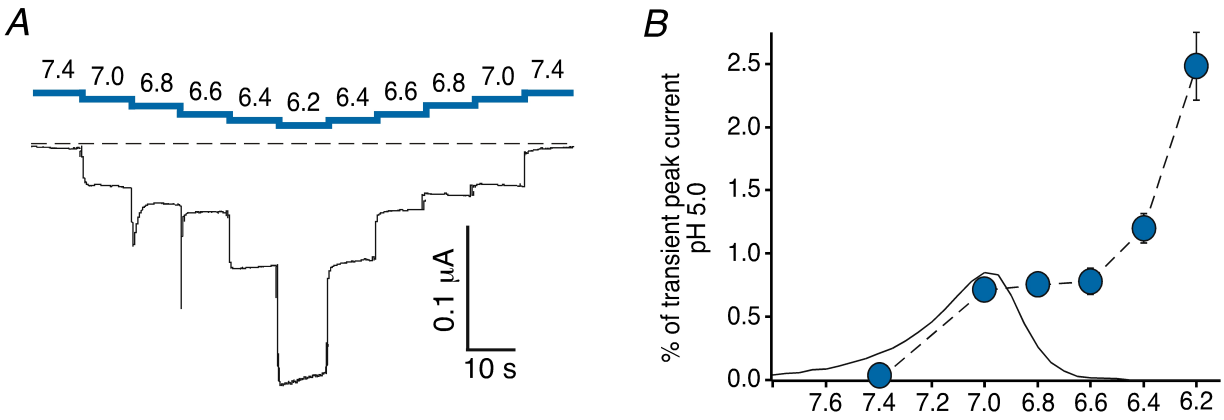

Figure 3.7. Small pH steps evoke sustained shark ASIC1b currents.
(A) pH was stepped from 7.4 to 6.2 in steps of 0.2 units (first step: 0.4 units; top). A representative current trace is shown (bottom). (B) Current versus pH relationship of sustained currents (filled circles; *n* = 12) measured as in A and the predicted window current (smooth curve). The window current was calculated by multiplying values at each pH of the activation and steady-state desensitization curve fits from Fig. 3C; the fit for the activation curve was refined for low H^+ concentrations by measuring transient currents also at pH 6.95 (*I* = 0 mA; *n* = 15).

At pH values below pH 7.0, however, the plot for the sustained current starts to deviate from the predicted window current. The additional sustained current, which cannot be explained by the window current, is likely carried by the nonselective sustained current that we observed at pH 6.4. Thus, the sustained current between 7.0 and 6.6 is a mixture of window current and the nonselective sustained current and at pH values below 6.6, the sustained current is solely carried by the nonselective sustained current. If this interpretation were correct, the nonselective sustained current of sASIC1b would start to activate just below pH 7.0, effectively being the so far most sensitive sustained ASIC current that is not a window current.

3.5 Discussion

Our study has two key findings: 1) we show that the presence of the “proton-sensitivity signature” can predict H^+-sensitivity of an ASIC, and 2) we show that H^+ sensitivity of ASICs evolved latest in cartilaginous fish. Moreover, we show that sASIC1b has a sustained current component, which is unusually sensitive to H^+.

3.5.1 The "H^+ sensitivity signature"

A recent study identified a few amino acids that are important for H^+-sensitivity of rat ASIC1a (Paukert *et al*., 2008). These amino acids are E63, H72/H73, and D78 and cluster in the proximal ectodomain. Substitution of E63 or D78 together with amino acids that mediate open channel block by Ca^{2+} (Paukert *et al*., 2004a) renders ASIC1a H^+-insensitive; substitution of the histidine pair H72/H73 has the same effect. The crucial role of a histidine at this position had previously also been shown for ASIC2a (Baron *et al*., 2001; Smith *et al*., 2007). The precise role of these amino acids for ASIC gating is unknown, but it has been proposed that protonation of H72/H73 induces channel opening (Paukert *et al*., 2008). All ASICs that contain these amino acids are H+-sensitive, with two exceptions: sASIC1b and zASIC2 (Paukert *et al*., 2008). In the present study we show that sASIC1b is indeed H^+-sensitive, reducing the number of H^+-insensitive ASICs containing the "H^+ sensitivity signature" to one; we speculate that zASIC2 contains some unknown sequence features that render this channel H^+-insensitive despite the presence of the critical amino acids.

The critical amino acids are not conserved in all H^+-sensitive ASICs (Paukert *et al*., 2008). For example, zASIC1.1 does not contain the crucial His residue. Thus, it is clear that at present we cannot predict with certainty H^+-sensitivity of an ASIC solely based on the amino acid sequence. However, the present study is an example that we can predict it with some fidelity, justifying the definition of a "H^+-sensitivity signature".

Other regions implicated in H^+-sensitivity of ASICs are a putative Ca^{2+}-binding site in the ion pore (Immke & McCleskey, 2003) and a cluster of acidic amino acids, the acidic pocket, that was identified in the crystal structure of chicken ASIC1 (Jasti *et al*., 2007). Both elements are supposed to hold a Ca^{2+} ion in the closed state. H^+ would compete with these Ca^{2+} ions and displace them during acidification, triggering the opening of the ion pore. Both elements individually are not absolutely necessary for H^+-sensitivity of an ASIC (Paukert *et al*., 2004a; Li *et al*., 2009), but likely contribute to H^+-sensitivity. The acidic pocket for example, determines apparent proton affinity of an ASIC (Sherwood *et al*., 2009). Crucial elements of the Ca^{2+}-binding site in the ion pore are two acidic amino acids (Paukert *et al*., 2004a) and are conserved in sASIC1b (Glu441 and Asp448). Similarly, the eight acidic amino acids, which form three carboxyl-carboxylate pairs composing the acidic pocket and a fourth pair outside the acidic pocket (Jasti *et al*., 2007), are also conserved in sASIC1b (Glu108, Glu235,

Asp253, Glu254, Asp361, Glu365, Asp423, and Glu432). Although the exact role of both elements for H^+-sensitivity of ASICs is still uncertain, their presence in sASIC1b is in agreement with its H^+-sensitivity.

3.5.2 When did H^+ sensitivity of ASICs evolve?

Previous studies (Coric *et al.*, 2005; Coric *et al.*, 2008) suggested that proton-gating first evolved in bony fish (Fig. 3.8) and that ASICs of primitive chordates have a different gating stimulus. Here we clearly show that this is not true for shark. sASIC1b generates typical ASIC currents, showing that H^+ sensitivity evolved latest in cartilaginous fish. Cartilaginous fish evolved some 80 million years earlier than bony fish, approximately 500 million years ago (Kumar & Hedges, 1998) (Fig. 3.8). What about the ASICs from chordates that diverged even earlier from higher vertebrates?

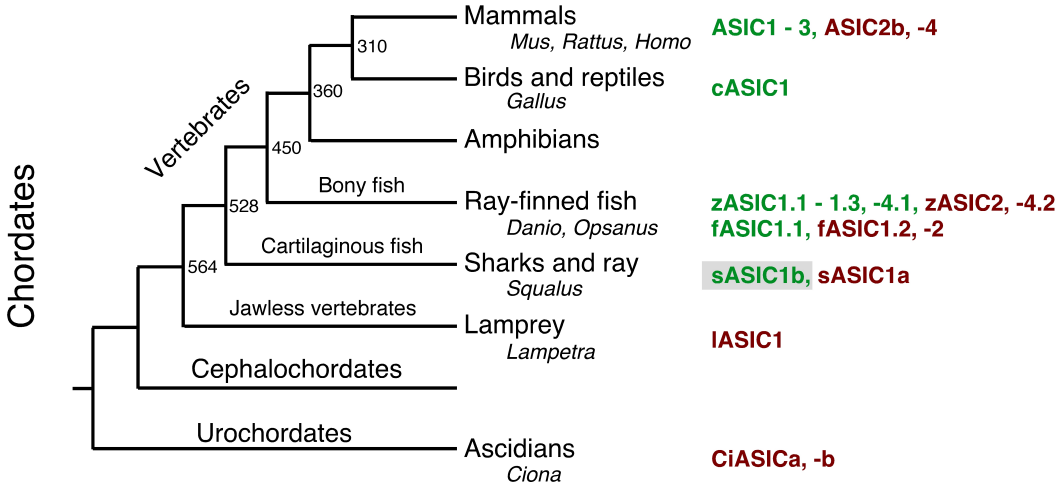

Figure 3.8. Phylogenetic tree illustrating the main branches of chordates.
Individual ASICs are shown on the right; proton-sensitive ASICs in green, presumably proton-insensitive ASICs in red; sASIC1b is shown on a grey background. Genera from which ASICs have been cloned are also indicated. An estimate of the time of some branching events is given (Kumar & Hedges, 1998).

ASIC1 from the jawless vertebrate lamprey is H^+-insensitive (Coric *et al.*, 2005) and does not contain the H^+ sensitivity signature (Paukert *et al.*, 2008). Since mammalian ASIC1a has a high H^+ affinity and a widespread expression in the nervous system, H^+ insensitivity of lamprey ASIC1 is a striking feature, suggesting a ligand different from H^+ for this ASIC. However, so far only ASIC1 has been cloned and characterized from lamprey and it remains an open question whether lamprey does also contain H^+-sensitive ASICs. Higher vertebrates, for example, contain H^+-insensitive ASICs, for

example ASIC2b and ASIC4 of mammals (Lingueglia *et al*., 1997; Gründer *et al*., 2000) and zASIC2 and zASIC4.2 of zebrafish (Paukert *et al*., 2004b), together with H^+-sensitive ASICs. If such channels existed also in lamprey, it would be possible that lamprey ASIC1 contributes to H^+-gated channels by formation of heteromeric channels, as it has been shown for other H^+-insensitive ASICs (Lingueglia *et al*., 1997; Chen *et al*., 2007).

Concerning the urochordate Ciona (Fig. 3.8), the Ciona genome contains a single ASIC gene, which gives rise to two splice forms (Coric *et al*., 2008). The cDNA sequence for one of these subtypes can be found in the public EMBL database. Similar to sASIC1b, this ASIC from Ciona contains the proton-sensitivity signature, suggesting that H^+-sensitivity of this subtype should also be re-evaluated. Irrespective of H^+-sensitivity of Ciona ASIC, H^+-insensitivity could also be a secondary, acquired feature. Given the close relationship of ASICs with peptide-gated channels from Cnidaria (Golubovic *et al*., 2007), it is tempting to postulate an agonist different from H^+ for ASICs from primitive chordates; however, the possibility that some of these ASICs are H^+-sensitive and that H^+ are the original gating stimulus of ASICs should not be dismissed.

3.5.3 The sustained current of shark ASIC1b

Whereas the typical ASIC current is a transient current, a few ASICs also generate sustained currents (Hesselager *et al*., 2004). However, these currents are usually generated only at unphysiological acidic pH. For example, homomeric rat ASIC3, a well studied subtype, generates sustained currents only at pH ≤5.0 (Waldmann *et al*., 1997). Nevertheless is it believed that ASIC3, a sensory neuron-specific ASIC, is a sensor of acidic and inflammatory pain (Deval *et al*., 2008). How can a channel that carries transient currents encode sustained acidification during a painful inflammation? This paradox has been solved by showing that pH activation and steady-state desensitization curves of ASIC3 overlap, allowing ASIC3 to carry a sustained “window current” at the pH values of overlap (Yagi *et al*., 2006). The window of overlap is tiny, however, limiting the pH range where ASIC3 can carry sustained currents from 7.3 to 6.7 (Yagi *et al*., 2006); moreover, ASIC1a, another highly H^+-sensitive ASIC, does not support such sustained window currents (Yagi *et al*., 2006).

Our results show that sASIC1b carries a bell-shaped window current at mild acidification between pH 7.4 and 6.6 (Fig. 3.7B), similar to ASIC3. Unique among homomeric ASICs, however, a second sustained current component developed already at only slightly more acidic pH below 7.0. Thus, the sustained current between pH 7.0 and 6.6 is a mix of a window current and a nonselective sustained current. The sustained current at pH 6.4 has no longer any contribution by the window current and is a pure nonselective sustained current (Fig. 3.7B). The tight overlap of window current and nonselective sustained current results in sustained sASIC1b currents over the whole pH range below pH 7.0. This behaviour is similar to heteromeric ASIC3/2a (Yagi *et al*., 2006), with the exception that the fractional sustained current of sASIC1b is up to 5-fold larger over the pH range from 7.0 to 6.2.

The relation of the nonselective sustained current at slight acidification (e.g. pH 6.4) and the slow current at pH 5.0 is not entirely clear. Cross-desensitization of the sustained current at pH 6.4 by the slow current (Fig. 3.2B) and unselectivity of both currents (Fig. 3.2C) suggest, however, that both currents are carried by the same state of the channel. This interpretation would imply that the slow current starts to develop at pH <7.0, gradually increases in amplitude with increasing acidification and gets slowly, but profoundly desensitized by pH values <6.2.

Other homomeric ASICs that generate sustained currents are zASIC4.1 and -4.2 (Paukert *et al*., 2004b; Chen *et al*., 2007). The sustained current of these subtypes differs from the sASIC1b sustained current in several ways: 1) it develops only slowly over 1 s (Chen *et al*., 2007) whereas the sASIC1b current develops at least ten times faster (Fig. 3.1); 2) it is insensitive to amiloride (Chen *et al*., 2007) whereas the sASIC1b current is sensitive to amiloride (Fig. 3.4B); 3) it depends on the presence of the N-terminal domain (Chen *et al*., 2007) whereas also the sASIC1b deletion mutant (M27) developed the sustained current (Fig. 3.6A). Thus, it seems that the sustained current of zASIC4.1 and 4.2 is unrelated to the sustained current of sASIC1b.

The sustained sASIC1b current endows this channel with the capacity to encode also sustained acidification. ASIC3, with which sASIC1b shares many features, is involved in detection of painful acidosis (Yagi *et al*., 2006; Deval *et al*., 2008). Although there is now clear evidence for nociception in bony fish (Sneddon, 2004), nociception in sharks, however, remains contested (Snow *et al*., 1993). Moreover, sASIC1b has been cloned from shark brain and its expression in DRGs is unknown, rendering a role for sASIC1b in nociception hypothetical. In the brain, sASIC1b would carry a

sustained depolarizing current during acidosis, suggesting that the extracellular pH has an important impact on neurons in shark brain.

4. The interaction between two extracellular linker regions controls sustained opening of acid-sensing ion channel 1

4.1 Abstract

Activation of acid-sensing ion channels (ASICs) contributes to neuronal death during stroke, to axonal degeneration during neuroinflammation, and to pain during inflammation. While understanding ASIC gating may help to modulate ASIC activity during these pathologic situations, at present it is poorly understood. The ligand, H^+, probably binds to several sites, among them amino acids within the large extracellular domain (ECD). The ECD is linked to the two transmembrane domains by the wrist region that is connected to two anti-parallel β-sheets, β1 and β12. Thus, the wrist region together with those β-sheets may have a crucial role in transmitting ligand binding to pore opening and closing. Here we show that amino acids in the β1-β2-linker determine constitutive opening of ASIC1b from shark. The most crucial residue within the β1-β2 linker (D110), when mutated from aspartate to cysteine, can be altered by cysteine-modifying reagents much more readily when channels are closed than when they are desensitized. Finally, engineering of a cysteine at position 110 and at an adjacent position in the β11-β12 linker leads to spontaneous formation of a disulfide bond that traps the channel in the desensitized conformation. Collectively our results suggest that the β1-β2 and β11-β12 linkers are dynamic during gating and tightly appose to each other during desensitization gating. Hindrance of this tight apposition leads to reopening of the channel. It results that the β1-β2 and β11-β12 linkers modulate gating movements of ASIC1 and may thus be drug targets to modulate ASIC activity.

4.2 Introduction

Acid-sensing ion channels (ASICs) are H^+-gated Na+ channels and are abundantly expressed throughout the central and the peripheral nervous system (Wemmie *et al*., 2006). They probably contribute to the excitatory postsynaptic current in many neurons (Baron *et al*., 2002; Wemmie *et al*., 2002; Askwith *et al*., 2004; Xiong *et al*., 2004; Weng *et al*., 2010) and to detection of painful acidosis in peripheral tissues

(Deval *et al*., 2008; Deval *et al*., 2010). ASIC1a is the most abundant ASIC subunit in the mammalian CNS and most ASICs in central neurons are homomeric ASIC1a or heteromeric ASIC1a/2a (Baron *et al*., 2002; Askwith *et al*., 2004; Vukicevic and Kellenberger, 2004). During prolonged acidosis that accompanies brain ischemia and autoimmune inflammation, ASIC1a gets activated and enhances brain injury and axonal damage, respectively (Xiong *et al*., 2004; Friese *et al*., 2007). Thus, a better understanding of ASIC1 gating is desirable and may lead to pharmacological interventions aimed at modulating ASIC1 activity during diverse neuropathological states (Sluka *et al*., 2009).

After a rapid drop in pH, ASICs open within milliseconds (Bässler *et al*., 2001). During prolonged acidification they desensitize; kinetics of desensitization varies over a 100-fold range from 10 msec (Coric *et al*., 2003; Paukert *et al*., 2004) to several seconds (Lingueglia *et al*., 1997). For most ASICs, desensitization is complete but some ASICs have small, sustained currents that do not desensitize in the continuous presence of protons (Waldmann *et al*., 1997; Hesselager *et al*., 2004; Springauf and Gründer, 2010). Such sustained currents could have a major contribution to the harmful effects of ASIC activity during prolonged acidosis. However, despite the importance of desensitization gating and sustained opening of ASICs, our molecular understanding of these processes is incomplete.

The crystal structure of chicken ASIC1 (cASIC1) has been solved at acidic pH (Jasti *et al*., 2007; Gonzales *et al*., 2009), probably representing the desensitized conformation of the channel. It provides a structural framework to understand ASIC gating (Gründer and Chen, 2010), in particular desensitization gating. The cASIC1 structure is characterized by the symmetric arrangement of three subunits. Each subunit has two transmembrane domains (TMDs) that are linked to the large extracellular domain (ECD) by an apparently flexible wrist. The ECD resembles a clenched hand and consists of five subdomains, namely the palm, thumb, finger, knuckle, and β-ball domains (Jasti *et al*., 2007).

In this study, we identified amino acids in the β1-β2- and β11-β12-linkers of the palm domain that determine the presence of a sustained current in sASIC1b. Moreover, our results indicate that the β1-β2- and β11-β12-linkers are dynamic during gating and come in close apposition in the desensitized state. Hindrance of this tight apposition destabilizes the desensitized state inducing sustained re-opening of the channel. Covalently linking the two linkers traps the channel in the desensitized state. These

linkers have a similar role in rASIC1a, suggesting that they have a conserved role for ASIC1 gating. The crucial role of these two linkers makes them interesting targets for drugs that modulate ASIC gating.

4.3 Materials and Methods

4.3.1 Molecular Biology

Chimeras of rat ASIC1a and shark ASIC1b were obtained by recombinant PCR. Amino acids substitutions were generated by site-directed mutagenesis using standard protocols. KAPPA HiFi polymerase (peqlab, Erlangen, Germany) was used for all PCR reactions and PCR- derived fragments were controlled by sequencing. All constructs were cloned in the oocyte expression vector pRSSP, which is optimized for functional expression in *Xenopus* oocytes (Bässler *et al*., 2001). Using the mMessage mMachine kit (Ambion, Austin, TX), capped cRNA was generated by SP6 RNA polymerase from linearized plasmids.

4.3.2 Electrophysiology

Surgical removal of oocytes was done as described elsewhere (Springauf and Gründer, 2010). Between 0.016 and 8 ng cRNA were injected into stage V or VI oocytes of *Xenopus laevis*, oocytes were kept in OR-2 medium (in mM: 82.5 NaCl, 2.5 KCl, 1.0 Na_2HPO_4, 5.0 HEPES, 1.0 $MgCl_2$, 1.0 $CaCl_2$, and 0.5 g/liter polyvinylpyrrolidone) at 19°C, and studied 24 – 72h after injection. Whole cell currents were recorded with a TurboTec 03X amplifier (npi electronic, Tamm, Germany) using an automated, pump-driven solution exchange system together with the oocyte testing carousel controlled by the interface OTC-20 (npi electronic) (Madeja *et al*., 1995). With this system, 80% of the bath solution (10–90%) is exchanged within 300 ms (Chen *et al*., 2006). Data acquisition and solution exchange were managed using CellWorks version 5.1.1 (npi electronic). Data were filtered at 20 Hz and acquired at 1 kHz. Holding potential was -70 mV, except when otherwise indicated. All experiments were performed at room temperature (20 - 25°C). The bath solution for two-electrode voltage clamp contained (in mM) 140 NaCl, 1.8 $CaCl_2$, 1.0 $MgCl_2$, and 10 HEPES. For solutions with a pH ≤ 6.6, HEPES was replaced by MES.

2-aminoethyl methanethiosulfonate (MTSEA) (Toronto Research Chemicals, North York, Canada) was dissolved in bath solution and kept on ice when not in use. Fresh solutions were prepared every 20 minutes to ensure desired concentrations. Wild-type channels showed no detectable changes upon exposure to MTS compounds, DTT or H_2O_2. Before application, pH was adjusted for bath solutions containing MTS compounds, DTT or H_2O_2.

4.3.3 Data analysis

Data were collected and pooled from at least two preparations of oocytes isolated on different days from different animals. Data were analyzed with the software IgorPro (Wave metrics, Lake Oswego, OR).

Concentration response curves were fit to the Hill-Function

$$I = 1/(1 + (EC_{50}/[H]^n)) ,$$

where EC_{50} is the pH at which half-maximal activation/desensitization of the transient current component was achieved, and n is the Hill-coefficient.

Current decay kinetics of the transient currents were fit with a mono-exponential function:

$$I = A_0 + Ae^{-1/\tau} ,$$

where A_0 is the relative amplitude of the non-desensitizing component, A is the relative amplitude of the desensitizing component and τ is the time constant of desensitization.

Current decay kinetics of the slow “sustained” currents of sASIC1b-wt were best fit with the sum of two exponential components

$$I = A_0 + A_1e^{-1/\tau 1} + A_2\text{-}^{1/\tau 2} ,$$

where A_0, A_1, and A_2 are the relative amplitudes of the various components, and τ_1 and τ_2 are the slow and fast time constants, respectively.

Results are reported as means ± S.E.M. They represent the mean of n individual

measurements on different oocytes. Statistical analysis was done with Student's unpaired *t* test.

4.4 Results

Fig. 4.1 illustrates the gating kinetics of rat ASIC1a (rASIC1a) to mild and strong acidification (pH 6.4 and 5.0). Application of pH 6.4 or 5.0 elicits transient currents that completely desensitize with a time constant τ = ~2 sec. Recently we characterized ASIC1b from shark (sASIC1b) that shares 70 % amino acid identity with rASIC1a but desensitizes strikingly different (Springauf and Gründer). As illustrated in Fig. 4.1, application of pH 6.4 elicits transient sASIC1b currents that decline at least 40- fold faster than that of rASIC1a (τ < 50 msec). More importantly, desensitization is incomplete and a sustained current remains as along as pH is acidic. The level of the sustained current is ~5% of the peak current amplitude (Fig. 4.1). pH 5.0 also elicits transient currents and, in addition, shortly after the initial peak a second current component develops with variable amplitude around 50% of the amplitude of the transient current (Fig. 4.1). This second current component desensitizes much slower than the initial transient current. We referred to the typical transient ASIC current as the 'transient current' and to the second slow current component at pH 5.0 as the 'slow current' (Springauf and Gründer, 2010). Thus, both the kinetics and the extent of desensitization are different between sASIC1b and rASIC1a. The transient and slow sASIC1b currents are both unselective whereas the transient current is Na^+-selective (Springauf and Gründer, 2010). Moreover, the slow current cross-desensitizes the sustained but not the transient current (Springauf and Gründer, 2010). These characteristics suggest that the sustained and slow sASIC1b currents share a conformation that is different from the typical transient open conformation. Thus, there are clearly two different open states for sASIC1b that can be separated macroscopically.

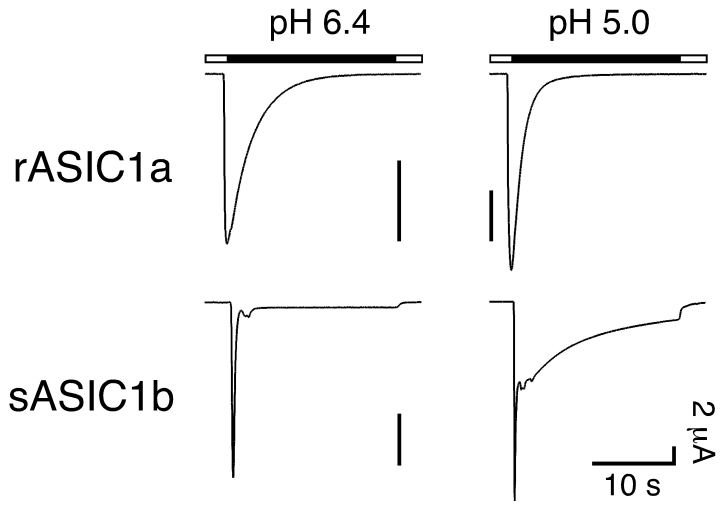

Figure 4.1. Representative current traces for rASIC1a (top) and sASIC1b (bottom) illustrating the different desensitization kinetics at mild and strong acidification (pH 6.4 and 5.0). The time constant of desensitization of transient rASIC1a currents was τ = 2.1 ± 0.2 sec at pH 6.4 (*n* = 13) and τ = 1.8 ± 0.2 sec at pH 5.0 (*n* = 13; *p* = 0.1). Desensitization was complete and no sustained current remained. Desensitization of the transient sASIC1b currents was much faster than for rASIC1a (τ < 50 msec, *n* = 13; *p* < 0.001) but incomplete. Desensitization of the second current component at pH 5.0 was best described by 2 time constants (τ_1 = 7 ± 0.4 sec and τ_2 = 2.1 ± 0.4 sec; *n* = 6). Note that current amplitudes at pH 5.0 were larger than at pH 6.4.

The slight delay of onset of the slow current at pH 5.0 suggests that the second unselective open state is reached from the desensitized state, which can be described by the following kinetic scheme:

$$C + H^+ \longleftrightarrow O_1 \cdot H^+ \longleftrightarrow D \cdot H^+ \longleftrightarrow O_2 \cdot H^+$$

This scheme is solely intended to illustrate the basic idea of two macroscopically separable open states, O_1 and O_2, and for the sake of simplicity it does not incorporate further closed and open states. The scheme implies that sASIC1b opens to a Na^+-selective open state O_1 from which it quickly reaches the desensitized state D, from which it reopens to an unselective open state O_2. It follows that the desensitized state of sASIC1b is energetically unstable, whereas for most other ASICs, including rASICa, it is stable in the continued presence of H^+ and channels do not reopen. Since the sustained sASIC1b current is comparatively small, at equilibrium most (> 90%) of the channels are probably in the desensitized state and few channels (< 10%) are in the open state O_2.

4.4.1 The proximal ectodomain controls sustained opening of ASIC1

To identify the amino acids that determine sustained opening of sASIC1b, we generated a series of chimeras, in which we exchanged different parts of the

extracellular domain (ECD) of sASC1b by corresponding sequences from rASIC1a, and measured currents at pH 6.4 and 5. First, we exchanged the whole ECD of sASIC1b. The resulting chimera (srs6) showed transient inward currents upon application of low pH (Fig. 4.2). At pH 5, currents desensitized completely with a time constant τ = 1.5 ± 0.2 sec (*n* = 14), not significantly different from rASIC1a (*p* = 0.44). Moreover, the desensitization rate at pH 6.4 was similar to that at pH 5 (Fig. 4.2).

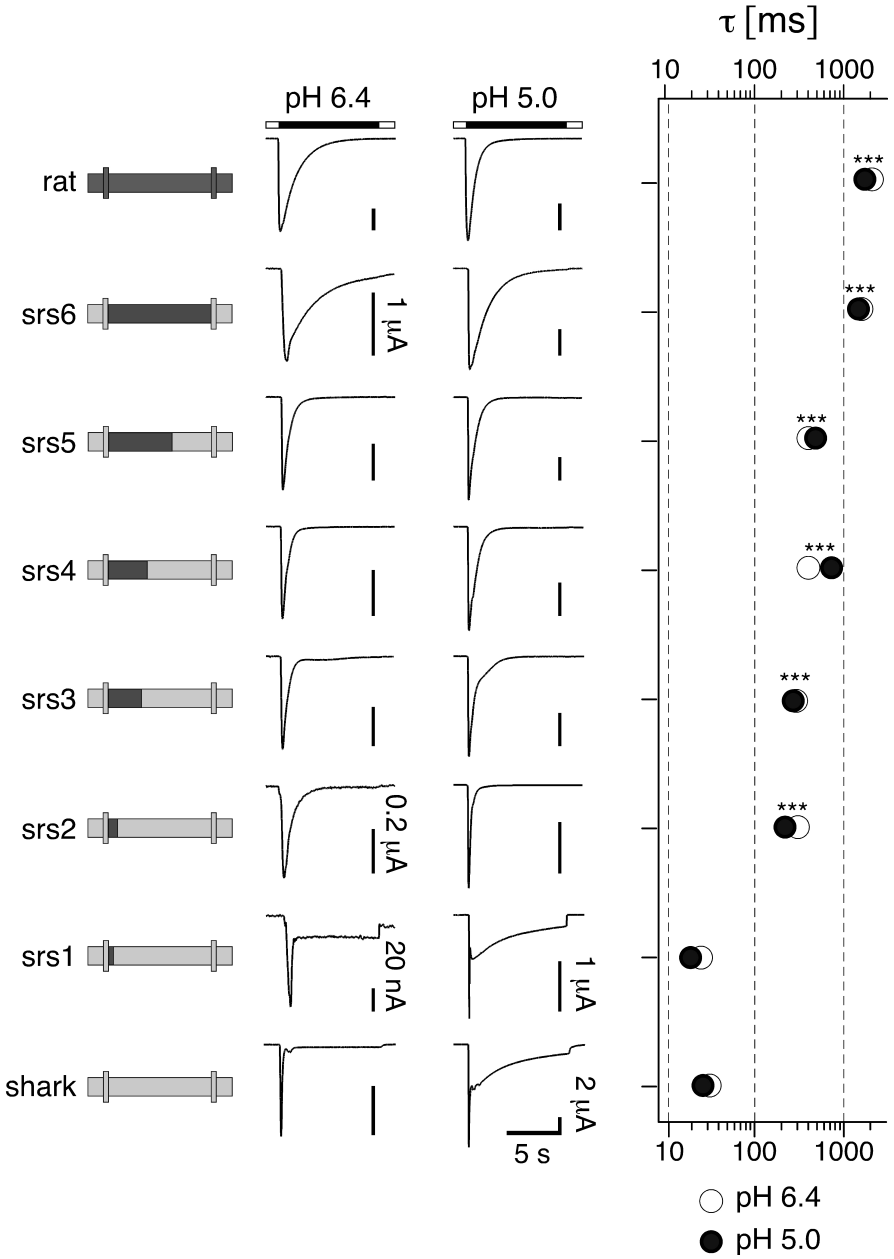

Figure 4.2. A small region shortly after TMD1 determines sustained opening of sASIC1b. Left, schematic drawings of rASIC1a and sASIC1b and chimeras. Middle, representative traces of currents at pH 6.4 and 5.0. Scale bars correspond to 2 µA, except when otherwise indicated. Right, time constants of desensitization of the transient current at pH 6.4 (open circles) and 5 (filled circles). n > 6. ***, p < 0.001 (compared to sASIC1b).

Thus, desensitization of this chimera was indistinguishable from rASIC1a, showing that the ECD determines the kinetics of desensitization and the presence of a sustained current in ASIC1. Therefore, we substituted gradually smaller parts of the ECD of sASIC1b. Substitution of either the first two-thirds or the first one-third of the ECD of sASIC1b (chimeras srs5 and srs4) yielded channels that desensitized ~3-times more rapidly than rASIC1a currents (at pH 5: τ = 0.7 ± 0.1 sec, *n* = 14, and τ = 0.5 ± 0.04 sec, *n* = 29, respectively; *p* < 0.001) and > 10-times more slowly than sASIC1b currents (*p* < 0.001). For both chimeras the desensitization rate at pH 6.4 was similar to that at pH 5 (Fig. 4.2). Most importantly, both chimeras desensitized completely to pH 6.4 and pH 5 and there was no sustained or slow current. Thus, the first one-third of the ECD of sASIC1b is necessary for the fast desensitization and the presence of the slow sustained current of this channel.

Substitution of either the first 123 or the first 24 amino acids of the sASIC1b ECD (chimeras srs3 and srs2) had essentially the same effect: the kinetics of desensitization was intermediate to rASIC1a and sASIC1b (at pH 5: τ = 0.3 ± 0.02 sec, *n* = 15, and τ = 0.2 ± 0.02 sec, *n* = 13, respectively; *p* < 0.001) and similar at pH 6.4 and pH 5. Moreover, there was no sustained or slow current. When we substituted only the first 14 amino acids of the ECD, we obtained a chimera (srs1) with a very different desensitization kinetics: desensitization of the transient current was very fast (τ < 50 msec) and incomplete. Thus, this chimera desensitized basically as sASIC1b wild type. In summary, the most striking difference in desensitization was observed between chimeras srs1 and srs2, which differ in only 7 amino acids.

The results obtained with the chimeras between sASIC1b and rASIC1a revealed that a small region of the ECD (residues 109 – 115) shortly after TMD1 is necessary for the presence of a sustained current at pH 6.4 and a slow current at pH 5. Moreover, in agreement with a previous report (Coric *et al*., 2003), this same region largely determines the kinetics of desensitization of the transient current; other regions that determine the kinetics of desensitization to a lesser extent seem to be scattered over the ECD. As is shown in Fig. 4.3, the critical region lies in a linker that connects β-sheet 1 of the palm domain to β-sheet 2 of the β-ball. We next analyzed in more detail the effect on desensitization of these 7 amino acids, Met109 – Tyr115, in the β1-β2 linker.

4.4.2 Amino acids 109 - 111 control sustained opening of ASIC1; amino acid 110 is especially important

A previous study identified an amino acid triplet in the proximal ECD as a determinant of the slow desensitization kinetics of rASIC1a (Coric *et al*., 2003). This triplet is S83QL in rASIC1a and P112FM in sASIC1b and falls into the critical region identified by our chimeras (Fig. 4.3). Therefore, we next substituted the PFM triplet of sASIC1b by the SQL triplet of rASIC1a. sASIC1b-SQL desensitized rapidly with a time constant τ < 50 msec (n = 10) and it still had a sustained current at pH 6.4 and a slow current at pH 5 (Fig. 4.4A), clearly showing that the PFM triplet is not necessary for sustained sASIC1b opening. However, the amplitude of the slow current at pH 5.0 was significantly (p < 0.001) decreased compared to sASIC1b-wt and was about 10% of the initial fast transient current amplitude. Unexpectedly, although due to the fast desensitization we cannot exclude some slowing of the desensitization of sASIC1b by the SQL substitution, the SQL triplet did not determine slow desensitization kinetics of the transient sASIC1b current (Fig. 4.4A).

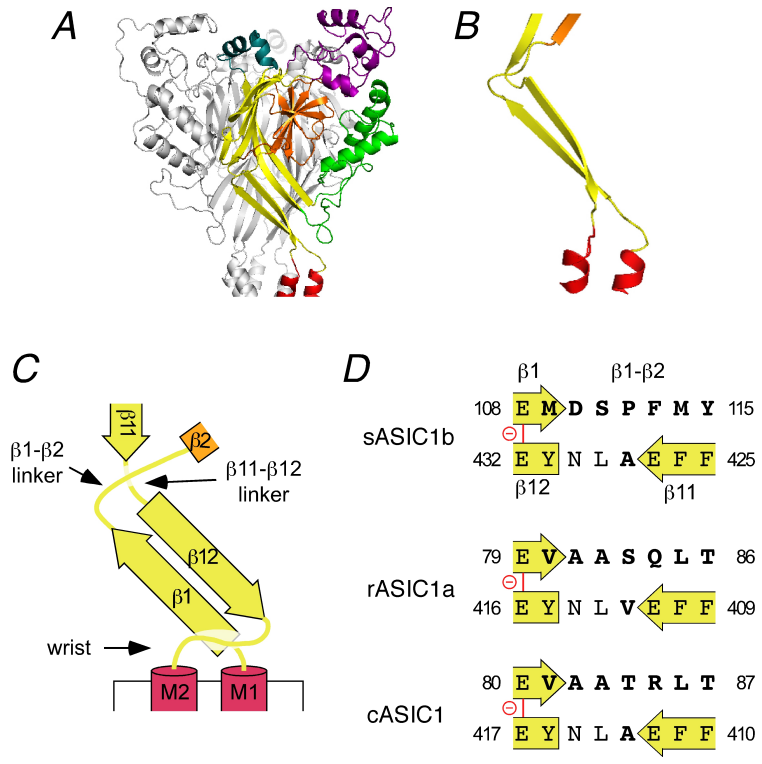

Figure 4.3. Residues 109 – 115 of sASIC1b localize to the β1- β2 linker. A, Ribbon representation of the desensitized cASIC1 structure. The different domains of the ECD are shown in different colors (TMDs in red, palm in yellow, thumb in green, knuckle in turquoise, finger in purple, and β-ball in orange). B, β-sheets 1 and 12 from one subunit and the linkers that connect them to β-sheets 2 and 11, respectively, are shown. C, Schematic representation of (B). D, Amino acid sequences of the β1-β2- and the β11-β12-linkers of sASIC1b, rASIC1a, and cASIC1, respectively. The carboxyl-carboxylate pair between β-sheets 1 and 12 is illustrated by a red line.

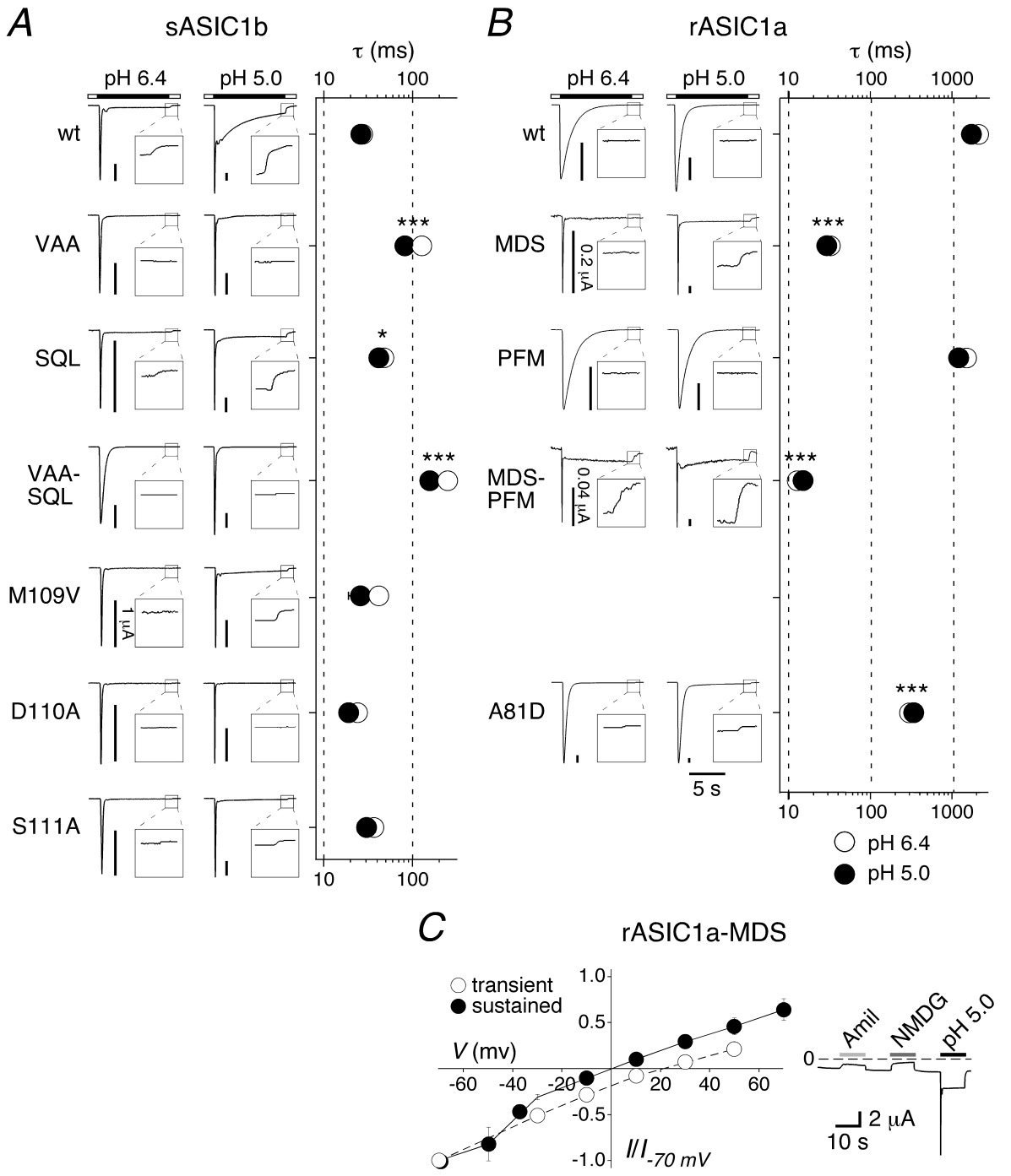

Figure 4.4. Aspartate 110 is most crucial for sustained opening of sASIC1b. A, B, Left, representative current traces at pH 6.4 and 5.0 for sASIC1b (A), rASIC1a (B), and amino acid substitutions in the β1-β2 linker. Scale bars correspond to 2 µA, except when otherwise indicated. The insets show the current decline after washout of acidic pH on a 4-fold expanded scale. Right, time constants of desensitization of the transient current at pH 6.4 (open circles) and 5 (filled circles). n > 8. *, p < 0.05, ***, p < 0.001 (compared to wild-type). C, Left, current–voltage relationship for the transient and the sustained current of rASIC1a-MDS at pH 5.0. Channels had been repeatedly activated at different holding potentials and currents normalized to the current at -70 mV. Absolute values of the current amplitudes at −70 mV were 7.2 ± 1.7 µA (transient current; n = 11), and 0.77 ± 0.13 µA (sustained current; n = 10), respectively. Right, representative current trace illustrating constitutive activity of rASIC1a-MDS. Amiloride (1 mM) and substitution of Na^+ by the large cation $NMDG^+$ reduced the background current revealing some constitutive activity of rASIC1a-MDS at pH 7.4.

We then substituted in sASIC1b the three amino acids just upstream of the PFM triplet, M109DS, by those of rASIC1a, V80AA. sASIC1b-VAA desensitized rapidly with a time constant τ < 100 msec (*n* = 16) but strikingly it no longer had a sustained current at pH 6.4 nor a slow current at pH 5 (Fig. 4.4A), clearly showing that the MDS triplet in sASIC1b is necessary for sustained sASIC1b opening. Combined substitution of both triplets, MDS and PFM, by VAASQL yielded a channel that had no sustained openings and desensitized with a time constant τ = 160 ± 11 msec (*n* = 23), similar to chimera srs2 (*p* = 0.13; Fig. 4.4A). These results demonstrate that both triplets, MDS and PFM, contributed to the kinetics of desensitization of the sASIC1b current, but that only the MDS triplet was necessary for sustained opening of sASIC1b.

To further define the role of individual amino acids within the MDS triplet for sASIC1b desensitization, we substituted the three amino acids individually by those found in rASIC1a, (V, A, A, respectively). sASIC1b with any of the three individual substitutions, M109V, D110A, and S111A, desensitized very rapidly (τ < 50 msec, *n* = 8, Fig. 4A). sASIC1b-M109V had no sustained currents at pH 6.4 but still at pH 5. In contrast, sASIC1b-D110A had no sustained currents at pH 6.4 or at pH 5 (Fig. 4.4A), not even at pH 4 (not shown). sASIC1b-S111A still had sustained openings at pH 6.4 and slow openings at pH 5. Collectively, these results show that the MDS triplet in the proximal ECD is necessary for sustained sASIC1b opening and that D110 has an especially crucial role within the triplet.

To further corroborate these findings we did inverse substitutions in rASIC1a (Fig. 4.4B). rASIC1a-PFM desensitized slightly faster than rASIC1a wild type (τ = 1.2 ± 0.14 sec, *n* = 10, compared with τ = 1.8 ± 0.16 sec, *n* = 13; *p* = 0.12) and had no sustained or slow current (Fig. 4.4B), showing that this triplet is not sufficient for sustained opening of rASIC1a. In sharp contrast, rASIC1a-MDS desensitized much faster than rASIC1a wild type (τ < 50 msec, *n* = 10; *p* < 0.001) and displayed robust sustained currents at pH 5 (Fig. 4.4B). Combined substitution of the two triplets, VAA and SQL, by MDSPFM had similar effects as substitution of VAA by MDS alone: fast desensitization of the transient current (τ < 50 msec, *n* = 7) and sustained openings at pH 6.4 and pH 5 (Fig. 4.4B). These findings clearly show that the MDS triplet is not only necessary for sustained opening of sASIC1b but also sufficient to introduce sustained opening into rASIC1a. Since D110 had an especially prominent role for sustained opening of sASIC1b, we substituted the corresponding amino acid in

rASIC1a, A81, by a D. rASIC1a-A81D desensitized significantly faster (τ = 340 ± 50 msec, n = 11; p < 0.001) than rASIC1a wild-type and showed sustained opening with an amplitude of 2% of the transient current at pH 5 (Fig. 4.4B), showing that a D at this position is a determinant of fast desensitization and is sufficient to introduce sustained opening in rASIC1a.

Sustained sASIC1b currents are unselective whereas transient currents are Na^+-selective (Springauf and Gründer, 2010). In agreement, reversal potentials of sustained rASIC1a-MDS currents were also significantly shifted by 20 mV to the left compared to transient currents (1 ± 2 mV compared with 21 ± 3 mV; n = 10; p < 0.001; Fig. 4.4C). The reversal potential of the transient current was also less positive than expected for a Na^+-selective ion pore. This result is likely explained by low constitutive activity of rASIC1a-MDS at pH 7.4, as revealed by amiloride block and sensitivity of the background current to exchange by the large cation $NMDG^+$ (Fig. 4.4C). Constitutive activity will lead to Na^+-uptake and consequently shift the Na^+ equilibrium potential. Thus, the MDS triplet introduces unselective sustained currents into rASIC1a; some sustained activity is even induced at pH 7.4.

4.4.3 Accessibility of residue 110 is state-dependant.

By which mechanism does an aspartate at position 110 (in sASIC1b) keep the ASIC1 pore constitutively open? One possibility is that this residue moves during the gating transitions of ASIC1 and that it sterically destabilizes the desensitized conformation. To get evidence for movement of this residue during gating of ASIC1, we assessed the accessibility of residue 110 of sASIC1b to modification by cysteine-reactive 2-aminoethyl methanethiosulfonate (MTSEA), a positively charged MTS reagent. Introduction of a cysteine at position 110 resulted in channels that desensitized rapidly and did not have a sustained current (Fig. 4.5A), similar to the introduction of an alanine at the same position (Fig. 4.4A). We first investigated MTS-modification in the closed state (Fig. 4.5A). Application of a low concentration (0.5 µM) of MTSEA in the interval between applications of pH 6, dramatically altered the currents of sASIC1b-D110C: peak amplitude gradually increased two-fold and a robust sustained current appeared, which had an amplitude of ~30% of the peak current. After 5 applications of 10 sec duration the modification of the current was complete (Fig. 4.5A).

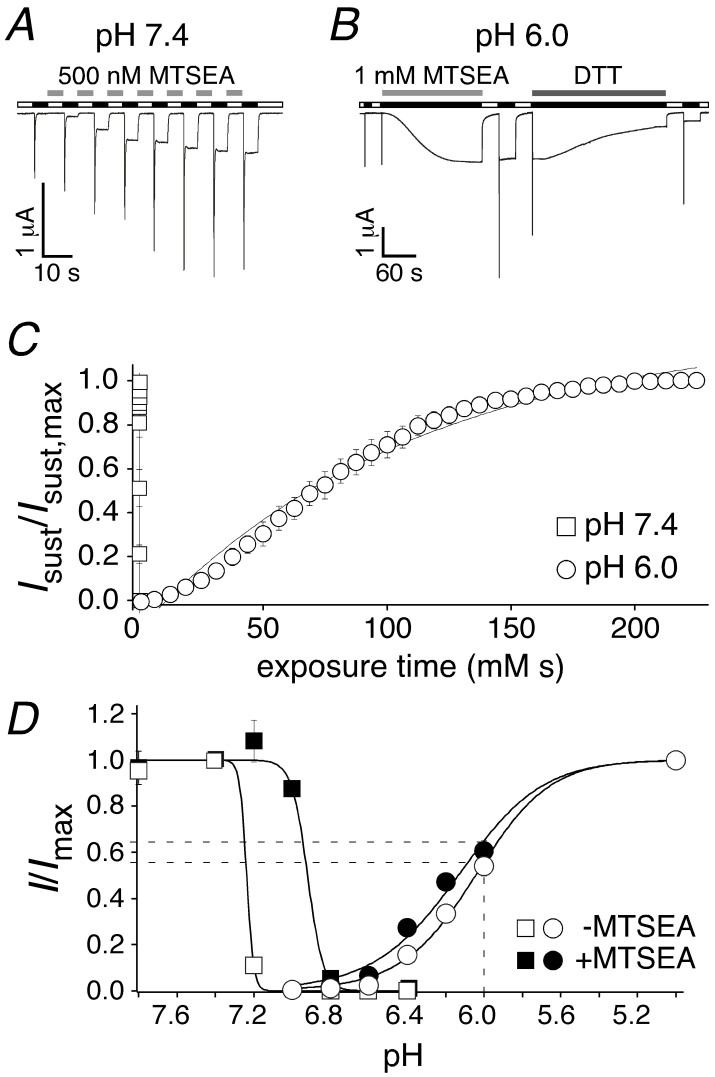

Figure 4.5. MTS-modification of sASIC1b-D110C leads to sustained opening. A, 500 nM MTSEA was applied for 5 sec in the interval between activation of the channel (at pH 7.4). Activation was with pH 6 for 5 sec. B, A higher concentration of MTSEA (1 mM) than in (A) was applied at pH 6 when channels were desensitized. Note also the different time scales in panels (A) and (B). The sustained currents could be reversed by application of 10 mM DTT. C, Increase in sustained currents as a function of exposure time (time exposed X concentration MTSEA) when MTSEA was applied at pH 7.4 (open squares) or at pH 6 (open circles). D, Activation curves (circles) and SSD curves (squares) for peak currents of sASIC1b-D110C before (open symbols) and after MTSEA modification (100 µM for 60 sec at pH 7.4; filled symbols). The dotted lines illustrate the expected increase in peak current at pH 6 by MTS modification.

For wild-type sASIC1b, MTSEA had no effect on the peak amplitude or on the appearance of the sustained current (not shown), suggesting that MTSEA specifically modified C110.

Application of a 2,000-fold higher MTSEA concentration (1 mM) at pH 6.0 (instead of pH 7.4) similarly led to the slow appearance of a sustained current (Fig. 4.5B), suggesting that MTSEA also modified the channel when it was in the desensitized conformation, albeit with a dramatically smaller reaction rate (see below). After

recovery at pH 7.4, the amplitude of the transient current also was increased, further suggesting MTSEA modification of sASIC1b-D110C at pH 6.0. Application of the reducing agent DTT (10 mM) reversed the increase in sustained current (Fig. 4.5B). Together these results suggest that MTSEA covalently modified C110 and that this modification strongly increased peak amplitude and enables sustained opening of sASIC1b. MTSEA-modification was faster at pH 7.4 than at pH 6 albeit a 2.000-fold smaller concentration used to modify the channel. Consequently, exponential fits of the fractional increase of the sustained current vs. exposure time (in mM x seconds; Fig. 4.5C) yielded a reaction rate of 100,000 M^{-1} sec^{-1} at pH 7.4 that was 22,000-fold higher than at pH 6 (4.6 M^{-1} sec^{-1}; $p < 0.005$). Thus at pH 7.4, C110 was modified by MTSEA with a rate comparable to mercaptoethanol in solution (Stauffer and Karlin, 1994), suggesting unhindered access to this residue in the closed conformation.

The increase of the peak current amplitude after MTSEA modification suggested an increased apparent H^+ affinity. However, MTSEA modification (100 µM for 60 sec) shifted apparent H^+ affinity of activation only slightly, showing that an increased apparent H^+ affinity cannot explain the large increase in peak current amplitude. In contrast, steady-state desensitization (SSD) curves were significantly shifted to the right by ~0.3 pH units ($p < 0.001$; Fig. 4.5D) so that larger concentrations of H^+ were needed to induce SSD. Similar to the appearance of a sustained current, this requirement for larger concentrations of H^+ to induce SSD after MTSEA modification further suggests that MTSEA destabilized the desensitized state of sASIC1b.

The profound difference in reaction rate at pH 7.4 versus 6.0 could be due to a dependence of the modification on the state of the channel (closed vs. desensitized) or on the pH (pH 7.4 vs. 6). To differentiate between these possibilities, we used the dependence of SSD on extracellular Ca^{2+} (Babini *et al* ., 2002) to find a single pH at which channels were predominantly in the desensitized or in the closed state, respectively, depending solely on the extracellular Ca^{2+} concentration (but not on pH). We determined SSD-curves in the presence of 1 mM and 20 mM Ca^{2+} with and without MTS modification. SSD curves were shifted by ~0.4 pH units by the different Ca^{2+} concentrations and by about the same amount by MTS modification (Fig. 4.6A). We chose pH 7.0 to determine the reaction rate of MTS modification because at this pH and 1 mM Ca^{2+}, all unmodified channels were in the desensitized conformation, whereas at 20 mM Ca^{2+}, ~50% of the unmodified channels were desensitized and the other 50% were closed (Fig. 4.6A).

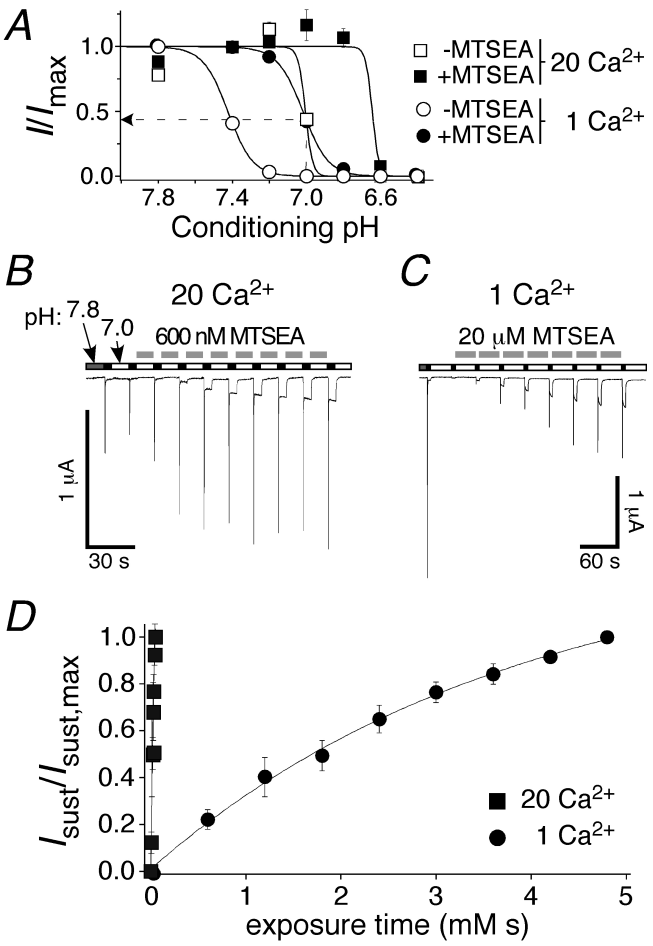

Figure 4.6. MTS-modification of sASIC1b-D110C is state-dependent. A, SSD curves for peak currents of sASIC1b-D110C in 1 mM Ca^{2+} (circles) and 20 mM Ca2+ (squares), before (open symbols) and after MTSEA modification (100 µM for 60 sec at pH 7.4; filled symbols). The dotted line illustrates the partial desensitization at pH 7 and in 20 mM Ca^{2+} (before MTS modification). B, 600 nM MTSEA was applied in 20 mM Ca^{2+} for 10 sec in the interval between activation (pH 6, 5 sec) of the channel. C, A higher concentration of MTSEA (20 µM) than in (B) was applied in 1 mM Ca^{2+} for 30 sec in the interval between activation (pH 6, 5 sec) of the channel. Note also the different time scales in panels (B) and (C). D, Increase in sustained currents as a function of exposure time (time exposed X concentration MTSEA) when MTSEA was applied in 20 mM Ca^{2+} (open squares) or in 1 mM Ca^{2+} (open circles). For both Ca^{2+} concentrations, conditioning pH was 7.0.

We argued that the partial desensitization with 20 mM Ca^{2+} might not strongly affect the reaction rate, because MTS modification happened so quickly at pH 7.4 that it should quickly absorb modified channels into the closed state. In fact, reaction rate at pH 7, 20 mM Ca^{2+}, was not significantly different (35,000 M^{-1} sec^{-1}, n = 4; p = 0.2) than at pH 7.4 and 1.8 mM Ca^{2+} but ~100-fold higher than with 1 mM Ca^{2+}, (320 M-1 sec-1, n = 4; p < 0.05; Fig. 6B and C), clearly demonstrating state-dependence of the MTS-modification. Reaction rate at pH 7, 1 mM Ca^{2+}, was ~70-fold higher than at pH 6, suggesting some pH dependence of the modification (Karlin and Akabas, 1998). But in any case the significantly faster reaction rate at pH 7 with 20 mM Ca^{2+} than

with 1 mM Ca^{2+} clearly shows that the modification of C110 by MTSEA was state-dependant and suggests that residue 110 is well accessible for MTSEA in the open conformation and moves upon desensitization to become less accessible.

The introduction at residue 110 of a long side chain with a positive charge had dramatic effects on sASICb currents. To confirm this result, we introduced a permanent positive charge at this position. The side chain of a lysine closely resembles the side chain of a cysteine modified by MTSEA (Fig. 4.7). As expected from this close resemblance, the kinetics of currents carried by sASIC1b-D110K was virtually identical to those carried by sASIC1b-D110C after MTSEA modification: the transient current was followed by a large sustained current that was much more pronounced than for wild-type sASIC1b (~60% of the peak current at pH 6.4 and >100% at pH 5; Fig. 7). This result confirms that, at position 110, a long side chain with a positive charge strongly favors sustained opening of sASIC1b.

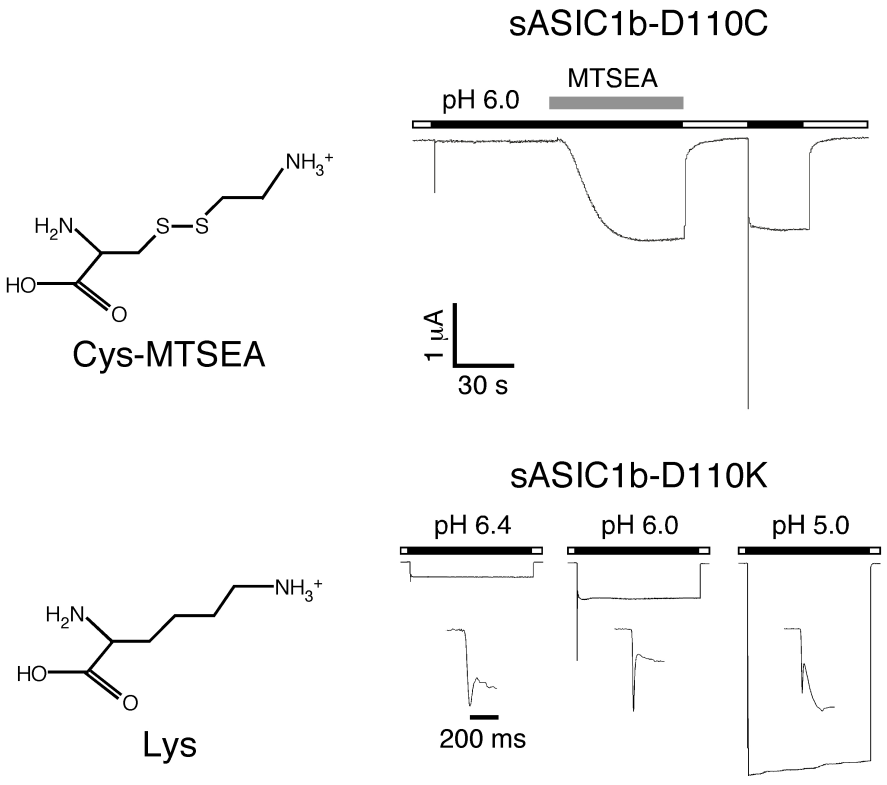

Figure 4.7. A Lys at position 110 mimics MTSEA-modification. Left, chemical structures of an MTSEA-modified cysteine and a lysine. Right, representative current traces for MTSEA-modification of sASIC1b-D110C (top) and for sASIC1b-D110K (bottom). Currents for sASIC1b-D110K are shown at three different pH values. The current rise time is also shown on an expanded time scale.

4.4.4 Residue 110 is in close contact with residue 428 in the β11- β12 linker

Results so far suggest that certain residues at position 110 destabilize the desensitized conformation of sASIC1b, leading to constitutive opening of the channel. Amino acids with short, neutral side chains (Ala, Cys) do not destabilize the desensitized conformation, whereas the desensitized conformation becomes slightly destabilized by a negatively charged side chain (Asp) and strongly destabilized by a large, positively charged side chain (MTSEA-modified Cys, Lys). In addition, state-dependence of MTS-modification shows that residue 110 becomes less accessible in the desensitized conformation, suggesting that in this conformation its side chain gets buried in a pocket of the protein.

What is the structural basis for destabilization of the desensitized conformation and sustained opening of sASIC1b by large, charged residues? Given the high homology of sASIC1b with chicken ASIC1 (cASIC1; 70% amino acid identity), we considered the crystal structure of cASIC1 as a good model for the desensitized state of sASIC1b and modeled an aspartate at the position corresponding to D110 of sASIC1b (A82). Structural analysis showed that an Asp residue at position 82 of cASIC1 is not easily accommodated because this residue is indeed buried. An Asp could form an H-bond with Asn415 but at the same time there would be unfavourable interactions with the main chain oxygens of Ala413, which would probably trigger some local structural changes.

The unfavourable interaction of D82 with the main chain oxygen atoms of Ala413 in the β11- β12 linker (Fig. 4.3) suggested that such an interaction might destabilize the desensitized conformation and lead to sustained opening of sASIC1b. To test this prediction, we substituted the residue corresponding to chicken Ala413 in sASIC1b (A428) by a negatively charged amino acid (D). The resulting channels (sASIC1b-A428D) had a normal transient current, followed by a sustained current that was much larger than the sustained current of wild-type sASIC1b (Fig. 4.8), confirming that this exchange further destabilized the desensitized state of sASIC1b. Since sASIC1b-D110A had no sustained current we made the double-substitution D110A-A428D. The resulting channels had a phenotype that very much resembled that of wild-type sASIC1b (Fig. 4.8), providing further support for an interaction of amino acid 110 and 428. If both amino acids have short side chains, no sustained currents develop, if one has a negatively charged side chain, robust sustained currents develop, and if both have a negatively charged side chain, the resulting channels

have a strong sustained current with an amplitude similar to the transient current.

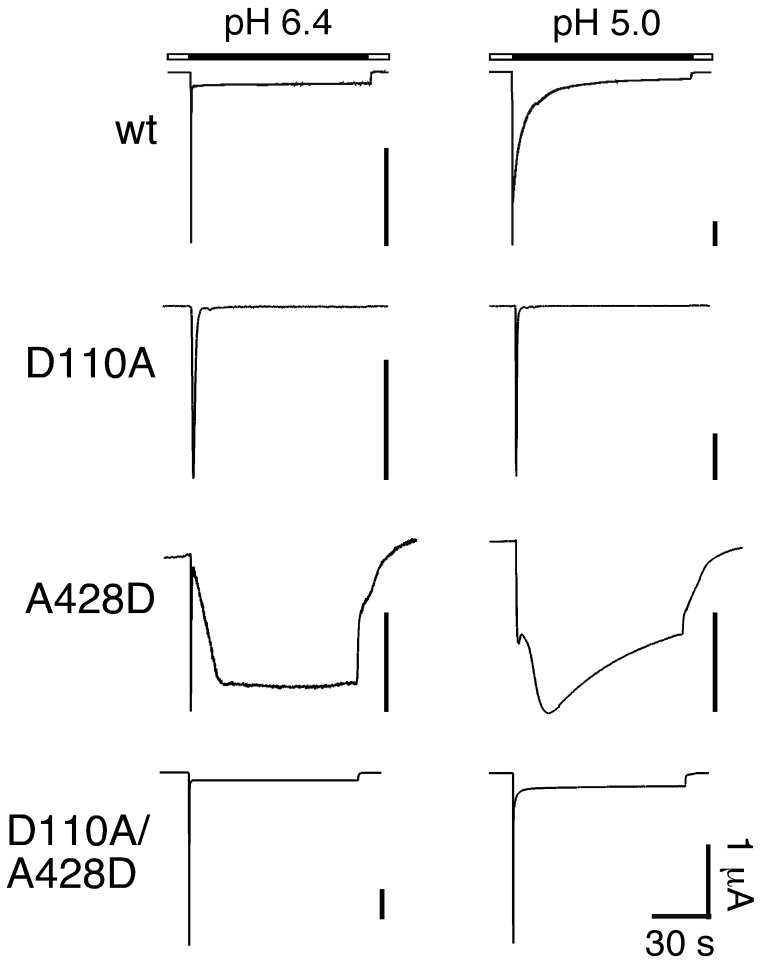

Figure 4.8. Representative current traces at pH 6.4 and 5.0 for sASIC1b-wt, -D110A, -A428D, and -D110A/A428D, respectively.

4.4.5 Cross-linking of residues 110 and 428 traps sASIC1b in the desensitized state

We searched for further evidence for a tight interaction of residues 110 and 428 in the desensitized conformation of the protein. When we modeled two cysteines at the corresponding residues in the cASIC structure and selected the best side chain rotamer conformations, the two S-atoms were at a distance of 2.9 Å (Fig. 4.9A), which would be compatible with the formation of an intramolecular disulfide bond. The discrepancy of ~1 Å between the observed and the ideal distance (2.05 Å) together with a non-perfect dihedral angle of ~120° (ideal is 90°) predicted a strained disulfide bond between C82 and C413.

To test this prediction we engineered two cysteines at positions 110 and 428 of

sASIC1b. After stimulation with pH 5, the resulting channels (sASIC1b-D110C/A428C) showed transient and sustained currents, both of comparatively small amplitude (Fig. 4.9C). Repeated activation with pH 5 further reduced current amplitudes (Fig. 4.9C), which is expected if a disulfide bond formed rapidly when the channels are desensitized in the presence of H^+, and if this disulfide bond trapped channels in the desensitized conformation.

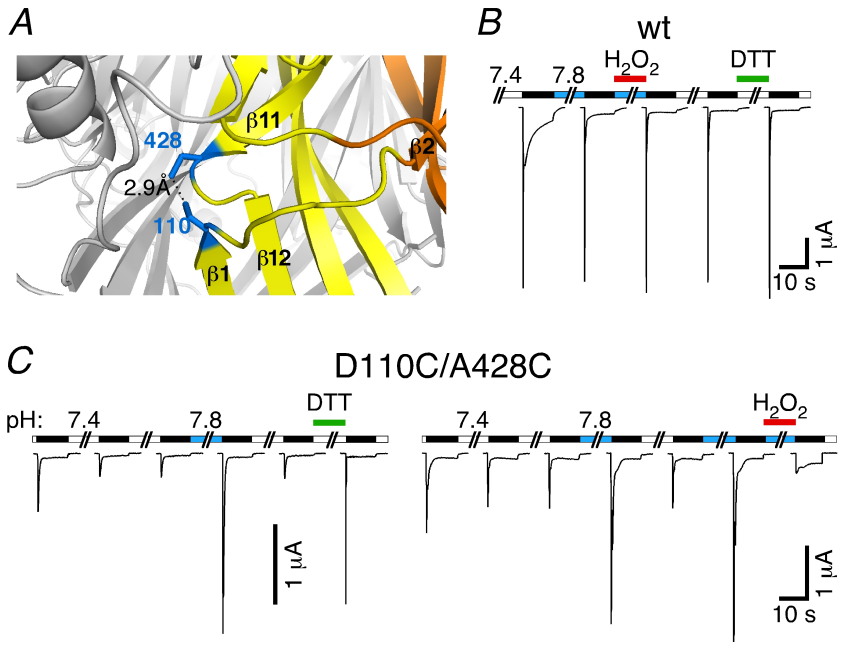

Figure 4.9. Cross-linking of residues 110 and 428 traps sASIC1b in the desensitized state. A, Left, detail from the cASIC1 crystal structure, in which two Cys residues had been modeled, one at position 82 and one at position 413 (corresponding to positions 110 and 428 of sASIC1b). Right, schematic representation with the two cysteines as blue bars. B, Reducing and oxidizing conditions had no effect on sASIC1b-wt currents. C, Left, sASIC1b-D110C/A428C current amplitude gradually decreased with repeated stimulation by ligand (pH 5.0). Switching the pH to 7.8 or reducing conditions strongly increased current amplitude. Right, oxidizing conditions strongly reduced current amplitude of sASIC1b-D110C/A428C.

We reasoned that the disulfide bond also might have formed spontaneously (at pH 7.4) and that spontaneous trapping explains the small current amplitudes when channels were activated the first time. In fact, switching the conditioning pH from 7.4 to 7.8 strongly increased the amplitude of the currents elicited by pH 5 (Fig. 4.9C), which is expected if the putative disulfide bond were under considerable strain and spontaneously hydrolyzes when the pH is slightly raised and the desensitized state further destabilized. Alternatively, the two Cys substitutions might have simply shifted the SSD curve. Application of the oxidizing reagent H_2O_2 (0.15 %) at pH 7.8 strongly reduced current amplitudes (Fig. 4.9C), which is not expected if Cys substitutions had

shifted the SSD curve and thus clearly argues for formation of a disulfide bond. Moreover, application of the reducing reagent DTT (10 mM) at pH 7.4 strongly increased current amplitudes (Fig. 4.9C), which is in agreement with hydrolysis of a disulfide bond and ensuing recovery from desensitization. Neither H_2O_2 nor DTT had an effect on sASIC1b wt (Fig. 4.9B). Together these results strongly suggest the spontaneous formation of a strained disulfide bond between C110 and C428, which trapped sASIC1b in the desensitized conformation. It follows that i) in the desensitized conformation both residues are in tight contact with each other, and that ii) both residues have to move a considerable distance away from each other for recovery from desensitization and the transition into the closed state.

We wanted to confirm the relevance of these findings for rASIC1a and introduced Cys residues at the corresponding positions of rASIC1a (residues 81 and 412; Fig. 4.3). For rASIC1a-A81C/V421C, at a conditioning pH 7.4, application of pH 6.4 induced currents of comparatively small amplitude. Repetitive activation further reduced current amplitudes (Fig. 4.10B). Such a sequential reduction is also known for ASIC1a-wt (Chen and Gründer, 2007) but was significantly more pronounced for the double-cysteine mutant (Fig. 4.10C), suggesting that a disulfide bond formed in the desensitized state at pH 6.4 and cumulatively trapped channels in this state. At conditioning pH 7.8 amplitudes were only slightly increased (Fig. 4.10B), suggesting that if a disulfide bond had formed it was under less strain than for sASIC1b. Application of 10 mM DTT, however, strongly increased the current amplitude (Fig. 4.10B), an effect that was not seen with rASICa wt (Fig. 10A) and which therefore strongly suggests formation of a disulfide bond that trapped channels in the desensitized state. In agreement with this conclusion, application of 0.15% H_2O_2 strongly decreased current amplitudes (Fig. 4.10B). Thus, rASIC1a-A81C/V421C reproduced the basic findings from sASIC1b- D110C/A428C, suggesting that the two critical residues also are in close apposition in rASIC1a.

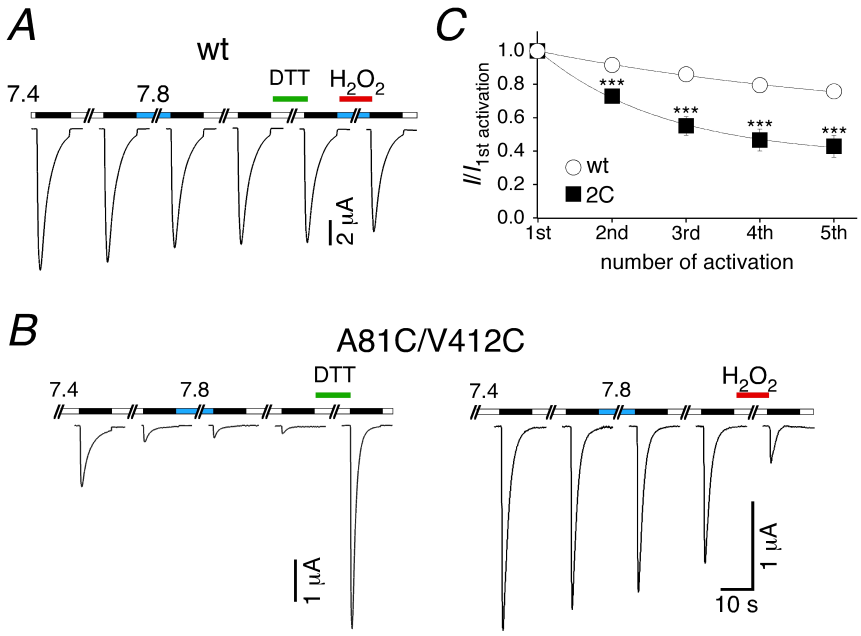

Figure 4.10. Cross-linking of residues 81 and 412 traps rASIC1a in the desensitized state. A, Reducing and oxidizing conditions had no effect on rASIC1a-wt currents. B, Left, rASIC1a-A81C/V412C current amplitude gradually decreases with repeated stimulation by ligand (pH 6.4). Switching the pH to 7.8 has no effect on current amplitude, whereas reducing conditions dramatically increased current amplitude. Right, oxidizing conditions reduced current amplitude of rASIC1a-A81C/V412C. C, Quantification of tachyphylaxis for rASIC1a-wt and -A81C/V412C ("2C"). Channels were repeatedly activated and current amplitudes normalized to the first amplitude. Repeated activation reduced rASIC1a-A81C/V412C currents significantly more strongly than wt currents. Absolute values of the initial amplitudes were 14.3 ± 2.5 µA (wt; n = 6), and 1.0 ± 0.2 µA (A81C/V412C; n = 6), respectively. Lines represent fits to a mono-exponential function. ***, $p < 0.001$.

4.5 Discussion

In this paper we present several-fold evidence that the interaction of the β1-β2- and β11-β12-linkers modulates desensitization gating of ASICs and that a pair of amino acids, each in one of the linkers, is especially crucial for this modulation. First, we identify a triplet of amino acids (M109DS) in the β1- β2-linker that determines sustained opening of sASIC1b (Figs. 2 and 4). Within this triplet, aspartate 110 has a predominant effect (Fig. 4.4). Second, we show that modification by MTS reagents of residue 110, when mutated to cysteine, strongly depends on the state of the channel: modification in the closed state happens at least 100-fold faster than in the desensitized state (Figs. 5 and 6), showing that residue 110 becomes partially buried in the desensitized state. Third, substitutions of residue 428 in the β11-β12 linker that tightly apposes with residue 110 in the desensitized conformation of cASIC also affect re-opening of sASIC1b (Fig. 4.8). Fourth, cysteines engineered at positions 110 and

428 lead to spontaneous formation of a disulfide bond that traps the channel in the desensitized state (Fig. 4.9). All these observations suggest the following model: β1-β2- and β11-β12-linkers are dynamic during ASIC gating and tightly appose in the desensitized conformation, occluding residue 110. Hindrance of this apposition destabilizes the desensitized state and leads to sustained re-opening. During recovery from desensitization, β1-β2- and β11-β12-linkers "open up" again, exposing residue 110 to solvent. Occlusion in the desensitized state and exposition in the closed state readily explains the state- dependence of MTS modification of residue 110. We found that introduction of the MDS triplet into rASIC1a is sufficient for robust sustained opening of the rASIC1a pore (Fig. 4.4). Moreover, a disulfide bond also formed between two cysteines in rASIC1, engineered at positions corresponding to 110 and 428, trapping rASIC1a in the desensitized state (Fig. 4.10). Thus, there is evidence that the interaction of this pair of amino acids has a general role for desensitization gating of ASIC1.

The spontaneous formation of the disulfide bond between residues 110 and 428 (Fig. 4.9) was surprising but is not without precedence. Two cysteines engineered into lobes of the ligand-binding domain of AMPA receptors also spontaneously form a disulfide bond, trapping the AMPA receptors in the desensitized state (Plested and Mayer, 2009). This spontaneous trapping has been interpreted as a significant mobility of the glutamate binding domains in the absence of ligand (Plested and Mayer, 2009). Similarly, spontaneous formation of the disulfide bond between residues 110 and 428 suggests conformational flexibility of the β1-β2- and β11-β12-linkers in the absence of H^+. Alternatively, ambient concentrations of H^+ in the extracellular medium and/or in the intracellular compartments, through which ASIC traffic on their way to the plasma membrane, may be high enough to induce opening and desensitization of ASICs with a low probability.

4.5.1 What is the basis for sustained openings?

We propose that in sASIC1b the interaction of D110 and A428 destabilizes the desensitized state, leading to re-opening of the ion pore. In this model, sustained currents would not reflect incomplete desensitization from the transient open state O_1 but rather re-opening from the desensitized state to a new open state O_2. Evidence for this model is first, the rebound of current that follows the transient current at low

pH (for example pH 5.0, Fig. 4.1; (Springauf and Gründer, 2010), and second, the different selectivity of the ion pore during transient and sustained openings (Springauf and Gründer, 2010). In the simplest case, it follows that a sustained current develops whenever channels enter the desensitized state. In fact, transient sASIC1b currents are always followed by sustained currents (Springauf and Gründer, 2010). This situation is different for rASIC3, an ASIC that shows transient currents at pH < 6.9 but sustained currents only at pH ≤ 5.0 (Waldmann *et al*., 1997; Salinas *et al*., 2009). For ASIC3, the development of sustained currents would thus require at least one additional H^+ binding step. Such additional protonation steps could also explain the slow sASIC1b currents, which develop at low pH and also desensitize (Fig. 4.1; (Springauf and Gründer, 2010). We speculate that slow structural relaxations accommodate β1-β2- and β11-β12-linkers at low pH (e.g. pH 5) and lead to slow desensitization of sustained currents.

A completely different way of generating sustained currents is by window currents, which are generated by the overlap of the activation and desensitization curves (Yagi *et al*., 2006). In the narrow window of overlap sustained currents are generated that can be calculated by the multiplication of the fractional activation and desensitization at a given pH. Thus, sustained window currents are mediated by the transient open state O_1 and do not require a separate open state O_2. Window currents have first been described for rASIC3 (Benson *et al*., 1999; Yagi *et al*., 2006) and are also generated by sASIC1b but only in the small pH range from 7.4 to 6.6 (Springauf and Gründer, 2010). Below pH 6.6, sustained sASIC1b currents are entirely unselective sustained currents (Springauf and Gründer, 2010), which we propose are mediated by the second open state O_2.

A sustained current that develops in the declining phase of a transient peak current is also characteristic for currents mediated by FMRFamide-activated Na^+ channel, FaNaC (Cottrell *et al*., 1990; Lingueglia *et al*., 1995), and Hydra Na^+ channels, HyNaCs (Golubovic *et al*., 2007; Dürrnagel *et al*., 2010), peptide-gated channels that are related to ASICs (Golubovic *et al*., 2007). The kinetics of the peptide-induced currents is very similar to sASIC1b currents only that the sustained currents are larger, amounting to 50-100% of the peak current amplitude (Lingueglia *et al*., 1995; Golubovic *et al*., 2007; Dürrnagel *et al*., 2010). Since HyNaCs are closely related to ASICs (Golubovic *et al*., 2007) and since their sustained currents are unselective cation currents (Golubovic *et al*., 2007; Dürrnagel *et al*., 2010) like the sustained

sASIC1b currents, we speculate that HyNaCs and perhaps FaNaC also re- open to a second open state from the desensitized state. Future studies will show whether this speculation is true and whether interactions of the β1-β2- and β11-β12-linkers also determine sustained opening of HyNaCs.

4.5.2 The role of the β1-β2- and β11-β12-linkers in desensitization gating

Results from previous studies that addressed desensitization gating of ASICs (reviewed in (Gründer and Chen, 2010) largely confirm our own findings. In ASIC3, residue 79 at the end of β-sheet 1 (corresponding to E108 in sASIC1b; Fig. 4.3), if replaced by a cysteine, cannot react with MTS reagents when channels are desensitized (Cushman *et al*., 2007), suggesting that it is deeply buried. In fact, in the crystal structure of desensitized cASIC1, β-sheets 1 and 12 tightly appose and E79 (E80 in cASIC1) forms a carboxyl-carboxylate pair with E417 (cASIC1) at the beginning of β-sheet 12 (Fig. 4.3; Jasti, 2007). In contrast, in the closed state residue 79 can react with MTS reagents with a rate of ~200 M^{-1} sec^{-1}, suggesting that the carboxyl-carboxylate pair forms only during desensitization and that the tight apposition between β-sheets 1 an 12 is not maintained in the closed state. The comparatively low reaction rate (reaction rate was 100,000 M^{-1} sec^{-1} for modification of D110 in the closed state; Figs. 4.5 and 4.6) indicates that residue 79 is partially buried also in the closed state of ASIC3. Moreover, MTS modification of ASIC3-E79C dramatically slowed desensitization (Cushman *et al*., 2007), suggesting that volume on residue 79 destabilizes the desensitized state by hindrance of the tight apposition of β-sheets 1 and 12. This is in agreement with our own results.

In rASIC1, the S83QL triplet in the β1-β2-linker (the triplet just following the MDS triplet; Fig. 4.3) is one determinant of desensitization kinetics (Coric *et al*., 2003), which suggests that it determines the energy barrier between open and desensitized states. This conclusion perfectly agrees with the notion that movement of the β1-β2-linker accompanies desensitization gating. In *Xenopus* ASIC1, the last residue of this triplet (M114 in sASIC1b), if replaced by a cysteine, is modified by MTS reagents with an equal rate (~100 M^{-1} sec^{-1}) in the closed and the desensitized states, suggesting that this residue is partially buried in both conformations of the protein (Li *et al*., 2010). Equal reaction rates do not provide evidence for rearrangement of this residue during desensitization. It was proposed that this residue interacts with a residue

(corresponding to N430 in sASIC1b; Fig. 4.3) in the β11-β12-linker (Li *et al*., 2010). No direct interaction was found, however, and both residues contribute independently to the stability of the desensitized state (Li *et al*., 2010). Thus, although those previous results confirm a general role of the β1-β2- and β11-β12-linkers for desensitization gating, our results highlight a tight interaction between D110 and A428 in those linkers of sASIC1b and show that this interaction controls sustained re-opening.

In summary, our results add to a better understanding of desensitization gating of ASICs and to the molecular basis of sustained ASIC currents. They identify the β1-β2- and β11-β12-linkers as a possible target for pharmacological modulation of ASIC activity.

5. General Discussion

5.1 The appearance of proton-sensitivity of ASICs

The first part of this work describes the identification of shark ASIC1b as a proton-sensitive ASIC and the characterization of the currents that are generated by this channel in response to various proton-concentrations and additionally sheds light on the development of proton sensitivity of Acid Sensing Ion Channels.

Several amino acids that were previously identified by mutational screening as crucial residues for proton sensitivity of ASIC1, namely Glu63, His72/His73 and Asp78 (Paukert et al., 2007), are entirely conserved in sASIC1b. Although previous publications reported the proton-insensitivity of shark ASIC1b (Coric et al., 2005) the striking conservation of these amino acids was the main reason for re-evaluating this issue.

The finding that sASIC1b indeed responded to extracellular acidification confirmed the importance of the four identified amino acids in sASIC1b and showed that we can predict the proton-sensitivity of an ASIC with some reliability, which also justifies the definition of a 'H^+ sensitivity signature'. Additionally, it reduced the number of proton-insensitive ASICs that contain the four crucial amino acids to one, which is zASIC2 from zebrafish. With respect to the remaining zASIC2 we speculate that this channel contains some unknown sequence features that might be responsible for the proton-insensitivity of zASIC2 and that cover the impact of the four crucial amino acids.

However, it has to be mentioned that this 'H^+ sensitivity signature' is not conserved in all ASICs that show sensitivity to protons. For example, the proton-sensitive zASIC1.1 does not contain the crucial histidine residues. Thus, there are still some exceptions that prevent an unequivocal prediction for proton sensitivity, solely based on the amino acid sequence.

The characterization of the proton sensitive shark ASIC1b led also to the question, when proton-sensitivity first appeared in ASICs. So far, shark ASIC1b is the most ancient ASIC that has been shown to be proton-sensitive, a fact that contradicts the earlier conclusion of an appearance of proton-sensitivity of ASICs with the rise of bony fishes.

Moreover, several other findings support the view that chordates even lower than cartilaginous fish express proton-sensitive ASICs. First of all, the genome of the

urochordate *Ciona* contains one ASIC gene that gives rise to two spliced forms (Coric et al., 2008) that also comprise the 'H^+ sensitivity signature'. This suggests that the proton-sensitivity of this ASIC should be also re-evaluated. Second, although the cloned ASIC1 from the jawless vertebrate lamprey was also identified as a proton-insensitive channel (Coric et al., 2005) and even though it does not contain the 'H^+ sensitivity signature' the lamprey genome possibly comprises other ASIC genes that contain the 'H^+ sensitivity signature' and thus also might be proton-sensitive. Even mammals contain ASICs such as ASIC2b and ASIC4, which are not proton-sensitive. However, ASIC2b was shown to be able to assemble with other proton-sensitive subunits to form heteromeric channels with distinct properties. If the genome of lamprey also contains other ASIC genes it could be possible that ASIC1 assembles with these subunits to form heteromeric and proton-sensitive channels. Recently, it was shown that lamprey ASIC1 can be converted into a channel that responds to extracellular acidification with non-desensitizing currents after replacement of only two residues in the proximal part of the extracellular domain (Li et al., 2010). One might speculate that the proton-insensitivity of ASICs from *Ciona* and lamprey are secondary acquired features caused by point-mutations early in evolution. On the other hand, the fact that the closely related HyNaC channels from the freshwater-polyp *Hydra magnipapillata* are activated by neuropeptides (Golubovic et al., 2007; Dürrnagel et al., 2010) suggests that ASICs from evolutionary early species could also be activated by other ligands than protons and that the first proton-sensitive ASIC evolved with the rise of cartilaginous fish.

5.2 Gating kinetics and the generation of sustained currents

In addition to the identification of shark ASIC1b as a proton-sensitive ion channel this work showed that the sustained current component is a striking feature of this channel and unique among the members of the ASIC subfamily.

Detailed characterization of this sustained current revealed several properties that distinguishes the sustained current of shark ASIC1b from the sustained currents of other ASICs:

(1) it is the most pH-sensitive sustained current (Fig. 3.7 A, B) that is not a window current (as known for ASIC3 (Yagi et al., 2006), and

(2) it can be blocked by amiloride (Fig. 3.5), different from the sustained currents of zebrafish ASIC4.1 and ASIC4.2 (Paukert *et al*., 2004*b*; Chen *et al*., 2007).

Although most ASICs exhibit only transient and completely desensitizing currents several studies pointed to an involvement of ASICs to acidic and inflammatory pain. But is it possible that channels with transient currents are able to function as sensors for long lasting stimuli? This paradox was solved when it was shown that pH activation and steady-state desensitizing curves of ASIC3 overlap (Yagi et al., 2007), thus providing a mechanism for ASIC3 to carry sustained currents. However, the window of overlap of those two curves is in a narrow pH range and the sustained currents of ASIC3 that are based on the window current are rather small compared to the transient currents elicited by strong acidification.

The first part of the results shows that sASIC1b also carries a bell-shaped window current at mild acidification between pH 7.4 and pH 6.6 (Fig. 3.7 A, B). However, also a second sustained current component developed at slightly more acidic pH values below pH 7.0. This shows that the sustained current between pH 7.0 and pH 6.6 is a mix of window current and an unselective sustained current. At pH 6.4 the window current no longer contributes to the sustained current (Fig. 3.7 A,B). Because the transient current was shown to be selective for sodium ions whereas the sustained current was an unselective current, we postulated that both current components are generated by different open states (O_1 and O_2) of the channel.

Further investigations uncovered the amino acids crucial for the generation of this sustained current in the β1-β2 linker region at the proximal part of the extracellular domain near the first α-helical transmembrane domain.

Powerful evidence for the importance of the amino acid triplet ($M^{109}DS$) and especially residue D^{110} in this linker region for generating sustained currents was provided by the observation that this sequence is not only necessary for the sustained current in shark ASIC1b but that it is also sufficient to introduce sustained currents in homomeric rat ASIC1a channels (Fig. 4.4).

Again, this approach revealed that a single aspartate (D^{110}) is sufficient for generating a sustained current effect (Fig. 4.4).

Furthermore, amino acid substitutions between shark ASIC1b and rat ASIC1a showed that the $M^{109}DS$ triplet induces not just a sustained current in ASIC1

channels but also influences the time constants of desensitization of shark ASIC1b and rat ASIC1a (Fig 4.4).

The picture that was drawn from these observations led to the conclusion that the amino acids in this linker region control the stability of the open state of the channel, which is partly displayed by the speed of desensitization, and the stability of the desensitized conformation, observable by the generation of the sustained current.

5.3 The crystal structure of chicken ASIC1 confirms observations of gating mutants and uncovers interacting regions

Since shark ASIC1b and chicken ASIC1 share 70% of their amino acids, the crystal structure of chicken ASIC1 (Fig. 1.5) also provides a good model for the desensitized state of shark ASIC1b.

The crystal structure provides information which can explain the importance of the amino acid triplet $M^{109}DS$ for the generation of the sustained current on the basis of unfavorable amino acid interactions in the desensitized state of the channel.

Modulation of the crystal structure of cASIC1 suggests that residue D^{110} in sASIC1b comes in close contact to residue A^{428} in the linker region between β11 and β12, near the second transmembrane domain. Mutation of D^{110} to an alanine yields a channel that no longer shows a sustained current (Fig. 4.8), whereas the A428D mutant displays a highly increased sustained current component compared to the wildtype shark ASIC1b (Fig. 4.8). Both mutant channels support predictions made by the crystal structure and endorse the idea that the sustained current of shark ASIC1b is indeed generated by unfavorable interactions between those two linker regions. Two neutral residues (alanine) at positions 110 and 428 do not show sterical forces and thus no sustained current is generated. When both positions carry negatively charged residues (aspartates) that are able to repel each other the sustained current was much more pronounced compared to the shark ASIC1b wildtype which carries one negatively charged (D^{110}) and one neutral residue (A^{428}).

Moreover, modeling of two cysteines at positions 110 and 428 and selection of the best side chain rotamer conformations revealed a distance between the S-atoms of both cysteines of less than 3 Å suggesting a possible formation of a disulfide bridge in the desensitized state of the channel (Fig. 4.9 A). Because of the discrepancy of 1 Å between the observed and the ideal distance of a disulfide bridge (ideal are 2.05 Å)

and the non-perfect dihedral angle of 120° (instead of the ideal 90°) we predicted a strained disulfide bond. Electrophysiological recordings of the shark ASIC1b double cysteine mutant firstly confirmed the prediction of a possible formation of a disulfide bond, which traps channels under standard conditions (pH 7.4) in the desensitized state. Raising the pH from 7.4 to 7.8 or by application of the reducing agent DTT at pH 7.4 easily hydrolyzes the disulfide bridge thus also providing evidence that this disulfide bond is under considerable strain (Fig 4.9 C).

Furthermore, it was also shown that cysteine mutations of the residues at corresponding positions in the mammalian rat ASIC1a also form disulfide bonds in the desensitized state (Fig 4.10 B). This observation strongly confirmed the relevance of the findings for the shark ASIC1b double cysteine mutant and suggests a general mechanism for the desensitization gating of ASIC1.

5.4 Cysteine-modification assays complement the static picture of the crystal structure

As shown previously, the crystal structure of chicken ASIC1 provided a valuable basis for uncovering possible interacting regions. Again, the aspartate at position 110 in shark ASIC1b was identified as the most crucial residue for the generation of a sustained current. Furthermore, in the desensitized state the position 110 is in close proximity to residue 428, as supported by the double cysteine mutants. Unfortunately, the crystal structure represents only a static picture of the desensitized state of the channel. In order to get a more dynamic image and to shed light on possible gating movements of the channel, MTS-modification assays were performed with promising results for the single cysteine mutant at position 110 (shark ASIC1b D110C).

MTS reagents are sulfhydryl reactive reagents that are commonly used for modification assays where they from disulfide bonds with cysteine residues of proteins, for example ion channels, and influence the function of modified channels.

With this assay it was shown that position 110 of shark ASIC1b was modified much faster in the closed state at pH 7.4 than in the desensitized state at pH 6.0 (Fig. 4.5). This finding led to the interpretation that residue 110 is accessible in the closed state but might be buried within the channel or is interacting with a different residue in the desensitized state. Moreover, this result clearly showed that position 110 is dynamic during the desensitization movement.

The MTS-modification assays provided additional evidence that the β1-β2 linker region belongs to the important regions that influence and direct the gating kinetics of shark ASIC1b.

Taken together, in this work the gating kinetics of the acid sensing ion channel shark ASIC1b were characterized and the unique sustained current of shark ASIC1b was discovered. Additionally, the regions that are important for the specific gating kinetics and the generation of the sustained current were identified and the direct interaction of two linker regions was uncovered on the basis of the crystal structure of chicken ASIC1 and was confirmed by the construction and electrophysiological characterization of appropriate channel mutants.

Taken together, the results of this thesis contribute to a better understanding of desensitization gating of ASICs and provide possible targets for pharmacological approaches seeking to modify the gating mechanisms of ASICs.

6. List of abbrevations

µA	microampere
µl	microliter
µM	micromoles per liter
τ	time constant
A	alanine
amil	amiloride
ASIC	acid-sensing ion channel
°C	degree Celsius
Ca^{2+}	calcium
$CaCl_2$	calcium chloride
C.elegans	*Caenorhabditis elegans*
cDNA	complement DNA
C^{l-}	chloride
cm	centimeter
C_m	membrane capacitance
CNS	central nervous system
CRD	cysteine-rich-domain
cRNA	complement RNA
D	aspartic acid
DEG	degenerin
DEL	degenerin-like protein
DEPC	diethylpyrocarbonate
DNA	deoxyribonucleic acid
DRG	dorsal root ganglion

ECM	extracellular matrix
EC_{50}	ligand concentration necessary for half– maximal activation
EDTA	ethylenediaminetetraacetic acid
ENaC	epithelial sodium channel
ERD	extracellular regulatory domain
F	phenylalanine
FaNaC	FMRFamide-gated sodium channel
Fig.	figure
FLR-1	fluoride resistant mutant-1
FMRFamide	phenylalanine-methionine-arginine- phenylalanine amide
G	glycine
GPCR	G-protein coupled receptor
h	hour
H^+	proton
HA	hemagglutinin
HG	histidine-glycine
H_3N^+-	amino terminus
5-HT	5-hydroxytryptamine (serotonine)
HEPES	4-(2-hydroxyethyl)-1-piperazineethanesulfonic acid
HyNaC	Hydra sodium channel
I	current
I_c	capacitative current
IC_{50}	ligand concentration necessary for half– maximal inhibition
ID	inner diameter

I_i	ionic current
I_m	membrane current
I_{max}	maximal current
INaC	intestinal sodium channel
K	lysin
K^+	potassium
KCl	potassium chloride
kDa	kiloDalton
L	leucine
M	moles per liter
M	methionine
MEC	mechanosensitive mutations
MES	2-(N-morpholino)ethanesulfonic acid
MDEG	mammalian degenerin
mg	milligram
Mg^{2+}	magnesium
$MgCl_2$	magnesium chloride
min	minute
ml	milliliter
mm	millimeter
mM	millimoles per liter
mRNA	messenger ribonucleic acid
mV	millivolt
MSD	membrane spanning domain
MΩ	MegaOhm

N	asparagine
n	number
Na^+	sodium
NaCl	sodium chloride
ng	nanogram
Na_2HPO_4	di-sodium hydrogen phosphate
nm	nanometer
NMDA	N-methyl-D-aspartic acid
$NMDG^+$	D(-)-N-Methylglucamine nitric oxide
OD	outer diameter
OR-2	oocyte ringer´s solution 2
OTC-20	oocyte testing carousel – 20
P	proline
p	probability
PNS	peripheral nervous system
post-TM1	post-transmembrane domain 1
PVP	polyvinylpyrrolidone
PPK	pickpocket
Q	glutamine
Q_m	membrane charge
R	arginine
R_i	resistance of the current electrode
RNA	ribonucleic acid
RPK	ripped pocket
S	serine

SD	standard deviation
sec	second
SEM	standard error of mean
T	threonine
Tab.	Table
TEVC	two electrode voltage clamp
TM	transmembrane domain
trunc.	truncated
U	units
UNC	uncoordinated locomotion mutant
UV	ultra violet
V	voltage
V	valine
V_{hold}	holding potential
V_m	membrane potential

7. References

Adams, C.M, Anderson, M.G, Motto, D.G, Price, M.P, Johnson, WA and Welsh, MJ (1998) Ripped pocket and pickpocket, novel *Drosophila* DEG/ENaC subunits expressed in early development and in mechanosensory neurons. *J Cell Biol* ,**140**, 143-52.

Akopian, AN, Chen CC, Ding, YN, Cesare P, and Wood JN (2000) A new member of the acid-sensing ion channel family. *Neuroreport*, **11**, 2217–2222.

Askwith CC, Wemmie JA, Price MP, Rokhlina T, Welsh MJ (2004) Acid-sensing ion channel 2 (ASIC2) modulates ASIC1 H^+-activated currents in hippocampal neurons. *J Biol Chem*, **279**, 18296-18305.

Babini E, Paukert M, Geisler HS, Gründer S (2002) Alternative splicing and interaction with di- and polyvalent cations control the dynamic range of acid-sensing ion channel 1 (ASIC1). *J Biol Chem*, **277**, 41597-41603.

Baron A, Schaefer L, Lingueglia E, Champigny G & Lazdunski M (2001). Zn^{2+} and H^+ are coactivators of acid-sensing ion channels. *J Biol Chem*, **276**, 35361-35367.

Baron A, Waldmann R, Lazdunski M (2002) ASIC-like, proton-activated currents in rat hippocampal neurons. *J Physiol*, **539**, 485-494.

Baron A, Voilley N, Lazdunski M and Lingueglia E (2008) Acid sensing ion channels in dorsal spinal cord neurons. *J Neurosci*, **28**, 1498-1508.

Bässler EL, Ngo-Anh TJ, Geisler HS, Ruppersberg JP & Gründer S (2001) Molecular and functional characterization of acid-sensing ion channel (ASIC) 1b. *J Biol Chem*, **276**, 33782-33787.

Benson CJ, Eckert SP, McCleskey EW (1999) Acid-evoked currents in cardiac sensory neurons: A possible mediator of myocardial ischemic sensation. *Circ Res*, **84**, 921-928.

Benson CJ, Xie J, Wemmie JA, Price MP, Henss JM, Welsh MJ, Snyder PM (2002) Heteromultimers of DEG/ENaC subunits form H^+-gated channels in mouse sensory neurons. *Proc Natl Acad Sci U S A*, **99**, 4752.

Cameron P, Hiroi M, Ngai J, Scott K. (2010) The molecular basis for water taste in *Drosophila*. *Nature*, **465**, 91-105

Canessa, C.M, Horisberger, JD and Rossier, BC (1993) Epithelial sodium channel related to proteins involved in neurodegeneration. *Nature*, **361**, 467-470.

Canessa, CM, Schild, L, Buell, G, Thorens, B, Gautschi, I, Horisberger, JD, Rossier, BC (1994) Amiloride-sensitive epithelial Na^+ channel is made of three homologous subunits. *Nature*, **367**, 463-467.

Chalfie, M and Wolinsky, E (1990) The identification and suppression of inherited neurodegeneration in *Caenorhabditis elegans*. *Nature*, **345**, 410-416.

Chalfie M and Au M (1989) Genetic control of differentiation of the *Caenorhabditis elegans* touch receptor neurons. *Science*, **243**, 1027–1033.

Chen CC, England S, Akopian AN & Wood JN (1998) A sensory neuron-specific, proton-gated ion channel. *Proc Natl Acad Sci U S A*, **95**, 10240-10245.

Chen X & Gründer S (2007). Permeating protons contribute to tachyphylaxis of the acid-sensing ion channel (ASIC) 1a. *J Physiol*, **579**, 657-670.

Chen X, Kalbacher H & Gründer S (2005) The tarantula toxin psalmotoxin 1 inhibits acid-sensing ion channel (ASIC) 1a by increasing its apparent H^+ affinity. *J Gen Physiol*, **126**, 71-79.

Chen X, Kalbacher H & Gründer S (2006a) Interaction of acid-sensing ion channel (ASIC) 1 with the tarantula toxin psalmotoxin 1 is state dependent. *J Gen Physiol*, **127**, 267-276.

Chen X, Paukert M, Kadurin I, Pusch M & Gründer S (2006b) Strong modulation by RFamide neuropeptides of the ASIC1b/3 heteromer in competition with extracellular calcium. *Neuropharmacology*, **50**, 964-974.

Chen X, Polleichtner G, Kadurin I & Gründer S (2007) Zebrafish Acid-sensing Ion Channel (ASIC) 4, Characterization of Homo- and Heteromeric Channels, and I dentification of Regions Important for Activation by H^+. *J Biol Chem*, **282**, 30406-30413.

Cook SP, Rodland KD, McCleskey EW (1998) A memory for extracellular Ca^{2+} by speeding recovery of P2X receptors from desensitization. *J Neurosci*, **15**, 9238- 9244.

Coric T, Zhang P, Todorovic N & Canessa CM (2003) The extracellular domain determines the kinetics of desensitization in acid-sensitive ion channel 1. *J Biol Chem*, **278**, 45240-45247.

Coric T, Zheng D, Gerstein M & Canessa CM (2005) Proton sensitivity of ASIC1 appeared with the rise of fishes by changes of residues in the region that follows TM1 in the ectodomain of the channel. *J Physiol*, **568**, 725-735.

Coric T, Passamaneck YJ, Zhang P, Di Gregorio A & Canessa CM (2008) Simple chordates exhibit a proton-independent function of acid-sensing ion channels. *Faseb J*, **22**, 1914-1923.

Coryell MW, Ziemann AE, Westmoreland PJ, Haenfler JM, Kurjakovic Z, Zha XM, Price M, Schnizler MK, Wemmie JA (2007) Targeting ASIC1a reduces innate fear and alters neuronal activity in the fear circuit. *Biol Psychiatry*, **62**, 1140-1148.

Cottrell GA, Green KA, Davies NW (1990) The neuropeptide Phe-Met-Arg-Phe-NH2 (FMRFamide) can activate a ligand-gated ion channel in Helix neurones. *Pflugers Arch*, **416**, 612-614.

Cushman KA, Marsh-Haffner J, Adelman JP, McCleskey EW (2007) A conformation change in the extracellular domain that accompanies desensitization of acid-sensing ion channel (ASIC) 3. *J Gen Physiol*, **129**, 345-350.

Darboux, I., Lingueglia, E., Pauron, D., Barbry, P. and Lazdunski, M. (1998) A new member of the amiloride-sensitive sodium channel family in *Drosophila melanogaster* peripheral nervous system. *Biochem Biophys Res Commun*, **246**, 210-216.

Davey, F., Harris, S.J. and Cottrell, G.A. (2001) Histochemical localisation of FMRFamide-gated Na^+ channels in *Helisoma trivolvis* and *Helix aspersa* neurones. J Neurocytol, **30**, 877-84.

Deval E, Noel J, Lay N, Alloui A, Diochot S, Friend V, Jodar M, Lazdunski M & Lingueglia E. (2008). ASIC3, a sensor of acidic and primary inflammatory pain. *EMBO journal*, **27**, 3047-3055.

Deval E, Gasull X, Noel J, Salinas M, Baron A, Diochot S, Lingueglia E (2010) Acid-Sensing Ion Channels (ASICs): *Pharmacology and implication in pain. Pharmacol Ther.*

De Weille, J and Bassilana, F (2001) Dependence of the acid-sensitive ion channel, ASIC1a, on extracellular Ca^{2+} ions. *Brain* , **900**, 277-281.

Donier E, Rugiero F, Jacob C, Wood JN. (2008) Regulation of ASIC activity by ASIC4-new insights into ASIC channel function revealed by a yeast two-hybrid assay. *Eur J Neurosci*, **28**, 74-86.

Driscoll, M and Chalfie, M (1991) The mec-4 gene is a member of a family of *Caenorhabditis elegans* genes that can mutate to induce neuronal degeneration. *Nature*, **349**, 588-593.

Dürrnagel S, Kuhn A, Tsiairis CD, Williamson M, Kalbacher H, Grimmelikhuijzen CJ, Holstein TW, Gründer S (2010) Three homologous subunits form a high affinity peptide-gated ion channel in *Hydra*. *J Biol Chem*, **285**,11958-11965.

Escoubas P, De Weille JR, Lecoq A, Diochot S, Waldmann R, Champigny G, Moinier D, Menez A & Lazdunski M (2000) Isolation of a *tarantula* toxin specific for a class of proton-gated Na^+ channels. *J Biol Chem*, **275**, 25116-25121.

Firsov D, Robert-Nicoud M, Gründer S, Schild L & Rossier BC (1999). Mutational analysis of cysteine-rich domains of the epithelium sodium channel (ENaC). Identification of cysteines essential for channel expression at the cell surface. *J Biol Chem*, **274**, 2743-2749.

Friese MA, Craner MJ, Etzensperger R, Vergo S, Wemmie JA, Welsh MJ, Vincent A & Fugger L (2007) Acid-sensing ion channel-1 contributes to axonal degeneration in autoimmune inflammation of the central nervous system. *Nature medicine*, **13**, 1483-1489.

Furukawa, Y, Miyawaki, Y and Abe, G (2006) Molecular cloning and functional characterization of the *Aplysia* FMRFamide-gated Na^+ channel. *Pflugers Arch*, **451**, 646- 656.

Gao J, Wu LJ, Xu L and Xu TL. (2004) Properties of the proton-evoked currents and their modulation by Ca^{2+} and Zn^{2+} in the acutely dissociated hippocampus CA1 neurons. *Brain Res*, **1017**, 197-207.

Garty H and Palmer LG. (1997) Epithelial sodium channels: function, structure, and regulation. *Physiol Rev*, **77**, 359–396.

Golubovic A, Kuhn A, Williamson M, Kalbacher H, Holstein TW, Grimmelikhuijzen CJ & Gründer S (2007) A peptide-gated ion channel from the freshwater polyp *Hydra*. *J Biol Chem*, **282**, 35098-35103.

Gonzales EB, Kawate T & Gouaux E. (2009). Pore architecture and ion sites in acid-sensing ion channels and P2X receptors. *Nature*, **460**, 599-604.

Goodman, M.B., Ernstrom, G.G., Chelur, D.S., O'Hagan, R., Yao, C.A. and Chalfie, M. (2002) MEC-2 regulates *C. elegans* DEG/ENaC channels needed for mechanosensation. *Nature*, **415**, 1039-42.

Grimmelikhuijzen, C.J., Dockray, G.J. and Schot, L.P. (1982) FMRFamide-like immunoreactivity in the nervous system of *Hydra*. *Histochemistry*, **73**, 499-508.

Gründer S, Geissler HS, Bässler EL & Ruppersberg JP (2000) A new member of acid-sensing ion channels from pituitary gland. *Neuroreport*, **11**, 1607-1611.

Gründer S, Chen X (2010) Structure, function, and pharmacology of acid-sensing ion channels (ASICs): focus on ASIC1a. *Int J Physiol Pathophysiol Pharmacol*, **2**, 73-94.

Gu G, Caldwell GA, and Chalfie M (1996) Genetic interactions affecting touch sensitivity in *Caenorhabditis elegans*. *Proc Natl Acad Sci U S A*, **93**, 6577– 6582.

Hattori T, Chen J, Harding AM, Price MP, Lu Y, Abboud FM, Benson CJ (2009) ASIC2a and ASIC3 heteromultimerize to form pH-sensitive channels in mouse cardiac dorsal root ganglia neurons. *Circ Res*, **105**, 279-286.

Hesselager M, Timmermann DB & Ahring PK (2004) pH Dependency and Desensitization Kinetics of Heterologously Expressed Combinations of Acid-sensing Ion Channel Subunits. *J Biol Chem*, **279**, 11006-11015.

Huang, M. and Chalfie, M (1994) Gene interactions affecting mechanosensory transduction in *Caenorhabditis elegans*. *Nature*, **367**, 467-470.

Immke DC & McCleskey EW (2003) Protons open Acid-sensing ion channels by catalyzing relief of Ca^{2+} blockade. *Neuron*, **37**, 75-84.

Jasti J, Furukawa H, Gonzales EB & Gouaux E (2007) Structure of acid-sensing ion channel 1 at 1.9 A resolution and low pH. *Nature*, **449**, 316-323.

Jeziorski, M.C, Green, K.A, Sommerville, J and Cottrell, GA (2000) Cloning and expression of a FMRFamide-gated Na^+ channel from *Helisoma trivolvis* and comparison with the native neuronal channel. *J Physiol*, **526**, 13-25.

Jones NG, Slater R, Cadiou H, McNaughton P & McMahon SB (2004) Acid-induced pain and its modulation in humans. *J Neurosci*, **24**, 10974-10979.

Kadurin I, Golubovic A, Leisle L, Schindelin H & Gründer S (2008) Differential effects of N-glycans on surface expression suggest structural differences between the acid-sensing ion channel (ASIC) 1a and ASIC1b. *The Biochemical journal*, **412**, 469-475.

Karlin A, Akabas MH (1998) Substituted-cysteine accessibility method. *Methods Enzymol*, **293**,123-145.

Katsura I, Kondo K, Amano T, Ishihara T, and Kawakami M (1994) Isolation, characterization and epistasis of fluoride-resistant mutants of *Caenorhabditis elegans*. *Genetics*, **136**, 145–154.

Kellenberger, S, Gautschi, I and Schild, L (1999) A single point mutation in the pore region of the epithelial Na^+ channel changes ion selectivity by modifying molecular sieving. *Proc Natl Acad Sci U S A*, **96**, 170-175.

Kellenberger, S and Schild, L (2002) Epithelial sodium channel/degenerin family of ion channels: a variety of functions for a shared structure. *Physiol Rev*, **82**, 735-767.

Kubo Y, Miyashita T, Murata Y (1998) Structural basis for a Ca^{2+}-sensing function of the metabotropic glutamate receptors. *Science*, **279**,1722-1725.

Kumar S and Hedges SB (1998) A molecular timescale for vertebrate evolution. *Nature*, **392**, 917-920.

Li T, Yang Y & Canessa CM. (2009). Interaction of the aromatics Tyr-72/Trp-288 in the interface of the extracellular and transmembrane domains is essential for proton gating of acid-sensing ion channels. *J Biol Chem*, **284**, 4689-4694.

Li T, Yang Y, Canessa CM (2010) Asn-415 in the {beta}11-{beta}12 linker decreases proton-dependent desensitization of ASIC1. *J Biol Chem*.

Littleton JT and Ganetzky B. (2000) Ion channels and synaptic organization: analysis of the Drosophila genome. *Neuron*, **26**, 35–43.

Liu, J, Schrank, B and Waterston, R.H (1996) Interaction between a putative mechanosensory membrane channel and a collagen. *Science*, **273**, 361-364.

Liu, L, Johnson, WA and Welsh, .J (2003) *Drosophila* DEG/ENaC pickpocket genes are expressed in the tracheal system, where they may be involved in liquid clearance. *Proc Natl Acad Sci U S A*, **100**, 2128-2133.

Liu, L, Leonard, AS, Motto, DG, Feller, MA, Price, MP, Johnson, WA and Welsh, MJ (2003) Contribution of *Drosophila* DEG/ENaC genes to salt taste. *Neuron*, **39**, 133-146.

Lingueglia E, Voilley N, Waldmann R, Lazdunski M, and Barbry P (1993) Expression cloning of an epithelial amiloride-sensitive Na^+ channel. *FEBS Lett*, **318**, 95–99.

Lingueglia, E, Champigny, G, Lazdunski, M and Barbry, P (1995) Cloning of the amiloride-sensitive FMRFamide peptide-gated sodium channel. *Nature*, **378**, 730-733.

Lingueglia E, de Weille JR, Bassilana F, Heurteaux C, Sakai H, Waldmann R & Lazdunski M (1997) A modulatory subunit of acid sensing ion channels in brain and dorsal root ganglion cells. *J Biol Chem*, **272**, 29778-29783.

Lingueglia, E, Deval, E and Lazdunski, M (2006) FMRFamide-gated sodium channel and ASIC channels: a new class of ionotropic receptors for FMRFamide and related peptides. *Peptides*, **27**, 1138-1152.

Mano, I and Driscoll, M (1999) DEG/ENaC channels: a touchy superfamily that watches its salt. *Bioessays*, **21**, 568-578.

Madeja M, Musshoff U & Speckmann EJ (1995) Improvement and testing of a concentration-clamp system for oocytes of *Xenopus laevis*. *J Neurosci Methods*, **63**, 211-213.

McDonald FJ, Yang B, Hrstka RF, Drummond HA, Tarr DE, McCray PB JR, Stokes JB, Welsh MJ, and Williamson RA (1999) Disruption of the beta subunit of the epithelial Na channel in mice: hyperkalemia and neonatal death associated with a pseudohypoaldosteronism phenotype. *Proc Natl Acad Sci U S A*, **96**, 1727–1731.

Mogil JS, Breese NM, Witty MF, Ritchie J, Rainville ML, Ase A, Abbadi N, Stucky CL, Séguéla P (2005) Transgenic expression of a dominant-negative ASIC3 subunit leads to increased sensitivity to mechanical and inflammatory stimuli. *J Neurosci*, **25**, 9893-9901.

Moosler A, Rinehart KL, Grimmelikhuijzen CJ (1996) Isolation of four novel neuropeptides, the hydra-RFamides I-IV, from Hydra magnipapillata. *Biochem Biophys Res Commun*, **229**, 596-602.

Mulle C, Léna C, Changeux JP (1992) Potentiation of nicotinic receptor response by external calcium in rat central neurons. *Neuron*, **8**, 937-945.

Palmer LG and Frindt G (1986) Amiloride-sensitive Na channels from the apical membrane of the rat cortical collecting tubule. *Proc Natl Acad Sci U S A*, **83**, 2727–2770.

Paukert M, Babini E, Pusch M & Gründer S (2004a). Identification of the Ca^{2+} blocking site of acid-sensing ion channel (ASIC) 1: implications for channel gating. *J Gen Physiol*, **124**, 383-394.

Paukert M, Sidi S, Russell C, Siba M, Wilson SW, Nicolson T & Gründer S (2004b) A family of acid-sensing ion channels from the zebrafish: widespread expression in the central nervous system suggests a conserved role in neuronal communication. *J Biol Chem*, **279**, 18783-18791.

Paukert M, Chen X, Polleichtner G, Schindelin H & Gründer S (2008) Candidate amino acids involved in H^+ gating of acid-sensing ion channel 1a. *J Biol Chem*, **283**, 572-581.

Perry, SJ, Straub, VA, Schofield, MG, Burke, JF and Benjamin, PR (2001) Neuronal expression of an FMRFamide-gated Na^+ channel and its modulation by acid pH. *J Neurosci*, **21**, 5559-5567.

Pietra F (2009) Docking and MD simulations of the interaction of the *tarantula* peptide psalmotoxin-1 with ASIC1a channels using a homology model. *Journal of chemical information and modeling*, **49**, 972-977.

Plested AJ, Mayer ML (2009) AMPA receptor ligand binding domain mobility revealed byfunctional cross linking. *J Neurosci*, **29**, 11912-11923.

Price, MP, Lewin, GR, McIlwrath, SL, Cheng, C, Xie, J, Heppenstall, PA, Mannsfeldt, AG, Brennan, TJ, Drummond, HA, Qiao, J, Benson, CJ, Tarr, DE, Hrstka, RF, Yang, B, Williamson, RA and Welsh, MJ (2000) The mammalian sodium channel BNC1 is required for normal touch sensation. *Nature*, **407**, 1007-1011.

Qadri YJ, Berdiev BK, Song Y, Lippton HL, Fuller CM & Benos DJ (2009 Psalmotoxin-1 docking to human acid-sensing ion channel-1. *J Biol Chem*, **284**, 17625-17633.

Rossier BC, Pradervand S, Schild L, and Hummler E (2002) Epithelial sodium channel and the control of sodium balance: interaction between genetic and environmental factors. *Annu Rev Physiol*, **64**, 877–897.

Roza C, Puel JL, Kress M, Baron A, Diochot S, Lazdunski M, Waldmann R (2004) Knockout of the ASIC2 channel in mice does not impair cutaneous mechanosensation, visceral mechanonociception and hearing. *J Physiol*, **558**, 659-669.

Sakai, H, Lingueglia, E, Champigny, G, Mattei, MG and Lazdunski, M (1999) Cloning and functional expression of a novel degenerin-like Na^+ channel gene in mammals. *J Physiol*, **519**, 323-333.

Salinas M, Lazdunski M & Lingueglia E (2009) Structural elements for the generation of sustained currents by the acid pain sensor ASIC3. *J Biol Chem*, **284**, 31851-31859.

Samways DS, Harkins AB & Egan TM (2009) Native and recombinant ASIC1a receptors conduct negligible Ca^{2+} entry. *Cell calcium*, **45**, 319-325.

Saugstad JA, Roberts JA, Dong J, Zeitouni S & Evans RJ (2004) Analysis of the membrane topology of the acid-sensing ion channel 2a. *J Biol Chem*, **279**, 55514-55519.

Schaefer, L, Sakai, H, Mattei, M, Lazdunski, M and Lingueglia, E (2000) Molecular cloning, functional expression and chromosomal localization of an amiloride-sensitive Na^+ channel from human small intestine. FEBS Lett, **471**, 205-210.

Schild, L, Schneeberger, E, Gautschi, I and Firsov, D (1997) Identification of amino acid residues in the alpha, beta, and gamma subunits of the epithelial sodium channel (ENaC) involved in amiloride block and ion permeation. *J Gen Physiol*, **109**, 15-26.

Sherwood T, Franke R, Conneely S, Joyner J, Arumugan P & Askwith C (2009) Identification of protein domains that control proton and calcium sensitivity of ASIC1a. *J Biol Chem*, **284**, 27899-27907.

Sluka KA, Winter OC, Wemmie JA (2009) Acid-sensing ion channels: A new target for pain and CNS diseases. *Curr Opin Drug Discov Devel*, **12**, 693-704.

Smith ES, Zhang X, Cadiou H & McNaughton PA (2007) Proton binding sites involved in the activation of acid-sensing ion channel ASIC2a. *Neurosci Lett*, **426**, 12-17.

Sneddon LU (2004) Evolution of nociception in vertebrates: comparative analysis of lower vertebrates. *Brain research*, **46**, 123-130.

Snow PJ, Plenderleith MB & Wright LL (1993) Quantitative study of primary sensory neurone populations of three species of elasmobranch fish. *The Journal of comparative neurology*, **334**, 97-103.

Springauf A, Gründer S (2010) An Acid-Sensing Ion Channel from Shark (Squalus Acanthias) Mediates Transient and Sustained Responses to Protons. *J Physiol*, **588**, 809-820

Sutherland, SP, Benson, CJ, Adelman, JP and and McCleskey, EW (2001) Acid-sensing ion channel 3 matches the acid-gated current in cardiac ischemia-sensing neurons. *Proc Natl Acad Sci U S A*, **98**, 711-716.

Take-Uchi, M, Kawakami, M, Ishihara, T, Amano, T, Kondo, K and Katsura, I (1998) An ion channel of the degenerin/epithelial sodium channel superfamily controls the defecation rhythm in *Caenorhabditis elegans*. *Proc Natl Acad Sci U S A*, **95**, 11775-11780.

Tavernarakis, N, Shreffler, W, Wang, S and Driscoll, M (1997) Unc-8, a DEG/ENaC family member, encodes a subunit of a candidate mechanically gated channel that modulates *C. elegans* locomotion. *Neuron*, **18**, 107-119.

Tavernarakis, N and Driscoll, M (1997) Molecular modeling of mechanotransduction in the nematode *Caenorhabditis elegans*. *Annu Rev Physiol***, 59**, 659-689.

Tavernarakis N and Driscoll M (2000) *Caenorhabditis elegans* degenerins and vertebrate ENaC ion channels contain an extracellular domain related to venom neurotoxins. *J Neurogenet*, **13**, 257– 264.

Ugawa, S, Ueda, T, Ishida, Y, Nishigaki, M, Shibata, Y, Shimada, S (2002) Amiloride-blockable acid-sensing ion channels are leading acid sensors expressed in human nociceptors. *J Clin Invest*, **110**, 1185-1190.

Vukicevic M, Kellenberger S (2004) Modulatory effects of acid-sensing ion channels onaction potential generation in hippocampal neurons. *Am J Physiol Cell Physiol*, **287**, 682-690.

Waldmann R, Champigny G, Bassilana F, Voilley N, and Lazdunski M (1995) Molecular cloning and functional expression of a novel amilo- ride-sensitive Na^+ channel. J Biol Chem, **270**, 27411–27414.

Waldmann R, Bassilana F, de Weille J, Champigny G, Heurteaux C & Lazdunski M (1997). Molecular cloning of a non-inactivating proton-gated Na^+ channel specific for sensory neurons. *J Biol Chem*, **272**, 20975-20978.

Waldmann R & Lazdunski M (1998). H^+-gated cation channels: neuronal acid sensors in the NaC/DEG family of ion channels. *Curr Opin Neurobiol*, **8**, 418-424.

Wemmie JA, Chen J, Askwith CC, Hruska-Hageman AM, Price MP, Nolan BC, Yoder PG, Lamani E, Hoshi T, Freeman JH, Jr. & Welsh MJ. (2002). The acid-activated ion channel ASIC contributes to synaptic plasticity, learning, and memory. Neuron, **34**, 463-477.

Wemmie, JA, Askwith, CC, Lamani, E, Cassell, MD, Freeman, JH Jr. and Welsh, MJ (2003) Acid-sensing ion channel 1 is localized in brain regions with high synaptic density and contributes to fear conditioning. *J Neurosci*, **23**, 5496-5502.

Wemmie JA, Price MP, Welsh MJ (2006) Acid-sensing ion channels: advances, questions and therapeutic opportunities. *Trends Neurosci*, **29**, 578-586.

Weng JY, Lin YC, Lien CC (2010) Cell type-specific expression of acid-sensing ion channels in hippocampal interneurons*. J Neurosci*, **30**, 6548-6558.

Wiemuth and Gründer (2010) A single amino acid tunes Ca^{2+} inhibition of brain liver intestine Na^{+} channel (BLINaC). *J Biol Chem*, **285**, 30404-30410

Xiong ZG, Zhu XM, Chu XP, Minami M, Hey J, Wei WL, MacDonald JF, Wemmie JA, Price MP, Welsh MJ & Simon RP (2004) Neuroprotection in ischemia: blocking calcium-permeable acid-sensing ion channels. *Cell*, **118**, 687-698.

Yagi J, Wenk HN, Naves LA & McCleskey EW (2006) Sustained currents through ASIC3 ion channels at the modest pH changes that occur during myocardial ischemia. *Circ Res*, **99**, 501-509.

Yamamura, H, Ugawa, S, Ueda, T, Nagao, M and Shimada, S (2004) Protons activate the delta-subunit of the epithelial Na^{+} channel in humans. *J Biol Chem*, **279**, 12529-12534.

Zerangue N, Schwappach B, Jan YN & Jan LY (1999) A new ER trafficking signal regulates the subunit stoichiometry of plasma membrane K(ATP) channels. *Neuron*, **22**, 537-548.

Zha XM, Wemmie JA, Green SH, Welsh MJ (2006) Acid-sensing ion channel 1a is a postsynaptic proton receptor that affects the density of dendritic spines. *Proc Natl Acad Sci U S A,* **103**,16556-16561

Zha XM, Costa V, Harding AM, Reznikov L, Benson CJ and Welsh MJ (2009) ASIC2 subunits target acid-sensing ion channels to the synapse via an association with PSD-95. *J Neurosci*, **29**, 8438-8446.

Zhang, P and Canessa, CM (2002) Single channel properties of rat acid-sensitive ion channel-1alpha, -2a, and -3 expressed in *Xenopus* oocytes. *J Gen Physiol*, **120**, 553-566.

Ziemann AE, Schnizler MK, Albert GW, Severson MA, Howard MA, 3rd, Welsh MJ & Wemmie JA (2008) Seizure termination by acidosis depends on ASIC1a. *Nature Neuroscience*, **11**, 816-822.